

Interpretation of Pneumatic and Chemical Data From the Unsaturated Zone Near Yucca Mountain, Nevada

By Gary L. Patterson, Edwin P. Weeks, Joseph P. Rousseau, and
Thomas A. Oliver

U.S. GEOLOGICAL SURVEY

Prepared in cooperation with the
U.S. DEPARTMENT OF ENERGY,
NEVADA OPERATIONS OFFICE, under
Interagency Agreement DE-AI08-92NV10874

Denver, Colorado
1996



9803090197 970627
PDR WASTE
WM-11 PDR

Interpretation of Pneumatic and Chemical Data From the Unsaturated Zone Near Yucca Mountain, Nevada

U.S. GEOLOGICAL SURVEY

Prepared in cooperation with the
U.S. DEPARTMENT OF ENERGY,
NEVADA OPERATIONS OFFICE, under
Interagency Agreement DE-AI08-92NV10874



CONTENTS

Abstract	1
Introduction	3
Purpose and Scope	4
Quality Assurance	5
Regional Hydrogeologic Setting of Yucca Mountain	6
Stratigraphic Framework	7
Correlation of the Lithostratigraphic and Hydrogeologic Frameworks	8
Ambient Pneumatic Pressure Monitoring	10
In Situ Pneumatic Pressure Response to Atmospheric Pressure Changes	10
Subsurface pressure Prior to the influence of ESF Excavation	12
North Ramp Boreholes	13
Pagany Wash Boreholes	16
Main Drift Boreholes	18
Synthesis of Subsurface Pressure Measurement	22
Tiva Canyon Welded Unit	22
Paintbrush Group Nonwelded Unit	23
Topopah Spring Lithophysal and Nonlithophysal Welded Tuffs	26
Pressures Monitored Below Perched Water	27
One-Dimensional Analyses of Permeability Using AIRK	29
Effects of Excavation of the ESF on In Situ SUBSURFACE Pneumatic-Pressure Measurements	40
Determination of Horizontal Permeability and the Vertical Anisotropy of the Topopah Spring Tuff Based on Modflowp Simulations	50
Model Structure	52
Model Parameters	55
Model Pressure Data	56
Initial Conditions	58
Parameter Estimation for Boreholes NRG#5, NRG-6, and NRG7	58
Parameter Estimation for Boreholes UZ#4 and UZ#5	65
Gas-Phase Circulation at Yucca Mountain Crest	67
Physical Processes	68
Barometric Pumping	69
Thermosyphon Pumping	70
Windpumping	72
Physical Measurements	75
Measurements in UZ-6s	75
Surface Airflow Measurements at Borehole UZ-6s	75
Flow Measurements at Depth	75
Surface Temperature and Relative Humidity Measurements	78
Measurements of Temperature at Depth	78
Measurements in Borehole UZ-6s	79
Measurements in Neutron Holes	81
Weather Records	82
Analysis of Flow Data from Borehole UZ-6s	82
Sources of Cross-Bed Flow to Borehole UZ-6s	89
Cross-Bed Leakage Through the PTn	89
Cross-Formational Flow Through Borehole UZ-6	90
Gas Chemistry Interpretations	91
Natural System Flow	92
The UZ-6/UZ-6s Local System	94
UZ6-UZ6s Tracer Test	95
Modflow Modeling of Thermally Driven Air Flow in the UZ-6/UZ-6s System	98

Conceptual Model	99
Model Structure	100
Model Pressure Potential Data	
Steady-State Calibration	
Borehole UZ-6s Simulation	106
Boreholes UZ-6/UZ6s Simulation	106
Conclusions	107
References	111

FIGURES

1. Location of study area	
2. Lithostratigraphic and hydrogeologic units in the Yucca Mountain area	
3. Borehole locations and trace of the Exploratory Studies Facility	
4. Stratigraphy and monitoring locations of instrumented boreholes	
5. Pressure record and the results of cross-spectral analysis on data from borehole UE-25 NRG#5 prior to the effects of ESF excavation	
6. Pressure record and the results of cross-spectral analysis on data from borehole USW NRG-6 prior to the effects of ESF excavation	
7. Pressure record and the results of cross-spectral analysis on data from borehole USW NRG-7a prior to the effects of ESF excavation	
8. Pressure record and the results of cross-spectral analysis on data from borehole UE-25 UZ#4 prior to the effects of ESF excavation	
9. Pressure record and the results of cross-spectral analysis on data from borehole UE-25 UZ#5 prior to the effects of ESF excavation	
10. Pressure record and the results of cross-spectral analysis on data from borehole USW SD-12 prior to the effects of ESF excavation	
11. Pressure record and the results of cross-spectral analysis on data from borehole USW UZ-7a prior to the effects of ESF excavation	
12. Pressure record and the results of cross-spectral analysis on data from borehole USW SD-7 prior to the effects of ESF excavation	
13. Casing configuration and monitoring zones at boreholes USW SD-9 and USW SD-7 (prior to the installation of the borehole liner)	
14. Pressure record from monitoring stations below perched water	
15. Selected onset of the effects of ESF excavation on pneumatic pressures at borehole UE-25 UZ#4	
16. Selected onset of the effects of ESF excavation on pneumatic pressures at borehole UE-25 UZ#5	
17. Pressure record and the results of cross-spectral analysis on data from borehole UE-25 UZ#4 after the effects of ESF excavation	
18. Pressure record and the results of cross-spectral analysis on data from borehole UE-25 UZ#5 after the effects of ESF excavation	
19. Selected onset of the effects of ESF excavation on pneumatic pressures at borehole UE-25 NRG#5	
20. Pressure record and the results of cross-spectral analysis on data from borehole UE-25 NRG#5 after the effects of ESF excavation	
21. Selected onset of the effects of ESF excavation on pneumatic pressures at borehole USW NRG-6	
22. Pressure record and the results of cross-spectral analysis on data from borehole USW NRG-6 after the effects of ESF excavation	
23. Selected onset of the effects of ESF excavation on pneumatic pressures at borehole USW NRG-7a	
24. Pressure record and the results of cross-spectral analysis on data from borehole USW NRG-7a after the effects of ESF excavation	
25. Selected onset of the effects of ESF excavation on pneumatic pressures at borehole USW SD-12	
26. Pressure record and the results of cross-spectral analysis on data from borehole USW SD-12 after the effects of ESF excavation	
27. Selected onset of the effects of ESF excavation on pneumatic pressures at borehole USW SD-7	
28. Pressure record and the results of cross-spectral analysis on data from borehole USW SD-7 after the effects of ESF excavation	

	effects of ESF excavation.....	
29.	Results of simulation of pressure amplitudes in boreholes UE-25 NRG#5, USW NRG-6, and USW NRG-7a due to a unit amplitude barometric pressure change of one-week period with the tunnel position updated weekly.....	
30.	Location of boreholes showing model boundaries.....	
31.	Gas temperature with depth during period of well exhaust, January-February, 1993.....	
32.	Sketch showing construction of upper part of well UZ6.....	
33.	Thermosyphon-generated flow from borehole USW UZ-6s, computed as the residual of measured flow minus those computed for barometric pumping and for wind pumping.....	
34.	Tracer test SF6 concentrations in boreholes UZ-6, UZ-6s, and UZ-N95.....	
35.	Comparison of simulated flow contributions to measure flow distribution with depth for calibrated model.....	
36.	Particle tracking backward for nodes representing layers 3 and 4 of borehole USW UZ-6s, showing modeled source of air.....	

TABLES

1.	Sensitivity of Topopah Spring residual amplitude to variations in t and k_2	35
2.	Sensitivity of Topopah Spring residual amplitude to variations in k_1	35
3.	Sensitivity of Topopah Spring Tuff residual amplitudes to variations in the $L_1\phi_1$ product.....	36
4.	Results of one dimensional air permeability analyses.....	39
5.	Summary of the first occurrence of pneumatic interference effects from the ESF.....	42
6.	Summary of Modflowp simulations to estimate permeabilities near boreholes NRG#5, NRG-6, and NRG7a.....	60
7.	Location of ESF used to simulate temporal effects of tunnel advancement.....	64
8.	Summary of Modflowp simulations to estimate permeabilities near boreholes UZ#4 and UZ#5.....	67
9.	Summary of analyses of air flow from borehole UZ-6s.....	88
10.	Summary of permeability determinations for Tiva Canyon Tuff near Borehole UZ6s.....	104

CONVERSION FACTORS

Multiply	By	To obtain
meters	3.281	feet
feet	0.3048	meters
square meters	1×10^{-6}	square kilometers
square kilometer	0.3861	square mile
cubic meters	0.001	liters
liters	0.2642	gallons
liters per second	0.06308	gallons per minute
liters per second	86.4	cubic meters per day
liters per second	543.44	barrels per day
millidarcies	9.869×10^{-16}	square meters
millidarcies	1.062×10^{-14}	square feet
centipoise	0.001	pascal seconds
meter squared per day	10.765	feet squared per day
pound per square inch	6.895	kilopascal
pound per square inch-l	1.450×10^{-4}	pascal-l
kilograms epr cubic meter	3.613×10^{-5}	pounds per square inch
kilogram	2.205	pounds

Temperature in degrees Celsius (°C) may be converted to degrees Fahrenheit (°F) as follows:

$$^{\circ}\text{F} = 1.8 \text{ }^{\circ}\text{C} + 32$$

Interpretation of Pneumatic and Chemical Data From the Unsaturated Zone Near Yucca Mountain, Nevada

By Gary L. Patterson, Edwin P. Weeks, Joseph P. Rousseau, and Thomas A. Oliver

Abstract

In-Situ pneumatic-pressure monitoring of instrumented boreholes throughout the Yucca Mountain area indicates that the lithostratigraphic units can be grouped into distinct pneumatic systems. The pneumatic-pressure records for stations in the Tiva Canyon Tuff display little attenuation or lag of the synoptic-barometric signal, which indicates that the Tiva Canyon Tuff has a large bulk permeability. The pneumatic-pressure records from stations within the Paintbrush Tuff nonwelded unit indicate that the synoptic-pressure signal is substantially attenuated and lagged by lower permeability subunits within the PTn. The attenuation and lag of the synoptic-pressure signal through the PTn varies across the site. Results of one-dimensional modeling of pressure data collected before effects of the ESF were observed indicate that the average bulk vertical permeability of the full thickness of the PTn ranges from 0.2 to 1.0 mm² near boreholes along the North Ramp of the Exploratory Studies Facility (ESF). Pressure data from stations within the Topopah Spring Tuff indicate that attenuation and lag in the Topopah Spring Tuff are negligible, with the exception of two boreholes that are affected by the presence of nearby faults and appear to contain zones of smaller permeability within the Topopah Spring Tuff. One-dimensional modeling indicates that the vertical permeability of the Topopah Spring Tuff is greater than 20 mm².

ESF excavation effects were detected in the pneumatic-pressure records of all boreholes with the exception of borehole UZ-7a, which is drilled entirely through the Ghost Dance Fault. Any ESF effects in UZ-7a may be masked by the effects of the fault itself. A Modflowp model was constructed to determine horizontal and vertical permeabilities of the Topopah Spring Tuff by simulation of the effects of excavation of the North Ramp of the ESF. Results of this modeling indicate that the bulk horizontal permeability ranges from 30 to 60 mm² and the bulk vertical permeability from 70 to 100 mm² in the vicinity of boreholes NRG-5, NRG-6, and NRG-7a.

The Modflowp model of the North Ramp was successful in providing parameter estimates that may be suitable for use in a general simulation model of repository performance. However, 7 of the 8 boreholes with discretized-pressure records discussed in this report appear to be affected by the presence of faults that were not included in the Modflowp simulation. Thus, a simple layered model that does not include detailed pneumatic characterization of faults and major fracture zones may fail to adequately represent the effects of many important pneumatic pathways that exist in the vicinity of the proposed repository.

A net annual exhaust of about 1×10^6 m³ of rock gas arising from thermosyphon and wind effects has been measured from borehole UZ-6s. Despite this large net exhaust, gas CO₂ chemistry for borehole UZ-6s changed very little over a 5 year period. The $\delta^{13}\text{C}$ composition of the gas (-17.5‰) strongly indicates a soil source for the CO₂, but the exposure along the flank of Solitario Canyon (the most obvious source for the exhausted gas) is limited. Thus, much of the gas must be derived from up dip migration from the eastern flank of the mountain. Based on chemistry data, about 40% of the thermosyphon-induced movement of air from well UZ-6s is derived from flow from the Topopah Spring Tuff to the Tiva Canyon Tuff through the breach in the PTn created by borehole UZ-6. Air flow from borehole UZ-6 to borehole UZ-6s was confirmed by a multiple well tracer tests and by a Modflow model. This air flow indicates

that no significant permeability barriers exist within the Topopah Spring Tuff between its outcrop in Solitario Canyon and borehole UZ-6, and that heat generated by waste emplacement in the Topopah Spring Tuff would likely result in gas-phase circulation cells between the repository and the outcrop that would discharge heat, moisture, and $^{14}\text{CO}_2$ to the atmosphere.

INTRODUCTION

Yucca Mountain, Nevada, is being studied by the U.S. Department of Energy as a potential site for the permanent storage of high-level radioactive waste. As part of the site characterization activities required to determine site suitability, the U. S. Geological Survey is engaged in studies to develop an understanding of the movement of gas and water vapor through the thick unsaturated rocks in the Yucca Mountain area. As part of these studies, several boreholes have been instrumented in the unsaturated zone and continuously monitored to record changes in pneumatic pressure at depth. The purposes of pneumatic monitoring are threefold: (1) measure *in situ* pneumatic pressure response to atmospheric pressure changes in order to determine the influence of lithostratigraphy, bulk properties, and major structural features on the natural gaseous-phase circulation system; (2) utilize the response of the system at depth to changes in atmospheric pressure to estimate pneumatic diffusivities and, ultimately, effective gas permeabilities of the lithostratigraphic layers; and (3) document and quantify the effects of excavation of the ESF on *in situ* pneumatic pressure and on the overall gaseous-phase-circulation system.

Gas and vapor flux through the unsaturated zone are driven by changes in barometric pressure, temperature induced density differences, and wind effects. Changes in barometric pressure at land surface result in corresponding changes in pneumatic pressure in the unsaturated sub-surface. The corresponding pressure change in the sub-surface is commonly amplitude-attenuated and time-lagged relative to the pressure change at the surface. The attenuation and lag are a function of the air-permeability and the associated bulk-pneumatic diffusivity of the rock layers at a given location.

Consequently, the sub-surface responses are conceptually controlled by the distribution and interconnection of fractures, the presence of faults and their ability to conduct gas and water vapor, and the moisture content and matrix permeability of the rock units.

Temperature induced density effects are significant only in hilly terrain, and are dominated by drier, cooler air entering along hillsides and moving through the sub-surface. This air becomes geothermally heated as it moves through the rock and eventually can move vertically upward to exhaust along hillcrests. This effect is referred to as the thermosyphon effect by mechanical engineers and that term is used in this report.

Wind effects are also only significant in hilly terrain and are the result of a drag effect along hillsides and a lift effect along hillcrests. Wind blowing against the side of a hill generally causes increased pressure that allows air to flow into the rock. Wind blowing over the crest of a hill generally causes lower pressure that allows air to flow out of the rock.

Purpose and Scope

This report summarizes pneumatic pressure data collected from instrumented boreholes throughout the Yucca Mountain area and flow, temperature, and chemistry data collected for open boreholes at the crest of Yucca Mountain. The report begins with a detailed discussion of the ambient pneumatic conditions in the vicinity of each instrumented borehole prior to the onset of the effects of Exploratory Studies Facility (ESF) excavation, including determinations of the vertical permeability to air of the major hydrogeologic units, based on a one-dimensional model. This discussion is followed by detailed descriptions of the changes imposed on those ambient conditions due to the advance of the tunnel boring machine (TBM). The effects of the ESF excavation are simulated with a three-dimensional gas-flow model to calculate horizontal permeabilities and vertical anisotropy of the Topopah Spring Tuff between boreholes along the north ramp of the ESF. This is followed by a discussion of gas circulation resulting from barometric, thermosyphon, and wind pumping along the

crest of Yucca Mountain as determined from interpretations of both physical and chemical data collected from open boreholes at Yucca Mountain Crest. These interpretations were tested using a three-dimensional gas-flow model. Interpretations of cross-formational flow through an open borehole were verified with a multiple borehole tracer test.

Several studies have contributed to the information presented in this report, but most of the information has been generated by Study 8.3.1.2.2.6.-Characterization of Gaseous-Phase Movement in the Unsaturated Zone and Study 8.3.1.2.2.3.-Characterization of Percolation in the Unsaturated Zone-Surface Based Study. Much of the information presented in the following sections dealing with geology and regional setting is modified from "Hydrogeology of the Unsaturated Zone, North Ramp Area of the Exploratory Studies Facility, Yucca Mountain, Nevada" edited by Rousseau, J.P., Kwicklis, E.M., and Gillies, D.C.

Quality Assurance

The bulk of the data described and interpreted in this report were collected in compliance with the approved U.S. Geological Survey, Yucca Mountain Project quality assurance (QA) program. However, some data cited and utilized in the report were collected prior to the implementation of the approved QA program. These data are non-qualified. Generally, the non-qualified data are used as background information or to corroborate findings and conclusions that are fully supportable using data that are fully qualified under the approved QA program. The use of non-qualified data generally is intended to add scientific confidence to the reports findings and conclusions, or to demonstrate that the non-qualified data are as scientifically valid as the fully qualified data, even though they are not "traceable" in the quality assurance sense.

In brief, two significant categories of non-qualified data were used in this report to corroborate interpretations of qualified data and to plan experiments for the collection of qualified data. The first of these categories involves the use of non-qualified data on flow distribution with depth in borehole UZ6s

(section on flow measurements at depth). These data were used to calibrate a Modflow model to corroborate the chemistry-interpretation-based finding that significant flow was occurring from the Topopah Spring Tuffs through borehole UZ-6 into the Tiva Canyon Tuff (section on the UZ-6-UZ-6s local flow system). The model was also used to identify optimal sampling locations for the UZ6-UZ-6s tracer test (section on UZ-6-UZ-6s local flow system). The other category involves the use of non-qualified gas chemistry data collected prior to 1993, which were used to corroborate interpretations of the qualified data collected in 1993. Data were collected prior to 1993 using the same techniques as those for the 1993 data, and provide similar results. When non-qualified data are used in the report they are identified as such in the text.

REGIONAL HYDROGEOLOGIC SETTING OF YUCCA MOUNTAIN

Yucca Mountain is located in southern Nevada (fig. 1) about 145 km northwest of Las Vegas within the Basin and Range physiographic province (Grayson, D.K.,1993). Basin and range physiography is represented by the north-to- northwest trending linear mountains and valleys that are a result of late Cenozoic structural activity. This region ranges in altitude from 86 m below sea level at Death Valley to about 3600 m above sea level.

Figure 1. Location of study area.

Within the Basin and Range physiographic province there are several topographic regions. Yucca Mountain is in the region named for Death Valley which is the most prominent desert basin. The Death Valley region is primarily in the northern Mojave Desert and extends northward into the Great Basin Desert. Yucca Mountain lies within the rain shadow of the Sierra Nevada Mountains which results in an arid climate with an average annual precipitation of about 165 mm (Hevesi and Flint, 1996), ranging

from 130 mm at the southern part of the mountain to 250 mm at the higher elevations in the northern part. Summer precipitation results primarily from localized convective-type storms that develop during monsoonal weather patterns (French, 1983; Houghton, 1969). Winter precipitation results primarily from frontal systems moving inland from the Pacific Ocean, and occurs as snow or rain.

Stratigraphic Framework

Yucca Mountain is underlain by a thick sequence of Miocene volcanic rocks and localized Quaternary to Pliocene alluvial deposits, and is broken into several east-tilted structural blocks that are bounded by north-trending normal faults (Buesch and Spengler, 1996). The central structural block of Yucca Mountain is bounded by Solitario Canyon and Bow Ridge faults on the west and east, respectively. In the northern part of the central block, northwest-trending washes and faults are the dominant physiographic surface and structural features. These northwest-trending strike-slip faults have variable amounts of strike-slip separation, but dip-slip separation is typically less than a few meters. Near the Bow Ridge fault, the eastern margin of the central block has numerous north-trending dip-slip faults with separations typically less than 10 m. In marked contrast, the central block to the south of Drill Hole Wash is characterized by numerous east-trending washes and north-trending faults. Several of these north-trending faults have dip-slip separations greater than 15 m.

Variations in lithostratigraphy and orientation of the layered Tertiary volcanic sequence at Yucca Mountain, Nevada are a direct result of the initial processes of eruption and deposition with cooling and crystallization in some ignimbrites and lava flows, and post-depositional processes of alteration and tectonics. Lithostratigraphic units are based on depositional, welding, crystallization, alteration, and fracture characteristics. Hydrogeologic properties such as variations in grain density, bulk density, porosity, permeability, and water content correlate with many of these lithostratigraphic features. Boundaries that separate fundamental variations in hydrologic properties and define the four major hydrogeologic units of the unsaturated zone (Montazer and Wilson, 1984) match those of mappable and

laterally continuous lithostratigraphic subzones (Buesch, Spengler, and others, 1996). Figure 2 shows the correlation between lithostratigraphic units and hydrologic units in the Yucca Mountain area and symbols used in stratigraphic columns in this report.

Figure 2. Lithostratigraphic and hydrogeologic units in the Yucca Mountain area.

The stratigraphic framework, from top to bottom, consists of Quaternary alluvial deposits that discontinuously overlie 11.4 to 13.4 m.y.-old formations of the Timber Mountain and Paintbrush Groups, the Calico Hills Formation, and the Crater Flat Group. Locally, the Timber Mountain Group is represented by the Rainier Mesa Tuff and the pre-Rainier Mesa Tuff bedded tuff. The Paintbrush Group consists of the Tiva Canyon, Yucca Mountain, Pah Canyon, and Topopah Spring Tuffs with interstratified informal units of bedded tuffs. Locally, rocks of the Crater Flat Group, represented by the Prow Pass Tuff or the Bullfrog Tuff, comprise the lower part of the unsaturated zone.

Correlation of the Lithostratigraphic and Hydrogeologic Frameworks

Lithologic units, described above, have been grouped into hydrogeologic units, based principally on major variations in the degree of welding and fracture characteristics. Beneath the alluvium, the four major hydrogeologic units include the Tiva Canyon welded unit, Paintbrush nonwelded unit, Topopah Spring welded unit, and the Calico Hills nonwelded unit (Montazer and Wilson, 1984). Lithostratigraphic units with the rank of subzone commonly correlate with boundaries of the four major hydrogeologic units. Each of the hydrogeologic units has the potential to be divided into subunits, and most of these subunits also correspond to the lithostratigraphic subzones.

The Tiva Canyon welded (TCw) hydrogeologic unit consists of crystallized moderately to densely welded tuff (Montazer and Wilson, 1984). The top of the TCw is the top of the vitric densely welded subzone of the crystal-rich member in the Tiva Canyon Tuff. The crystal-rich vitric densely

welded subzone is typically eroded, and occurs only locally in the central block in borehole NRG#2A (Geslin and others, 1995). The base of the TCw is typically the contact between crystallized, columnar subzone of the lower nonlithophysal zone and vitric moderately welded subzone of the crystal-poor member of the Tiva Canyon Tuff (Buesch, Spengler, and others, 1996; Moyer and others, 1996). In the southwest part of the central block, the base of the TCw is the contact of the vitric densely and moderately welded subzones (Buesch, Spengler, and others, 1996; Moyer and others, 1996).

The Paintbrush nonwelded (PTn) hydrogeologic unit consists of rocks with low density and high porosity that are interstratified with rocks with high density and low porosity (Montazer and Wilson, 1984). In the northern part of the central block of Yucca Mountain, the top of the PTn typically corresponds with the lithostratigraphic contact of the columnar subzone of the lower nonlithophysal zone and the vitric moderately welded subzone in the crystal-poor member of the Tiva Canyon Tuff. The base of the PTn is in the crystal-rich member of the Topopah Spring Tuff and typically corresponds with the contact of the vitric moderately and densely welded subzones where the transition from nonwelded to densely welded rocks is commonly less than 2 m thick.

The Topopah Spring welded (TSw) hydrogeologic unit consists of crystallized moderately to densely welded tuff (Montazer and Wilson, 1984; Buesch, Spengler, and others, 1996; Moyer and others, 1996). The top of the TSw correlates with the top of the vitric densely welded subzone of the crystal-rich member in the Topopah Spring Tuff, or locally where there is no vitric densely welded subzone, the top is the dense subzone of the nonlithophysal zone. The base of the TSw is the contact of the vitric densely welded and moderately welded subzones of the crystal-poor member in the Topopah Spring Tuff.

The Calico Hills nonwelded (CHn) hydrogeologic unit, which has been defined only for the unsaturated zone, consists of all rocks below the base of the crystal-poor densely welded zone of the Topopah Spring Tuff where they occur above the water table, except locally where the Crater Flat (CFu) hydrogeologic unit occurs above the water table (Montazer and Wilson, 1984).

AMBIENT PNEUMATIC PRESSURE MONITORING

Figure 3 is a map of the Yucca Mountain area showing the location of the Exploratory Studies Facility and boreholes discussed in this report. Boreholes UE-25 NRG#5, USW NRG-6, USW NRG-7a, USW SD-9, USW SD-7, USW SD-12, UE-25 UZ#4, UE-25 UZ#5 and USW UZ-7a were used primarily to collect *in situ* pressure measurements from discreet subsurface locations. Boreholes USW UZ-6 and USW UZ-6s and various neutron holes were used for composite borehole pressure measurements, flow measurements, and gas chemistry. The designation USW and UE-25 will be dropped from the borehole names for the remainder of the report.

Figure 3. Borehole locations and trace of the Exploratory Studies Facility.

***In Situ* Pneumatic Pressure Response to Atmospheric Pressure Changes**

In situ pneumatic pressures have been monitored in nine boreholes that are discussed in this report. Two of these boreholes, UZ#4 and UZ#5, are located in Pagany Wash; four boreholes, SD-9, NRG-7a, NRG#5, and NRG-6, are located in Drill Hole Wash, UZ-7a is located in WT-2 Wash, SD-12 is located in Antler Wash, and SD-7 is located on the flank of Highway Ridge (figure 3.). Boreholes UZ-7a, SD-12, and SD-7 are along the north-south (main) drift of the ESF and the others are along the east-west (north ramp) drift.

SD-12, UZ-7a, NRG-6, NRG-7a, UZ#4, and UZ#5 were instrumented with downhole pressure transducers that measure absolute pneumatic pressure. Individual monitoring stations in these boreholes were back-filled or packed with porous stemming materials (polyethylene beads or coarse sand) to couple the monitoring zone to the formation rock of interest. Isolation of individual instrument stations in these boreholes was achieved with intervening lifts of stemming materials consisting of grout and sand (Kume and Rousseau, 1994; Rousseau and others, 1995). In this report the absolute

pressure data from permanently instrumented boreholes have been converted to pressure potential by subtracting the long term mean from the absolute reading. This effectively removes the gravity component of the total pressure measurement and allows these data to be directly compared with pressure potential data collected from other boreholes.

At NRG#5 and SD-7, downhole pressures potentials are sensed at the ground surface through individual tubes that are connected to open ports located along the length of an impermeable membrane liner. The liner is inflated to seal the formation wallrock from direct communication with the atmosphere. Pressure potentials are measured using a differential pressure transducer at the ground surface that is referenced to atmospheric pressure at the time measurements are taken. A second pressure transducer is used to measure atmospheric pressure. This measurement is added back to the differential pressure measurement to compute the pneumatic pressure potential at the location of the port. It is assumed that the gas in the tubes extending from depth to land surface is of the same composition and at the same temperature as gas in the adjacent rock. Thus, the weight of the "hanging" column of air in the tube exactly compensates for the weight of gas in the unsaturated zone profile, so the readings represent the differences in pressure potential produced by barometric fluctuations.

At SD-9 and early monitoring at SD-7, pneumatic pressures were also measured at the ground surface in a manner similar to that for NRG#5 and SD-7. However, downhole pressures were sensed through access tubes inserted into the annular spaces between a pair of nested casings and between the outer casing and formation wallrock, as described later.

Throughout this report the term pressure should be taken to mean pressure potential. In the few instances where absolute measurements are referred to, the term absolute pressure will be used to differentiate those measurements from the pressure potentials.

In addition to visual inspection, the downhole pressure data were analyzed using cross-spectral estimation techniques (Bendat and Piersol, 1986) to describe the character of the time-varying response of downhole pressure to changes in the synoptic barometric signal.

The power spectral density of barometric pressure and the transfer function from barometric pressure to downhole pressure were estimated using the Spectrum subroutine from the Matlab signal Processing Toolbox (Little and Shure, 1988). Generally, this subroutine uses Fourier transform algorithms that can detect narrow-band frequency signals that are buried in wide-band noise. The barometric signal is a broad frequency-band pressure fluctuation that contains predominant semi-diurnal, and longer period (synoptic) frequencies. The synoptic frequencies, associated with the passage of storm fronts, provide a longer term pressure fluctuation and, therefore, provide a better developed downhole pressure response. For these analyses, the synoptic barometric frequency having the greatest power spectral density was selected and the residual amplitude (RA) and phase lag (PL) of that signal at each downhole sensor were calculated using the following relations:

$$RA = (Re^2 + Im^2)^{0.5} \text{ and } PL = \tan^{-1}(Im/Re) \text{ (rate of measurement)}$$

where Re and Im are the real and imaginary parts of the transfer function respectively.

These cross-spectral analyses are helpful in comparing pressure responses between stations within individual boreholes. However, because the period of the synoptic pressure signal varies over time, some of the differences seen in the analyses among different boreholes may be the result of differing time periods, data collection frequency, and different length of the data record. Ideally these analyses would be performed on long continuous data sets representing 1 or 2 years of monitoring. Because data sets of that length are not available for most of the boreholes discussed in this report, the use of these analyses is limited to events and conditions that can be supported by visual inspection of the record or other supporting information.

SUBSURFACE PRESSURE PRIOR TO THE INFLUENCE OF ESF EXCAVATION

Stratigraphic columns and the location of monitoring ports or stations for the instrumented boreholes discussed in this report are shown on figure 4.

Figure 4. Stratigraphy and monitoring locations of instrumented boreholes.

North Ramp Boreholes

Borehole NRG#5 is located in Drill Hole Wash, has a surface elevation of 1252 m and was drilled in 1993 to a total depth of 412 m. In May 1995 a 244 m borehole liner with monitoring ports at approximately 15 m intervals was installed (fig. 4.).

Figure 5a and b show barometric and downhole pressure records from NRG#5 from July 19 to August 2, 1995. These records are typical of the pressure data collected prior to the effects of ESF excavation in this borehole. Also shown on figures 5a and b are the results of cross-spectral analyses using pressure data from July 17 to August 17, 1995. Visual inspection of the data yields the following relations among monitoring zones.

Figure 5. a and b. near here.

Pressures from Zones 1 and 2, within the lower lithophysal and columnar units of the Tiva Canyon Tuff, almost exactly reflect the surface barometric pressure. This indicates that the permeabilities of the Tiva Canyon units through the columnar unit are sufficiently large that they offer no resistance to the downward propagation of the surface barometric signal. Pressures from Zone 3, within the Yucca Mountain Tuff unit, are substantially attenuated and lagged. The calculated residual amplitude is 61 percent of the barometric signal and the calculated phase lag is 12.2 hours as compared to 18 minutes for Zone 2. This indicates that one or more of the intervening units between the columnar unit and the Yucca Mountain Tuff have sufficiently low air permeability to impede the downward propagation of the barometric signal. Pressures from Zone 4, within the Pah Canyon Tuff, are further attenuated and lagged as reflected by the calculated residual amplitude of 38 percent and increased phase lag of 31.6 hours. Pressures from zone 5, in the pre-Pah Canyon bedded tuff, zones 6 and 7, in

the Topopah Spring upper nonlithophysal unit, and zones 8 and 9 in the Topopah Spring upper lithophysal unit, all exhibit similar responses to barometric changes at the surface. The residual amplitudes are calculated to be from 31 to 29 percent of the barometric signal and phase lags are calculated to be from 46.8 to 48.3 hours. Pressures from Zone 10, which is also in the upper lithophysal unit of the Topopah Spring Tuff, exhibit a much larger residual amplitude (39 percent) and shorter phase lag (37.7 hours) than any of the overlying zones within the Topopah Spring Tuff. The data from Zone 10 indicate that there is a pathway by which the surface barometric signal can bypass the overlying lithologic units and affect the downhole pressure at a depth of at least 227 m. The simplest explanation based on the proximity of NRG#5 to the Drill Hole Wash Fault, is that the fault has created a path by which barometric pressure can bypass the lower permeability units that cause most of the attenuation and lag. The fact that this effect does not occur in the overlying Topopah Spring Tuff stations implies that there is a zone of lower permeability separating the 227 m station from the overlying stations.

Borehole NRG-6 is located in Drill Hole Wash, has a surface elevation of 1248 m and was drilled in 1993 to a total depth of 335 m. In November 1994, this borehole was instrumented to monitor 8 zones. Figure 4 shows the lithologic log and location of monitoring stations used to collect pneumatic pressure data from borehole NRG-6.

Figure 6 shows barometric and downhole pressure records from NRG-6 from May 21 to June 4, 1995. These records are typical of the pressure data collected prior to the effects of ESF excavation in this borehole. Also shown on figure 6 are the results of cross-spectral analyses using pressure data from February 22 to August 12, 1995. Visual inspection of the data yields the following relations among monitoring zones.

Figure 6. Figure 6 near here.

Pressures responses at the upper station (G), in the Tiva Canyon columnar unit, are much more attenuated than those in the columnar unit at NRG#5. The calculated residual amplitude is 56 percent and the phase lag is 1.8 hours. Data from other boreholes indicate that the overlying Tiva Canyon lower lithophysal and hackly units have sufficient permeability that the surface barometric signal is not attenuated. One plausible explanation for the observed attenuation at NRG-6 is that the attenuation is caused by localized transient infiltration associated with unusually high precipitation during late 1994 and early 1995. The downward propagation of the barometric signal relies on the air filled porosity of the formation material. High saturation associated with infiltration pulses could act as a temporary impediment to the pressure signal by reducing the pore space available to transmit the pressure wave. The effect of this transient infiltration is not readily apparent in the pressure records from other monitored boreholes. Pressures from station F, in the Pah Canyon Tuff, are further attenuated (calculated residual amplitude of 36 percent) and the phase lag is increased to 31.5 hours. This is almost identical to the results obtained at borehole NRG#5 and also indicates the presence of low permeability units at the base of the Tiva Canyon Tuff and within the bedded units. Stations E through A (Topopah Spring upper nonlithophysal through middle nonlithophysal) have residual amplitudes of 29 and 30 percent with phase lags between 42 and 44 hours. This is similar to the results described for borehole NRG#5.

Borehole NRG-7a is located in Drill Hole Wash, has a surface elevation of 1283 m and was drilled in 1994 to a total depth of 461 m. In October 1994, this borehole was instrumented to monitor 5 zones. Figure 4 shows the lithologic log and location of monitoring stations used to collect pneumatic pressure data from borehole NRG-7a.

Figure 7 shows barometric and downhole pressure records from NRG-7a from August 1 to August 15, 1995. These records are typical of the pressure data collected prior to the effects of ESF excavation in this borehole. Also shown on figure 7 are the results of cross-spectral analyses using

pressure data from January 25 to October 8, 1995. Visual inspection of the data yields the following relations among monitoring zones.

Figure 7. Figure 7 near here.

Pressures at station E (in the Tiva Canyon hackly unit) reflect the barometric signal with no attenuation and a short lag time calculated to be 30 minutes. Pressures at station D, within the Yucca Mountain Tuff, have a calculated residual amplitude of 80 percent and a phase lag of 15.9 hours. This residual amplitude is larger than that of NRG#5 and may indicate a higher permeability in the Tiva Canyon crystal-poor vitric zone at NRG-7a. Pressures from stations A, B, and C, within the Topopah Spring upper nonlithophysal and upper lithophysal units, are greatly attenuated and lagged as evident from calculated residual amplitudes of only 13 and 12 percent and phase lags of more than 60 hours. This magnitude of attenuation and lag is larger than that seen at either NRG#5 or NRG-6 and is likely a reflection of one or more low permeability units in the lower part of the Paintbrush Tuff nonwelded unit.

Pagany Wash Boreholes

Borehole UZ#4 is located in Pagany Wash, has a surface elevation of 1200 m and was drilled in 1994 to a total depth of 112 m. In July 1995, this borehole was instrumented to monitor 8 zones. Figure 4 shows the lithologic log and location of monitoring stations used to collect pneumatic pressure data from borehole UZ#4.

Figure 8 shows barometric and downhole pressure records from UZ#4 from July 17 to July 31, 1995. These records are typical of the pressure data collected prior to the effects of ESF excavation in this borehole. Also shown on figure 8 are the results of cross-spectral analyses using pressure data from July 21 to July 31, 1995. This data set is very short because the onset of ESF effects occurred shortly

after this borehole was instrumented. Visual inspection of the data yields the following relations among monitoring zones.

Figure 8. Figure 8 near here.

Shallow stations H and G, within alluvium and the Tiva Canyon crystal-poor vitric zone, show similar responses to the surface barometric signal. Pressures from these stations are somewhat attenuated and lagged, but perhaps because of the short period of record cross-spectral analysis fails to compute residual amplitudes or phase lags for these stations. The record indicates that most of the attenuation occurs below the crystal-poor vitric unit. Pressures from stations F through A, within various Paintbrush Tuff nonwelded units through the upper non-lithophysal unit of the Topopah Spring Tuff, all exhibit largely attenuated and lagged responses. Residual amplitudes range from 15 to 21 percent and the phase lags are calculated to be from 15.9 to 26.5 hours.

Borehole UZ#5 is located in Pagany Wash, has a surface elevation of 1204 m and was drilled in 1994 to a total depth of 111 m. In June 1995, this borehole was instrumented to monitor 8 zones. Figure 4 shows the lithologic log and location of monitoring stations used to collect pneumatic pressure data from borehole UZ#5.

Figure 9 shows barometric and downhole pressure records from UZ#5 from July 10 to July 24, 1995. These records are typical of the pressure data collected prior to the effects of ESF excavation in this borehole. Also shown on figure 9 are the results of cross-spectral analyses using pressure data from June 30 to July 27, 1995. This data set is very short because the onset of ESF effects occurred shortly after this borehole was instrumented. Visual inspection of the data yields the following relations among monitoring zones.

Figure 9. Figure 9 near here.

The record from UZ#5 is similar to that from UZ#4. Most of the attenuation and lag occur across the Tiva Canyon crystal-poor vitric unit. Residual amplitudes from stations F through A, within various Paintbrush Tuff nonwelded units through the upper nonlithophysal unit of the Topopah Spring Tuff, range from 14 to 19 percent and phase lags range from 10.9 to 21.2 hours.

Main Drift Boreholes

Borehole SD-12 is located in WT-2 Wash, has a surface elevation of 1324 m and was drilled in 1994 to a total depth of 701 m. In December 1995, this borehole was instrumented to monitor 16 zones. Figure 4 shows the lithologic log and location of monitoring stations used to collect pneumatic pressure data from borehole SD-12.

Figure 10 shows barometric and downhole pressure records from SD-12 from January 16 to January 30, 1996. These records are typical of the pressure data collected prior to the effects of ESF excavation in this borehole. Also shown on figure 10 are the results of cross-spectral analyses using pressure data from November 28, 1995 to January 20, 1996. Visual inspection of the data yields the following relations among monitoring zones.

Figure 10. Figure 10 near here.

Pressures from stations P through M, within various units of the Tiva Canyon Tuff, all exhibit residual amplitudes greater than 96 percent of the surface barometric signal and phase lags shorter than 18 minutes, which is consistent with other boreholes showing that the Tiva Canyon Tuff is highly permeable to air. Pressures from station L, within the pre-Pah Canyon bedded tuff, are attenuated (69 percent residual amplitude) and lagged (7.4 hour phase lag) indicating the lower permeability of the overlying bedded and nonwelded units. Pressures from stations K through D, within the Topopah Spring Tuff from the upper nonlithophysal unit through the upper part of the lower nonlithophysal unit,

are further attenuated (residual amplitudes from 50 to 52 percent) and lagged (28 to 29.7 hour phase lags) indicating that the signal is impeded through the Crystal-rich vitric zone at the top of the Topopah Spring Tuff. Pressures from station C, within the lower nonlithophysal unit of the Topopah Spring Tuff, exhibit a larger residual amplitude (57 percent) and shorter phase lag (18.8 hours) than those from the overlying stations. This relation is similar to that of NRG#5 which is attributed to effects from the Drill Hole Wash Fault. In borehole SD-12 these effects can be attributed to the presence of the Ghost Dance Fault, which likely provides a downward path for the barometric pressure signal that then propagates horizontally to effect the lower station ad SD-12. Analogous to NRG#5, the fact that this fault effect is not propagated uniformly throughout the Topopah Spring Tuff stations must imply the presence of a less permeable zone between station C and the overlying stations. The lower most stations in borehole SD-12 (A and B) are located in the Crystal-poor vitric zone at the base of the Topopah Spring Tuff and within the Calico Hills Formation. During the drilling of this borehole it was noted by on-site observers that the core from the crystal poor vitric zone was wet. In several boreholes in the vicinity of Yucca Mountain, perched water occurs at or near the base of the Topopah Spring Tuff (Patterson, 1996). It is likely that this unit in borehole SD-12 is also at or near saturation. The pressure record at both stations within and below the crystal poor vitric zone indicates that essentially all of the synoptic barometric signal is attenuated. This is consistent with the idea of the presence of a perched water zone or nearly saturated zone that would effectively bar the downward propagation of the surface barometric signal.

Borehole UZ-7a is located in WT-2 Wash, has a surface elevation of 1293 m and was drilled in 1995 to a total depth of 235 m. This borehole is unique in that it was drilled through the Ghost Dance Fault zone such that all lithologic units are within the fault. In October 1995, this borehole was instrumented to monitor 10 zones. Figure 4 shows the lithologic log and location of monitoring stations used to collect pneumatic pressure data from borehole UZ-7a.

Figure 11 shows barometric and downhole pressure record from UZ-7a from November 11 to November 25, 1995. These records are typical of the pressure data collected prior to the effects of ESF

excavation in this borehole. Also shown on figure 11 are the results of cross-spectral analyses using pressure data from October 23 to December 15, 1995. Visual inspection of the data yields the following relations among monitoring zones.

Figure 11. Figure 11 near here.

Pressures from stations J through G, within the lower lithophysal, columnar, and crystal-poor vitric units of the Tiva Canyon Tuff, plot similarly to the barometer with little attenuation. Residual amplitudes range from 96 to 100 percent and the phase lags range from 0.5 to 2.5 hours. The increase in phase lag from 0.9 hours in the columnar unit to 2.5 hours in the crystal-poor vitric unit may indicate a slightly smaller permeability in the crystal-poor vitric unit, but the large residual amplitude is inconsistent the presence of a significant impediment to flow. Pressures from stations F through D, within the pre-Pah Canyon bedded tuff, Topopah Spring crystal-rich vitric unit, and Topopah Spring upper lithophysal unit, plot similarly and display smaller residual amplitudes (73 to 79 percent) and longer phase lags (5.2-6.0 hours). This is consistent with other boreholes that indicate lower permeabilities of nonwelded and bedded units of the Paintbrush Tuff. The magnitude of the attenuation in this borehole is smaller because the impeding layers have been altered by movement along the fault although they retain some of the characteristics that cause lower permeabilities than the fractured welded units. Pressures from stations C through A, within the upper lithophysal, middle nonlithophysal, and lower lithophysal units of the Topopah Spring Tuff, also plot similarly, with residual amplitudes from 54 to 57 percent and phase lags from 14.5 to 16.0 hours. These residual amplitudes are larger than those seen in the Topopah Spring Tuff in Drill Hole Wash and are due to downward propagation of the barometric pressure through the fault zone.

Borehole SD-7 is located on Highway Ridge, has a surface elevation of 1363 m and was drilled in 1995 to a total depth of 816 m. During drilling, perched water was encountered at a depth of about 480 m within the bedded tuffs at the base of the Calico Hills Formation, just above the contact with the

Prow Pass Tuff. In April 1996, a 244 m long borehole liner with monitoring ports at 15 m intervals was installed. Figure 4 shows the lithologic log and location of monitoring ports used to collect pneumatic pressure data from borehole SD-7.

Figure 12 shows barometric and downhole pressure record from SD-7 from April 30 to May 14, 1996. These records are typical of the pressure data collected prior to the effects of ESF excavation in this borehole. Also shown on figure 12 are the results of cross-spectral analyses using pressure data from April 4 to May 17, 1996. Visual inspection of the data yields the following relations among monitoring ports.

Figure 12. Figure 12 near here.

Zone 1 in the Tiva Canyon Tuff, crystal poor vitric unit responds almost instantaneously to barometric pressure changes with little attenuation of the surface signal. Cross-spectral analysis calculates a residual amplitude of 98 percent and a phase lag of about 12 minutes. Zone 2, in the Pre-Tiva Canyon Tuff bedded tuff is somewhat more attenuated and lagged with a residual amplitude calculated to be 88 percent and a phase lag of 3.1 hours. Zone 3, which is located at the contact between the crystal-rich vitric unit and the upper nonlithophysal unit of the Topopah Spring Tuff is significantly more attenuated and lagged than the upper zones with a calculated residual amplitude of 55 percent and a phase lag of 21.7 hours. All of the remaining zones (within various units of the Topopah Spring Tuff) plot essentially together and have calculated residual amplitudes of 56 percent and phase lags between 23.4 and 23.9 hours.

These data indicate that the Tiva Canyon Tuff units above the bedded tuff unit have large permeabilities and provide little impediment to downward propagation of the barometric signal. The primary impediment to downhole propagation of the surface barometric signal occurs near the top of the Crystal rich vitric zone of the Topopah Spring Tuff. Also evident from these data is that the vertical

permeability of the Topopah Spring Tuff units must be large to allow instantaneous equilibration of the downhole pressures throughout the monitored intervals.

Synthesis of Subsurface Pressure Measurement

The computed phase lags and residual amplitudes of the *in situ* pressure data indicate that individual lithostratigraphic units can be conveniently grouped into four distinct pneumatic systems: 1) the Tiva Canyon welded tuffs; 2) the Paintbrush Group nonwelded units that include the crystal-poor vitric base of the Tiva Canyon Tuff, the Yucca Mountain and Pah Canyon Tuffs (with associated bedded tuffs), and the crystal-rich top of the Topopah Spring Tuff; 3) the Topopah Spring lithophysal and nonlithophysal welded units; and 4) the pre-Topopah Spring bedded tuff, the nonwelded tuffs of the Calico Hills Formation, and the pre-Calico Hills Formation bedded tuff. This grouping conforms to the definition of the major hydrogeologic units presented in Figure 2. The general responses observed in each of these pneumatic units to the propagation of atmospheric pressure changes from land surface to depth are discussed in the sections that follow.

Tiva Canyon Welded Unit

For the most part, pneumatic pressure records for the Tiva Canyon welded unit display very little attenuation and lagging of the synoptic pressure signal (figures 5 through 12). The only significant exception is the pneumatic pressure record from station G, located at the base of the Tiva Canyon columnar unit at NRG-6. Figure 6 indicates that the residual amplitude of the pressure signal at this instrument station is only 56 percent of the synoptic signal, and that its phase lag is on the order of 9.6 hours. These spectral parameters are significantly different from those of other pressure records from the Tiva Canyon monitoring stations. The residual amplitudes of the synoptic signal from all other monitoring stations in the Tiva Canyon welded unit are on the order of 96 percent or greater, and phase lags in these stations are less than 3 hours. Temporary pneumatic sealing of near-surface fractures and

shallow soil cover by localized infiltrating water seems to be a plausible explanation for the small residual amplitudes in the Tiva Canyon at borehole NRG-6. This explanation is also consistent with the occurrence of unusually high precipitation during late 1994 and early 1995. Spectral analysis of earlier data from station G, beginning in February of 1995 indicate that the residual amplitude was only 43 percent with a phase lag of 9.6 hours (reference NRH). Both of these analyses are for data collected prior to the effects of ESF excavation, thus the increasing residual amplitude and decreasing phase lag are likely the result of drying out of the surface materials following the transient infiltration events. It is likely that transient infiltration occurred at other boreholes but the effects are not readily apparent in the pneumatic records.

Paintbrush Group Nonwelded Unit

The Paintbrush Group nonwelded unit (PTn) includes the crystal-poor vitric zones (Tpcpv1,2) at the base of the Tiva Canyon, the crystal-rich vitric zones (Tptrv2,3) at the top of the Topopah Spring Tuff, as well as the intervening Yucca Mountain, Pah Canyon, and associated bedded tuffs. Across the study area the Paintbrush Group nonwelded unit becomes thinner from north to south and in the monitored boreholes this unit is thickest at UZ#4 (84 m) and thinnest at UZ-7a (24 m).

Pneumatic pressure records from monitoring stations located immediately above and below the Paintbrush Group nonwelded unit (figures 5 through 12), indicate that the residual amplitude and phase lag of the synoptic pressure signal across the PTn are larger at boreholes SD-7, SD-12, and UZ-7a in the southern portion of the study area and are smallest in boreholes NRG-7a, UZ#4, and UZ#5.

Examination of the pneumatic pressure data from instrument stations located within and across various subunits of the PTn indicates that the pressure attenuating and lagging characteristics of these subunits are different from one location to another, and that the composite thickness of the PTn is insufficient to uniquely account for differences in the magnitude of the residual amplitude and phase lag of the synoptic pressure signal transmitted across this unit as discussed below.

At NRG-7a only one instrument station is located within the PTn. Instrument station D (figure 7) is located in a bedded unit above the Pah Canyon Tuff, approximately midway between the top of the crystal-rich, densely welded vitric zone of the Topopah Spring Tuff and the bottom of the crystal-poor, densely welded vitric zone of the Tiva Canyon Tuff. The decrease in the residual amplitude of the synoptic pressure signal across the upper 30 m of the PTn is approximately 20% (80% residual amplitude at instrument station D). At instrument station C, located in the upper nonlithophysal subunit of the Topopah Spring Tuff, the residual amplitude is only about 13% - a decrease of 67% across the lower 39 m of the PTn. At NRG-7a, most of the decay in the synoptic pressure signal occurs across the lower half of the PTn section. With only one instrument station in the PTn at NRG-7a, finer discrimination of the attenuating characteristics of individual subunits is not possible.

At NRG#5 (figure 5a) most of the attenuation of the synoptic signal occurs across the Yucca Mountain Tuff, between instrument stations 2 and 3 (38% reduction in the residual amplitude) and across the upper Pah Canyon Tuff and bedded tuff subunits between instrument stations 3 and 4 (23% reduction in the residual amplitude). Very little signal attenuation, if any, is associated with the relatively thick (5.5 m), crystal-rich vitric zone at the base of the PTn. The upper 30 m of the PTn at NRG#5 accounts for approximately 61%, and the lower 27 m accounts for only about 8% of the total synoptic signal attenuation across the PTn.

Attenuation of the synoptic pressure signal across the composite PTn at NRG-6 is minimal in comparison to other monitored boreholes. Most of the synoptic signal attenuation in this borehole (figure 6) appears to occur across the Tiva Canyon section (43% residual at instrument station G located at the base of the Tiva canyon columnar subunit). (See also the discussion of possible transient infiltration effects discussed above). Between instrument stations F and G, a distance of 15 m, the residual amplitude of the synoptic signal is reduced by about 20%. These instrument stations bound the crystal-poor vitric zone of the Tiva Canyon Tuff and the PTn, and a bedded tuff unit of the PTn. The change in residual amplitude is only about 7% between instrument stations E and F that bound an 26-

meter section of the Pah Canyon and crystal-rich vitric zone of the PTn and Topopah Spring Tuff. Station E straddles the contact between the crystal-rich vitric zone of the PTn and the upper nonlithophysal subunit of the Topopah Spring. The video log and fracture density log of NRG-6 (Rousseau and Patterson, 1996) indicate intense fracturing across this contact, with individual fracture openings that are several inches across. The lack of significant signal attenuation across the PTn at NRG-6 may be more a reflection of the effects of localized fracturing (faulting?) than a reflection of the relative thinness of the PTn at this location.

Instrument stations at UZ#4 and UZ#5 were positioned to examine the pneumatic characteristics of individual subunits within the PTn. Amongst the monitored boreholes, the thickness of the PTn is greatest at UZ#4 and UZ#5. Instrument stations in both of these boreholes bound the three PTn bedded units with instrument stations that are located at the top and bottom of the Yucca Mountain Tuff and the Pah Canyon Tuff (figure 4). Instrument stations are also located in the crystal-poor vitric and crystal-rich vitric zones of the PTn. The total attenuation of the synoptic pressure signal (residual amplitude equal to 16% and 14%) across the PTn is almost identical at both UZ#4 and UZ#5. Most of signal attenuation occurs across the crystal-poor vitric zone (79% and 81% reduction in the surface amplitude). Minimal attenuation occurs across the crystal-rich vitric zone and the other bedded and nonwelded tuffs of the PTn.

In boreholes SD-12 and SD-7, the PTn is relatively thin and the associated total signal attenuation through the PTn is smaller than at other boreholes (50% and 56% respectively). The assumption that the higher residual amplitudes in the Topopah Spring Tuff units is merely due to the thin PTn at these boreholes may not be valid. In borehole SD-12, effects of the nearby Ghost Dance Fault are apparent in station C (373 m depth) and residual amplitudes decrease upward from the bottom such that the larger residual amplitudes could be the result of the Ghost Dance Fault providing a pathway for the barometric signal to bypass the impeding layers of the PTn. The situation is not as readily apparent in the record from borehole SD-7. Although the residual amplitudes in the Topopah Spring units are larger than in

the crystal-rich vitric unit, there is no change in residual amplitude through the Topopah Spring units from bottom to top and the difference between 56% and 55% is within the error of the cross-spectral analysis.

Pneumatic pressure data from monitoring stations within the PTn and from monitoring stations located above and below this unit indicate that the pneumatic characteristics of the individual subunits are quite different from one location to another. The total thickness of the PTn alone is not sufficient to account for the total residual amplitude and phase lag of the synoptic pressure signal seen in the upper nonlithophysal subunit of the Topopah Spring Tuffs. Differences in the pneumatic diffusivities of individual subunits within the PTn are obviously present. These differences are more than likely a reflection of local differences in the saturation of individual subunits and/or a reflection of the presence or absence of open fractures within these subunits, especially at UZ#4 and UZ#5. In the absence of localized fracturing, the very low matrix porosities of the crystal-rich vitric and crystal-poor vitric zones render the pneumatic permeabilities of these units particularly sensitive to small changes in moisture content. Locally the pneumatic characteristics of the crystal-rich vitric zone appear to be dominated by fracturing. This is especially true at NRG-6, UZ#4 and UZ#5 (Rousseau and Patterson, 1996).

Topopah Spring Lithophysal and Nonlithophysal Welded Tuffs

Pressure data from instrument stations located in the Topopah Spring lithophysal and nonlithophysal welded tuffs exhibit negligible attenuation and lagging of the pneumatic pressure signals transmitted across the crystal-rich vitric zone of the Paintbrush Group nonwelded units (figures 5 through 12). Pressure signals appear to be transmitted nearly instantaneously throughout the entire Topopah Spring Tuff section. Pressure data from nearly all the Topopah Spring Tuff instrument stations indicate that the fractures within the Topopah Spring Tuff are apparently very permeable and highly interconnected within both the lithophysal and nonlithophysal subunits.

The only boreholes to display any significant variation in pneumatic pressures within the Topopah Spring welded units are NRG#5 (fig. 5b) and SD-12 (fig.10). The residual amplitude of the pneumatic pressures from instrument station 10 (figure 5) in borehole NRG#5, is 39 percent, while the residual amplitude of station 9 is only 29 percent. There is also a reduction in the phase lag between these stations of about 10 hours. This relation can be explained by invoking a nearby breach in the attenuating ability of the PTn such that the barometric pressure signal can bypass the PTn and affect the downhole pressure at a depth of 227 m. The most likely cause of the breach in the PTn in the vicinity of borehole NRG#5 is the Drill Hole Wash Fault. A similar situation exists in borehole SD-12 where station C exhibits a larger residual amplitude and smaller phase lag than the overlying stations. In this borehole, the likely pathway for the pneumatic signal is through the Ghost Dance Fault.

Pressures within the Topopah Spring Tuff at boreholes SD-12 and SD-7 all exhibit similar residual amplitudes and phase lags and the residual amplitudes are large when compared to those of other boreholes. Both of these boreholes are within about 230 m of the Ghost Dance Fault (fig. 3) and as discussed above, the higher pressures within the Topopah Spring Tuff at these boreholes may be the result of downward propagation of the surface signal along the Ghost Dance Fault followed by lateral propagation to the borehole once the impeding layers of the PTn have been breached.

Pressures Monitored Below Perched Water

Pressures at boreholes SD-9 and SD-7 were monitored from inside the annular space of nested casings that were open between the bottom of a perched water zone and the top of the water table (fig 13). In borehole SD-12, station A lies within the Calico Hills Formation and station B lies within the crystal-poor vitric unit at the base of the Topopah Spring Tuff (fig.4). At borehole SD-9 perched water was encountered during drilling near the base of the Topopah Spring Tuff and at borehole SD-7 perched water was encountered during drilling near the base of the Calico Hills Formation (Patterson, 1996). During the drilling of borehole SD-12 it was noted by on-site observers that the core from the crystal-

poor vitric zone at the base of the Topopah Spring Tuff was wet (Rousseau, oral communication, 1996). Figure 14 shows pressure records measured below the perched water zones in all three boreholes. The pressure records at all three boreholes indicate that essentially all of the synoptic barometric signal is attenuated. This is consistent with the idea of the presence of a perched-water zone or highly saturated zone that would have extremely low permeability to air and would effectively bar the downward propagation of the surface barometric signal. The small fluctuations seen in the record would likely be the result of horizontal propagation of the barometric signal from outside the margin of the perched water reservoir.

Figure 13. Figure 13 near here.

Figure 14. Figure 14 near here.

One-Dimensional Analyses of Permeability Using AIRK

The AIRK program (Weeks, 1978) is a code for determining the vertical permeability to air of a sequence of sedimentary beds, based on the simulation of pressure fluctuations at depth in response to atmospheric pressure changes at land surface. As for the ground-water flow codes discussed later, AIRK was formulated assuming an immobile liquid phase, and pressure responses at depth were assumed to respond linearly to pressure changes at land surface, in effect assuming that air is a slightly compressible fluid. As shown by Weeks (1978), the latter assumption is valid so long as pressure variations are no greater than 10% of their mean value.

Use of AIRK (and of the ground-water flow codes described below) to simulate air flow through fractured porous media are subject to a number of limitations. One limitation is that the fractured medium must be sufficiently fractured that it may be considered an equivalent porous medium at the scale of the model. Based on monitoring results in various boreholes prior to the time when ESF effects are apparent indicate that pressure responses in some, but not all, of the wells behave as would be expected in a uniform porous medium—that is, pressure responses decrease monotonically with depth. Wells NRG-5 and SD-12 show distinctly larger response below a certain depth in the Topopah Spring Tuff that is not compatible with a one-dimensional model. Thus, application of these models is somewhat suspect as applied to monitoring results from those wells.

Use of a porous-media-based model to simulate highly fractured porous media is also complicated the fact that flow and transport are affected by permeability and porosity effects at two very different scales. The fracture network consists of relatively few, large-aperture “pores” that have large

permeability and small storage. The matrix blocks include many small pores that have low permeability (many orders of magnitude less than the fracture network), but significantly greater storage. These media are characterized as having “double-porosity”, in which flow and transport are affected at different time scales. Adequacy of a single-porosity model to simulate flow in such media is dependent on the time scale of the simulation. If pressures in the matrix blocks equilibrate with those in the fracture network more quickly than the time period of simulation interest, the medium may be treated as a single-porosity medium, with the effective porosity being that of the matrix blocks and the permeability that of the fracture network. The time required for pressure equilibration between matrix and fractures may be estimated from the theoretical time that a block of matrix material of assumed ideal shape would require to equilibrate with a step change in pressure over its surface. Carslaw and Jaeger (1959, fig. 12) provide graphs of average pressure potential in a slab, a cylinder, and a sphere following such an instantaneous pressure change at the medium surface that indicates near-equilibrium for any of the three solids for values of the dimensionless parameter $\frac{kPt}{\mu l^2 \phi_a}$ of about 0.2-0.8, depending on the block shape. For this parameter, k is intrinsic permeability, m^2 , P is mean pressure in Pa, t is time in seconds, μ is air viscosity in Pa-s, l is the radius or half thickness, m, and ϕ_a is drained porosity. Based on a midpoint value between the blocks being spheres and being semiinfinite slabs, or a value of the dimensionless parameter of 0.5, pressures in the matrix blocks and in the fracture network should equilibrate after $t > \frac{0.5\mu l^2 \phi_a}{kP}$, and simulations involving larger time scales presumably could be reliably made without concern for double-porosity effects.

Many determinations of the matrix permeability for cores taken from the Topopah Spring Tuff indicate values in the range of $1-10 \times 10^{-6} \mu m^2$. Assuming that the geometric mean of these values, $k = 3 \times 10^{-18} m^2$, is appropriate, and further assuming $l = 0.3$ m, $\phi_a = 0.05$, mean pressure = 85,000 Pa, and $\mu = 1.8 \times 10^{-5}$ Pa-s, $t = 1.6 \times 10^5$ seconds, or about 2 days. Although this computation indicates that effects of double porosity should be observable in pressure data collected in response to diurnal atmospheric pressure fluctuations, the effects are not readily apparent, and simulations were made both using AIRK

and Modflowp assuming no double-porosity effects. Nonetheless, the above computations imply that model interpretations based on the single-porosity model should be used with caution.

The AIRK code numerically solves the one-dimensional partial differential equation for gas flow through porous media using the finite-difference method. Air flux measurements across land surface resulting from atmospheric pressure changes generally are not available, and AIRK uses only pressure potentials in its simulations. Pressure distribution with depth is thus governed by the lumped parameter, pneumatic diffusivity:

$$D_p = \frac{k k_{ra} P}{\mu_a \phi_a} \quad (1)$$

where

D_p is effective pneumatic diffusivity, [$L^2 T^{-1}$];

k is intrinsic permeability, [L^2];

k_{ra} is the relative permeability of the medium to air at the prevailing moisture content, [L^0];

P is mean pressure during the observation period, [$ML^{-1} T^{-2}$];

μ_a is the absolute viscosity of air at the prevailing temperature, [$ML^{-1} T^{-1}$]; and

ϕ_a is the interconnected air-filled porosity at the prevailing moisture content, [L^0].

The code uses face-centered nodes to represent blocks of material that are conveniently divided into layers of different permeability to air, as determined by screen locations. The advantage of the face-centered nodes is that the specified pressure is at the node face and vertical layer boundaries are readily specified. The bottom layer (layer 1) is designated as extending from the base of the model to the position of the second sampling port from the model base (screen 2), and each additional sampling port becomes a layer boundary, with the upper boundary of the top layer being at land surface. The base of the model is assumed to be impermeable, and the top of the uppermost active layer is a specified pressure boundary, with the pressure updated each time step to that given by the user.

Initial conditions are defined by interpolating pressures given for each screen for the start of the simulation. The base of the model is specified as a no-flow boundary, and the pressure gradient should always be zero at that location. This is accomplished in the code by assuming that the pressure profile with depth in the bottom layer may be represented by a sine curve segment extending from $z=0$ at screen 2 to $z=\pi/2$ at the base of the model. The amplitude of the sine curve is determined by fitting the sine curve through the pressure difference between screen 1 (the bottom screen) and screen 2, and pressures at each node in layer 1 are interpolated along the resultant sine curve and algebraically added to the pressure specified for screen 2. Interpolation is linear for all upper screens.

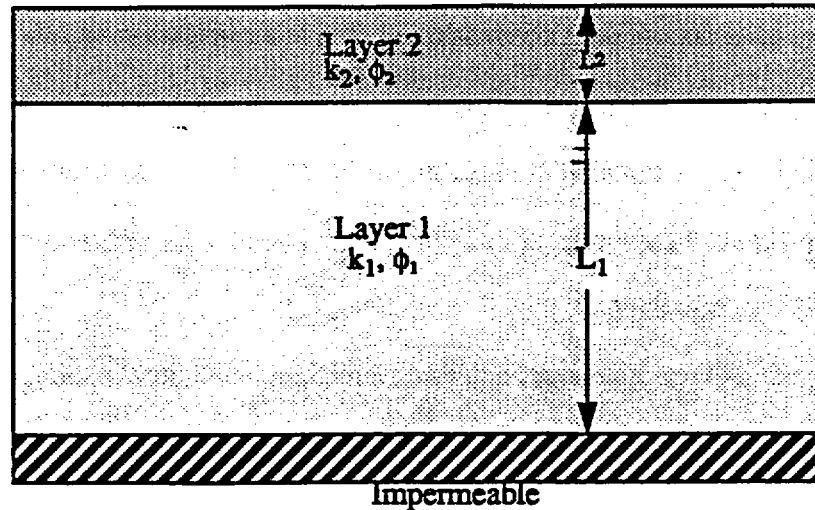
In using AIRK, the permeability of layer 1 is determined first, based on its specified airfilled porosity to allow diffusivity to be specified. Pressures are simulated for the position of the bottom screen, based on pressures at the position of screen 2 (the top of the layer) being specified as those measured each time step. The permeability is varied through an automatic search procedure until the sum-of-square (SOS) difference between measured and simulated pressures is minimized. At this point nodes representing layer 2 are added to the model, retaining those representing layer 1, and the specified pressure boundary becomes that measured in screen 3 (the top of layer 2). Permeability of layer 2 is varied until the SOS difference is minimized between the measured and simulated pressures for screen 2. This process is continued until all layers have been added, with atmospheric pressure being that specified for the top of the model.

The AIRK program was originally formulated to determine the vertical permeability to air of layered sequences of sedimentary materials, based on installations designed to provide pressure sampling ports at layer boundaries. In that work, the deepest unsaturated zones field tested were less than 100 m thick, and responses varied significantly with depth on a daily basis, allowing analysis of relatively short term data. At Yucca Mountain, the unsaturated zone is a few hundred meters thick, and consists of a highly permeable fractured rock aquifer, the Topopah Spring Tuff, overlain by the much less permeable PTn, and that unit is overlain by the even more permeable Tiva Canyon Tuff, as

discussed above. The resultant pressure responses include very small pressure differences between atmosphere and the base of the Tiva Canyon Tuff (so small that reliable permeability values are difficult to obtain). Quite substantial pressure differences do occur across the PTn, and the permeabilities identified from these records should be reliable, so long as the boundary condition resulting from the presence of the Topopah Spring Tuff is adequately represented, as described below. Because the Topopah Spring Tuff is much more permeable than the PTn, pressure potentials resulting from atmospheric pressure changes vary so little with depth in the unit that only minimum values of permeability can be estimated.

Because of these large differences between hydrologic conditions at Yucca Mountain and those for which AIRK was developed and previously applied, sensitivity tests of the program were made, with particular regard to estimating an effective average permeability of the full thickness of the PTn from the amplitude of the pressure response in the Topopah Spring Tuff. For these tests, the system was considered to consist of a highly permeable lower layer and a substantially less permeable upper layer, as shown schematically below.

Land Surface



For the base case simulations, conditions typical of Yucca Mountain were assumed, including a thickness of the Topopah Spring Tuff (L_1) of 330 m and of the PTn (L_2) of 55 m. Airfilled porosities of the Topopah Spring Tuff (ϕ_1) and PTn (ϕ_2) are assumed equal to 0.04 and 0.2, respectively. Base case permeabilities are $k_1=30 \mu\text{m}^2$ and $k_2=0.5 \mu\text{m}^2$. Pressure at land surface is represented as a sine function of variable period τ , unit (1 kPa) amplitude and zero phase lag. Either five or ten cycles were simulated, based on dividing each cycle into 32 equally spaced time steps to ensure that cyclic steady-state conditions were obtained. The period was varied using the time step size to represent τ varying from 1 to 7.1 days.

Measurements at various monitoring and flexible-liner boreholes indicate that residual amplitude (RA), the ratio of the amplitude at depth to that at land surface, is nearly constant throughout the monitored interval of the Topopah Spring Tuff. It was hypothesized that RA depends mainly on L_2 , k_2 , τ , and ϕ_2 , and simulations were made systematically varying τ and ϕ_2 to determine their relative effects. Results of these simulations are summarized in table 1.

Table 1. Sensitivity of Topopah Spring residual amplitude to variations in t and k_2

$k_2\tau$, $\mu\text{m}^2\text{-days}$	Topopah Spring Tuff Residual Amplitude	
	$\tau = 7.11$ days k_2 varied	$k_2 = 0.5 \mu\text{m}^2$ τ varied
0.71	0.028	0.031
1.07	.0524	.0550
1.42	.078	.080
2.84	.175	.175
3.55	.221	.221

Amplitudes vary somewhat for small $k_2\tau$ values depending on whether k_2 or τ is varied, but values are constant for larger values. For amplitudes large enough to be reliably determined, it appears adequate to say that the amplitude is proportional to $k_2\tau$. The base case is shown in bold type.

Sensitivity of the amplitude ratio and presumably the PTn permeability to variations in the permeability of the Topopah Spring Tuff, k_1 , was also determined, along with determining the amplitude at depth within the Topopah Spring Tuff at a depth of 300 m, by varying only k_1 in the base case., as shown in table 2.

Table 2. Sensitivity of Topopah Spring residual amplitude to variations in k_1

$k_1, \mu\text{m}^2$	Topopah Spring Tuff Residual Amplitude	
	At PTn Contact	At 300 m Depth
5	0.242	0.192
10	.225	.221
20	.221	.214
30	.221	.215
60	.221	.218

These simulations show that the amplitude is significantly affected if k_1 is only 10 times as large as the base case value of $0.5 \mu\text{m}^2$ for k_2 , but amplitudes at depth in the Topopah Spring Tuff are

attenuated as well. For k_1 greater than about $20 \mu\text{m}^2$, or 40 times k_2 , all determinations of PTn permeability are essentially independent of the value of k_1 . Thus, measurements indicating that amplitude did not vary with depth in the Topopah Spring Tuff indicate that, for a PTn permeability of $0.5 \mu\text{m}^2$, the vertical permeability of the Topopah Spring Tuff is at least $20 \mu\text{m}^2$, but cannot be quantitatively determined from the data. Separate sensitivity simulations (results not tabulated) indicate that, for a PTn permeability of $0.2 \mu\text{m}^2$, the permeability of the Topopah Spring Tuff must be on the order of 40 Darcies to avoid significant differences in residual amplitude with depth in that formation. Thus, the minimum permeability of the Topopah Spring Tuff that still prevents significant variations in residual amplitude with depth is somewhat sensitive to the magnitude of the permeability of the PTn. For the range of PTn permeabilities determined in this study, the lack of variation with depth of the residual amplitude of the Topopah Spring Tuff indicates that its permeability must be at least tens of μm^2 .

Conceptually, the air-filled porosity throughout the lower layer thickness provides a reservoir for air storage, and RA should vary with the $L_1\phi_1$ product, as shown in table 3.

Table 3. Sensitivity of Topopah Spring Tuff residual amplitudes to variations in the $L_1\phi_1$ product

$L_1\phi_1$ Product	Topopah Spring Residual Amplitude		
	6.6 m	13.2 m	26.4 m
$L_1=165$ m	0.337 ($\phi_1=.04$)	0.221 ($\phi_1=.08$)	0.129($\phi_1=.16$)
$L_1=330$ m	0.338 ($\phi_1=.02$)	0.221 ($\phi_1=.04$)	0.131 ($\phi_1=.08$)

Results of this analysis indicate that residual amplitudes for the PTn are significantly affected by the thickness—air-filled porosity product of the underlying highly permeable Topopah Spring Tuff member, and that the reliability of estimates of PTn permeability will be dependent on how closely that product can be estimated. Substantial data on total and water-filled porosity have been collected from many cores, and the effective air-filled porosity should be reasonably well determined as the difference between these values.

Pressure data collected at boreholes NRG#5, SD-7, and SD-9 prior to the effects of the TBM becoming apparent were analyzed using the AIRK program. Results need to be interpreted in light of the above sensitivity analyses— k 's only for the PTn are reliable, and then only if the Topopah Spring Tuff thickness—air-filled porosity is reliably estimated. PTn permeabilities computed using AIRK are also highly dependent on the assumed air-filled porosity for the PTn. Such data are available for only some of the boreholes for which determinations were made. Values used in the North Ramp Modflowp model, described below, were based on porosity and saturation data from cores taken at borehole NRG-6. The average value so determined is assumed for boreholes NRG#5, borehole SD-9, and borehole SD-7. Kwiklis (1996) used core data to obtain somewhat different air-filled porosity values for borehole NRG-7a, and an analysis is repeated using those values. In addition, because the Modflowp model uses a PTn ϕ of 0.34, a simulation was made using that value so that all results can be directly compared.

For boreholes NRG#5 and SD-7, pressure measurements are available for different depths in the Topopah Spring Tuff. Prior to the appearance of effects of a short circuit through the PTn provided by the ESF, the data for these different depths almost exactly coincide, indicating that the vertical permeability to air of the Topopah Spring Tuff is probably greater than $20 \mu\text{m}^2$. Although pressure data are not available for separate Topopah Spring Tuff depths in borehole SD-9, it was assumed that the unit is similarly permeable in that borehole. Consequently, for all three boreholes, the Topopah Spring Tuff was considered to consist of a single layer extending from the PTn contact to the Calico Hills Formation contact, which was considered an impermeable boundary. Similarly, data are available to discretize the Tiva Canyon Tuff in some of these boreholes, but that unit is also so permeable that the data are unreliable. Hence, the Tiva Canyon Tuff was also treated as consisting of a single layer extending from land surface to the top of the PTn.

Determination of air permeability for borehole NRG#5 was initially based on dividing the PTn into three layers, but the two layers from 40 to 74 m provided nearly identical permeability values, thus

the layers were combined for the final simulation. Data were available to determine the permeability of two layers of the PTn in borehole SD-7, and one layer in SD-9. Estimates of the permeability of the full thickness of the PTn as a single layer was also made for each borehole. Results of the determinations are presented in Table 4. Data for boreholes NRG-6 and NRG-7a, previously analyzed by Kwicklis (1996), were reanalyzed to provide permeability values for the lumped thickness of the PTn, both for values of Topopah Spring Tuff ϕ (0.06) used by Kwicklis and for $\bar{\phi}$ (0.043) used in the Modflowp model.

Table 4. Results of one dimensional air permeability analyses

Borehole and Date	Formation	Depth Interval	Permeability μm^2	Airfilled Porosity
NRG#5 07/11- 07/17/95	Topopah Spring	91-365	150	0.043
	Lower PTn	74-91	2.0	.34
	Upper PTn	40-74	0.7	.34
	Combined PTn	40-91	0.7	.34
	Tiva Canyon	0-40	3000	.04
SD-7 04/12- 04/23/95	Topopah Spring	122-452	30	.043
	Lower PTn	108-122	0.4	0.34
	Upper PTn	90-108	3.7	0.34
	Combined PTn	90-122	1.0	0.34
	Tiva Canyon	0-90	200	.04
SD-9 06/22- 07/12/96	Topopah Spring	66-420	30*	0.043
	PTn	0-66	0.4	.34
NRG-6 02/23- 03/17/95	Topopah Spring	85-395	500 (10-50)	.06
	Lower PTn	55-85	3 (2.1)	.38
	Upper PTn	40-55	0.6 (.45)	.28
	Combined PTn	40-85	1.	.34
	Combined PTn Topopah Spring Tuff $\phi=0.043$	40-85	0.9	.34
	Tiva Canyon	0-40	3 (3.1)	.16
NRG-7a	Topopah Spring	118-448	20 (10)	0.06
	PTn	47-448	0.7 (.65)	0.25
	PTn (Topopah Spring Tuff $\phi=0.043$)	47-448	0.6	0.34
	Tiva Canyon- PTn	0-47	1.0 (1.3)	0.12
* This is an assumed value, and was assigned to the Topopah Spring Tuff as a lower layer boundary condition for the SD-9 data simulation.				

Data for boreholes NRG#5, SD-7, and SD-9 were analyzed for other periods than those shown, and the PTn permeability values are similar for those analyses. Values computed for boreholes NRG-6

and NRG-7a are for a different period of record than that analyzed by Kwicklis, and differ somewhat in some cases from his values. His values are given in parentheses.

Some values for the Topopah Spring Tuff and Tiva Canyon Tuff are quite different than those shown by Kwicklis (1996), as the values listed here are those returned by the search procedure, whereas Kwicklis set them to be minimum plausible values. Kwicklis also used the rationale that the minimum plausible permeability was that at which simulated effects began to show departure ($10 \mu\text{m}^2$). The rationale for the sensitivity analyses described above was to select the minimum permeability for which the Topopah Spring Tuff measurements at depth did not show separation ($20 \mu\text{m}^2$). Permeability values of hundreds to thousands μm^2 , determined for either the Tiva Canyon Tuff or Topopah Spring Tuff, seem implausibly large, and may represent the effects of simulating "noise", or measurements that differ from each other for adjacent screens that are within the accuracy of the measurements. The lack of separation of the data with depth in the Topopah Spring Tuff does indicate that the permeabilities must be greater than $20 \mu\text{m}^2$ as a minimum. Thus, the results indicate that permeabilities of the Topopah Spring Tuff and Tiva Canyon Tuff are very large, with the exception of the one value determined for the Tiva Canyon Tuff at borehole NRG-6. However, the uppermost station at this borehole has not been included because the computed attenuation for the station is greater than 1. Thus, the lower lithophysal unit of the Tiva Canyon Tuff, outcropping at the borehole site, is very permeable. Possibly, the indicated low permeability for this station arises from the fact that the screened interval is in a block of relatively unfractured rock, and represents local conditions and the effect of scale on permeability determinations or may be a reflection of transient infiltration as discussed above.

EFFECTS OF EXCAVATION OF THE ESF ON *IN SITU* SUBSURFACE

PNEUMATIC-PRESSURE MEASUREMENTS

Pneumatic pressure interference effects associated with construction of the ESF have been observed in all monitored boreholes with the possible exception of UZ-7a. Borehole UZ-7a is drilled

within the fault plane of the Ghost Dance Fault and thus all zones exhibit a large response to the surface barometric signal which may effectively mask any possible effects of ESF excavation. The first occurrence of a pneumatic interference for each affected borehole in the study area is summarized in Table 5.

Table 5. Summary of the first occurrence of pneumatic interference effects from the ESF

Borehole	Date Event First Observed	Position of the TBM Referenced to ESF Stations (Distance from North Ramp Portal)	Horizontal Offset Distance to Affected Borehole, in feet (meters)	Lithostratigraphic Unit Exposed at the Face of the North Ramp Tunnel
NRG#4	06/16/95	10 + 68.3 (1,068.3 m)	82 (25)	pre-Pah Canyon Tuff (Tpb2)
UZ#4	08/12/95	12 + 61.8	1,361 (415)	Upper Nonlithophysal Topopah Spring (Tptm)
UZ#5	08/12/95	12 + 61.8	1,237 (377)	Upper Nonlithophysal Topopah Spring (Tptm)
NRG#5	09/14/95	16 + 56.3	305 (93)	Upper Nonlithophysal Topopah Spring (Tptm)
NRG-6	10/01/95	20 + 02.1	1,807 (551)	Upper Lithophysal Topopah Spring (Tptrl, Tptpul)
NRG-7a	10/21/95	23 + 46.8	85 (26)	Upper Lithophysal Topopah Spring (Tptrl, Tptpul)
SD-9	11/07/95	26 + 54.7	603 (184)	Middle Nonlithophysal Topopah Spring (Tptpmn)

Table 5. Summary of the first occurrence of pneumatic interference effects from the ESF

SD-12	03/23/96	46 + 23.0	161 (49)	Middle Nonlithophysal Topopah Spring (Tptpmn)
SD-7	06/05/96	55 + 98.0	348 (106)	Middle Nonlithophysal Topopah Spring (Tptpmn)

Detection of the first occurrence of a pneumatic disturbance effect may not coincide exactly in time with key excavation events in the North Ramp Tunnel (i.e. penetration of a fault, removal of a confining or pneumatic impeding layer, etc.)(Rousseau and Patterson,1996). Many of the recorded dates for pneumatic disturbance events, Table 5, appear in the pneumatic record several days after the actual construction event. The apparent lag effect can be attributed to two primary causes. First, changes in the frequency and amplitude of the synoptic pressure signal as registered downhole are used to determine when a tunnel disturbance effect has occurred. The wave length of this signal is on the order of 96+ hours, depending on the time of year (larger in the summer, shorter in the winter). To observe a change in *in situ* pressure using this signal requires at least a half wavelength of record (i.e. two days or more) before changes in the amplitude and frequency become apparent. Second, the rate of advance of the TBM tends to obscure detection of the first arrival of the pneumatic disturbance because theoretically this disturbance is initially propagated as a spherical wave front, a weak disturbance that decays as $1/r^3$ where r represents the radius of the tunnel. This disturbance gradually evolves into a cylindrical wave front, a stronger disturbance that decays as $1/r^2$, as the TBM advances closer and closer to the affected borehole. Obviously, if the TBM is advancing very rapidly the spherical or weak disturbance may not be readily discernible given the half wavelength delay time (2+ days) needed to confirm a change in the frequency and/or amplitude of the *in situ* pressure signal. There are many first occurrences that are recorded on a Sunday, 2 days following the Friday shut down of tunneling operations. Pressure disturbances that are clearly propagated along fault planes were detected in advance of actual fault penetration at UZ#4 and UZ#5, but only because the TBM was shut down for

ten days and did not actually penetrate the fault until eight days after tunneling operations were resumed. At NRG-6 the pneumatic disturbance was not observed until two days after the Drill Hole Wash Fault structure was penetrated for reasons cited above.

The first occurrence of interference effects are subtle and sometimes difficult to see in the record. They are usually manifested in a change in relation between stations or the onset of diurnal or synoptic signal effects that were not previously identified.

Penetration of the PTn (crystal-rich vitric zone at the base of the PTn) in the North Ramp Tunnel occurred on June 20, 1995 (Rousseau and Patterson, 1996). NRG#4 (not discussed in this report) was the first borehole to register a pneumatic disturbance to the ambient pressure system. This disturbance was first observed on June 16, 1995, when the face of the North Ramp Tunnel was in the pre-Pah Canyon Tuff (Tpbt2), and the crystal-rich vitric zone at the base of the PTn was still undisturbed. The horizontal offset distance of NRG#4 from the face of the North Ramp Tunnel on June 16, 1995 was approximately 25 m. The pneumatic interference effects observed at NRG#4 are the result of the removal of the PTn pneumatic impeding layer, thus exposing the Topopah Spring subunits directly to the atmospheric pressure signal.

Pneumatic disturbance effects at UZ#4 and UZ#5 were first observed on August 12, 1995 (figures 15 and 16). On this date the face of the North Ramp tunnel was approximately 18 m east of the intersection of a north to northwest-trending, west dipping, normal fault (Rousseau and Patterson, 1996). This fault was first exposed in the North Ramp tunnel when the TBM advanced to position 12 +80 (1280 m west of the North Ramp portal). This fault as exposed in the North Ramp tunnel is a zone approximately 1 meter wide and consists of several small, but discrete, west-dipping offsets. The breccia zone of this fault is approximately 50 m wide on the ground surface. The pneumatic disturbance observed at UZ#4 and UZ#5 on August 12, 1995 was transmitted along this fault zone over a distance of 377 to 415 m. The pneumatic pressure responses in all of the PTn and Topopah Spring Tuff instrument stations in these two boreholes were effected. Pressure records and results of cross-

spectral analyses on data collected after the effects from ESF excavation are shown on figures 17 and 18. Residual amplitudes at stations within the Yucca Mountain and Pah Canyon Tuffs increased on the order of 40 percent while those from stations in the Topopah Spring crystal-rich vitrophyre and upper nonlithophysal increased on the order of 60 percent. The lower stations display larger residual amplitudes and shorter phase lags after the ESF excavation effects because the barometric signal is now being applied below the PTn units.

Figure 15. Figure 15 near here.

Figure 16. Figure 16 near here.

Figure 17. Figure 17 near here.

Figure 18. Figure 18 near here.

The first indication of a pneumatic disturbance to the pressure record at NRG#5 occurred on September 14, 1995 (figure 19) when the face of the North Ramp Tunnel was approximately 93 m from this borehole and in the lower section of the upper nonlithophysal subunit of the Topopah Spring. Pneumatic disturbance effects were recorded in all of the PTn and Topopah Spring Tuff instrument stations in this borehole. Pressure records and the results of cross-spectral analyses on data collected after the effects of ESF excavation are shown on figure 20. Residual amplitudes from all zones above the Pah Canyon Tuff were not noticeably effected by the ESF. From the pre-Pah Canyon bedded tuff through the 193 meter deep zone in the upper lithophysal unit of the Topopah Spring Tuff, residual amplitudes increased on the order of 40 to 50 percent. The residual amplitude from the 227 meter deep zone of the upper lithophysal unit, previously discussed as being effected by the Drill Hole Wash Fault,

increased only on the order of 10 percent and is about 20 percent smaller than the zones above it. This supports the idea that there is a zone of lower permeability between 193 and 227 m that inhibits communication between these zones and limited the effect of the Drill Hole Wash Fault above the 227 meter zone. Generally, the fact that tunnel effects propagated downward to the 227 meter station indicates that there is limited communication between that station and the overlying stations. This implies that prior to the ESF interference, all zones in the Topopah Spring Tuff were probably effected by the Drill Hole Wash Fault, with the zones above 227 m having residual amplitudes that were elevated on the order of 10 percent.

Figure 19. Figure 19 near here.

Figure 20. Figure 20 near here.

Pneumatic interference effects are present in the pneumatic pressure record for NRG-6 beginning on October 1, 1995 (figure 21). These disturbance effects were recorded approximately two days after the TBM intersected the northern boundary of the Drill Hole Wash Fault structure on September 29, 1995. The intersection of this fault structure with the North Ramp tunnel occurs near survey control point 20 +02 (2002 m west of the North Ramp portal, and is approximately 551 m northwest of NRG-6. Recognition of this disturbance effect at NRG-6 was not immediately apparent. Several months of additional pressure data at NRG-6 were required to confirm that there was indeed a change in the amplitude and phase lag of the synoptic pressure signal in the NRG-6 pressure records for the Topopah Spring instrument stations. Numerical model simulations using the Site Unsaturated-Zone Model conducted by Lawrence Berkeley National Laboratory (written communication, R. Ahlers to B. Bodvarsson, May 1, 1996) were able to help confirm and isolate the approximate date that these changes first occurred. The numerical model simulation results corroborate the results of the post-TBM

interference cross-spectral analysis of the pneumatic pressure record at NRG-6 (Figure 22). Residual amplitudes in all stations within the Topopah Spring Tuff at NRG-6 increased about 20 percent due to ESF excavation. NRG-6 is located south of the inferred boundaries of the Drill Hole Wash Fault. It is likely that the weak pressure disturbance seen at NRG-6 is a reflection of pressure changes that are propagated both along, and perpendicular to, the alignment of this fault. It is clear from these data that faults in Drill Hole Wash are open in the Topopah Spring Tuff. This also may indicate that the relatively high residual amplitudes in the Topopah Spring Tuff stations prior to the ESF effects may have been the result of the surface barometric signal propagating through the Drill Hole Wash Fault.

Figure 21. Figure 21 near here.

Figure 22. Figure 22 near here.

At NRG-7a pneumatic interference effects were first observed after the North Ramp Tunnel had advanced past the northwest trending Drill Hole Wash Fault. The southern boundary of this fault was encountered when the TBM had advanced to position 22 +60 (2260 m from the North Ramp portal) on October 16, 1995, placing NRG-7a approximately 100 m west of this fault. A pneumatic disturbance at NRG-7a was not detected until the TBM had advanced to within 26 m of this borehole on October 21, 1995 (figure 23), five days after crossing the southern boundary of the Drill Hole Wash fault. The sequence of events surrounding the first observed occurrence of a pneumatic disturbance at NRG-7a indicate that secondary, near-field fracturing associated with the Drill Hole Wash Fault is apparently very limited immediately south of where the North Ramp tunnel crosses the Drill Hole Wash Fault, however, it should also be noted that the rate of advance of the TBM, approximately 22 m/day may have obscured early detection of the first arrival of the pneumatic interference effect. Pressure records and the results of cross-spectral analyses for data collected after the effects of ESF excavation are

presented on figure 24. The residual amplitudes of all zones within the Topopah Spring Tuff increased on the order of 50 percent and the phase lags decreased by about 50 hours.

Figure 23. Figure 23 near here.

Figure 24. Figure 24 near here.

At SD-12 pneumatic interference effects became recognizable through visual inspection on March 23, 1996 (figure 25) when the TBM was at station 46+23 (4,623 m). The TBM was only 49 m from the borehole when these effects became apparent which is surprising because the TBM was within a zone of steeply dipping, intense fractures that began at station 42+00 and ended at station 52+00. This fracture zone is coincident with the location of maximum displacement and deformation of the nearby Ghost Dance Fault, but is not considered to be part of the Ghost Dance Fault (Warren Day, oral communication, 1996). This zone would be expected to be highly permeable to air and thus to have affected the borehole at a greater distance. There is some evidence that in fact the earliest effects were subtle, and not visually identifiable. Time does not permit the further analysis of the data required to fully assess the possibility of earlier effects at SD-12 for inclusion in this report, but these analyses will be included in an upcoming report to be completed in 1997. The fact that the large fracture zone would have large storage capability may have caused the pneumatic effects from the ESF excavation to occur gradually in borehole SD-12 and mask the initial onset until the effects were large enough to see in the record. Pressure record and the results of cross-spectral analyses on data collected after the effects of ESF excavation were identified are shown on figure 26. Residual amplitudes of all stations below the Tiva Canyon crystal-poor vitric unit increased on the order of 20 percent, excluding the two deepest stations discussed above in relation to the presence of perched water.

Figure 25. Figure 25 near here.

Figure 26. Figure 26 near here.

At borehole SD-7 pneumatic interference effects became apparent June 5, 1996 (figure 27) when the TBM was at station 55+98 (5,598 m) in the middle nonlithophysal Unit of the Topopah Spring Tuff. The ESF effects are reflected in the simultaneous initiation of downhole responses to the diurnal barometric signal. When these effects first occurred, the TBM had already gone 30 to 40 m beyond the nearest approach of the ESF to borehole SD-7. This is the only borehole where this has occurred and may reflect somewhat lower horizontal permeability in the rock mass between the ESF and the borehole such that the pressure did not propagate horizontally until a more permeable zone was encountered. Pressure record and cross-spectral analyses on data collected after the effects of ESF construction are shown on figure 28. The residual amplitudes in the Topopah Spring Tuff units increased on the order of 25 percent and the phase lags decreased about 10 hours. Similarly to the pre ESF data, these data indicate that the vertical permeability of the Topopah Spring units must be large because of the simultaneous response of all of the deeper zones.

Figure 27. Figure 27 near here.

Figure 28. Figure 28 near here.

Determination of Horizontal Permeability and the Vertical Anisotropy of the Topopah Spring Tuff Based on Modflowp Simulations

A Modflowp-based (Hill, 1992) numerical model was formulated to estimate the permeability to air of the PTn and Topopah Spring Tuff, based on pressure responses due to tunnel construction observed at boreholes NRG#5, NRG-6, and NRG-7a. Particular emphasis was placed on determining the horizontal permeability and the ratio of horizontal to vertical permeability of the Topopah Spring Tuff, as these data cannot be reliably estimated from the monitoring data in the absence of tunnel effects, and those data derived from air permeability testing (LeCain, 1996) are for much smaller scale than those available from tunnel response. Permeabilities determined from these simulations may be useful in a more complete model of the repository that account for heat and moisture movement from the waste sources.

Use of a ground-water based flow code to simulate air flow through unsaturated fractured porous media requires some explanation and much qualification. Ground-water flow codes typically are formulated assuming that the porous medium is saturated with a single slightly compressible homogeneous fluid. The unsaturated rocks being simulated, on the other hand, are partly saturated with water, and the fluid of interest is highly compressible, resulting in the governing flow equation being nonlinear. However, water movement through the rocks comprising Yucca Mountain is partly by slow, diffuse movement that results in liquid saturations that vary little on the time scale to be modeled for simulating tunnel effects on gas flow, so the air-filled porosity can be considered constant with time. Water movement also occurs as intermittent, rapid focused recharge that bypasses the main volume of the unsaturated zone. Such recharge may affect saturations and air-filled porosity briefly immediately after precipitation events, but probably would not affect air permeability determinations based on long-term (monthly) data. Airflow simulations may be made using the linear ground-water flow equation if the pressure variations about the mean pressure are no more than about 10% (Weeks, 1978). For naturally induced pressure-potential differences arising from atmospheric pressure fluctuations,

temperature-induced density effects, and wind pumping, pressure fluctuation typically are no more than about 1% of the mean pressure, ensuring that the effects of nonlinearity in the gas-flow equation arising from high gas compressibility will be quite small.

Questions also arise in using a porous-media based code to simulate fluid movement through fractured porous media, particularly in regard to whether the unit is sufficiently fractured that it may be modeled as an equivalent porous medium. The answer to this question depends on whether the model scale is large relative to the representative elementary volume of the fracture-matrix continuum. In a system dominated by flow in discrete fractures, it would be anticipated that monitoring stations that did not intersect the fractures would be bypassed by barometrically-induced flow from the tunnel, and stations near the tunnel might show less response than those more distant but within the zone of influence of the fracture. Based on examination of data from monitoring boreholes NRG-6, NRG-7a, and NRG#5, deeper stations at borehole NRG#5 do show greater response than in the shallower stations prior to tunnel construction, illustrating this effect. However, most observed pressure responses, which have been made at distances of 10's to 100s of meters from the ESF, both vertically and horizontally, indicates that, in general, the responses decrease monotonically with radial distance from the ESF. Thus, the Topopah Spring Tuff must be extensively fractured, and an equivalent porous media model may be appropriate to examine pressure responses at a scale of 10s to 100s of meters. However, the Topopah Spring Tuff is variably fractured, as can be seen by exposures in the ESF, and the initial response of various boreholes appears highly dependent on the timing of the intersection of faults or of more broken rock by the ESF.

Faults at Yucca Mountain appear to behave both as highly permeable conduits and as low-permeability barriers. Presumably, the highly fractured breccia zones are very permeable, whereas fault gouge along the base of the faults appear to create low-permeability barriers to flow. These effects are perhaps best illustrated by the residual amplitudes for borehole UZ-7a prior to the time ESF effects were discerned. Monitoring stations D-F, extending through the PTn and well into the Topopah Spring

Tuff, show large and nearly uniform residual amplitudes, indicating that even the PTn is highly fractured at this location. However, monitoring stations A-C show a much reduced residual amplitude, again nearly constant among these stations. Thus, the lower stations are separated from the highly permeable breccia zone by a low-permeability layer. These features likely are nearly vertical and extend through all or most of the Topopah Spring Tuff thickness. However, the preliminary conceptual model for the equivalent porous medium used here assumes that the media properties of both the PTn and the Topopah Spring Tuff are areally uniform, and neither the conduit effects of breccia zones or the barrier effects of gouge planes are simulated. Thus, the identified permeability of fractured rock surrounding the monitoring boreholes incorporates the effects of the breccia zones as larger block permeability and the effects of gouge as smaller block permeability. Use of the bulk permeability values determined below thus must be used with caution and the full recognition that simulations based on these values might poorly represent the system. In prior studies, it has frequently been found that pressure response might be well-represented by a uniform-property model, but transport, in terms both of rate and direction, is poorly simulated.

As for the AIRK model, these Modflowp simulations assume that the highly fractured Topopah Spring Tuff may be modeled as a single-porosity medium, and the simulation results are subject to the same limitations discussed for that model.

Model Structure

The Modflowp model of pressure fluctuations produced by the ESF in the North Ramp area was formulated to include only the PTn and the Topopah Spring Tuff members. The Tiva Canyon Tuff was assumed to be so permeable, based on numerous shut-in pressure data collected at several boreholes, as discussed above, that atmospheric pressure changes are assumed to be transmitted instantaneously to the top of the PTn throughout the model area. This assumption allows substantial simplification of the model representation, as the complex topography representing the Tiva Canyon Tuff outcrop can be

ignored. The Calico Hills formation, which immediately underlies the Topopah Spring Tuff, is assumed to be impermeable to air. This assumption is plausible, as perched water occurs in either the Calico Hills or in the basal vitrophyre of the Topopah Spring Tuff in much of the model area.

The modeled region includes a slab that extends 1780 m (38 nodes) along the ESF north ramp trace (fig. 3) from the Bow Ridge Fault intersection with the ESF, 2100 m south (38 nodes) from the ESF, and is 385 m thick, represented by 31 layers. The surface of the slab is a specified pressure boundary, all other boundaries are no-flow boundaries, and general head boundary condition nodes are specified for tunnel locations on one boundary. These nodes always have the same pressure potential as that specified for the surface of the model.

Model discretization included layers of 10-m thickness throughout the depth penetrated by the ESF, with layers increasing in thickness below that deepest penetration to include the total Topopah Spring Tuff thickness of 330 m, as determined from the geologic log for borehole NRG-6. A total of 25 layers is used to simulate the Topopah Spring Tuff. The PTn was assumed to include a uniform thickness of 60 m throughout the model area, and is represented by six layers of 10-m thickness. The Modflowp code uses block-centered finite-difference nodes, rather than face-centered nodes as used in the AIRK code. Hence, the specified head is in the center of the nodes representing the uppermost layer of the PTn, and the simulated thickness of the PTn is 55 m.

The model was oriented with rows following the tunnel trace. Row 1 is 5 m wide to approximate the half-width of the ESF. Row spacing was kept constant at 10 m width until past the location of borehole NRG#5, was then expanded for a distance but decreased again to include borehole NRG-6 at the center of a 10-m wide row. Spacing of the 38 columns was also variable from 10 to 90 m, with the smallest spacing in the vicinity of the borehole locations.

The tunnel was simulated using the ghbc (general head boundary condition) option in the Modflowp code. The layer(s) in which the tunnel occurred for a given column was determined based on the difference in altitude between the PTn-Topopah Spring Tuff contact and the ESF spring line.

Altitude of the contact was determined by three-point extrapolation of the altitudes of the ESF contact, and those in boreholes NRG#5 and NRG-6 for locations east of borehole NRG#5 and of altitudes in boreholes NRG#5, NRG-6, and NRG-7a west of borehole NRG#5. For locations at which the centerline of the tunnel was near a layer boundary, ghbc nodes were placed in the adjacent layer as well. Conductances for the ghbc nodes was adjusted upward by trial and error until modeled heads in the nodes were within 1% of those specified. This approach was used to allow a minimum effective conductance, as large conductances degrade the performance of the conjugate-gradient solver used in this problem.

A check of the probable magnitude of pressure losses in the ESF due to ventilation air flow was made to ensure that the losses could be ignored. The computations were made as follows. Ventilation flow was reported as 60,000 cfm (Alan Flint, oral communication) or about 30 m³/s. Assuming a tunnel diameter of 7.6 m, the tunnel cross-sectional area is 46 m², so flow velocity is 0.65 m/s. Kinematic viscosity, ν , for air at the altitude of Yucca Mountain and a temperature of 20 °C is about 1.8X10⁻⁵ m²/s, so the Reynolds number for airflow in the tunnel is about 3X10⁵. Assuming a relative roughness of 0.05, pressure drop in the tunnel is on the order of 2 Pa/1000 m (Streeter, 1962, p. 218), and is not important to this modeling effort. These theoretical results are corroborated by non-qualified pressure data collected in Alcove 2, located about 200 m from the mouth of the tunnel. After subtracting a mean position pressure difference of 0.3409 kPa, the alcove data for the period September 21-October 10, 1995, overlie those for well NRG#5 almost exactly. Periods when tunnel ventilation is in operation can be detected from temperature data recorded in the alcove, but not from the pressure data. Although the alcove station is located too near the tunnel mouth to fully represent tunnel effects at distance, the lack of detectable effects corroborates the above engineering calculations.

Model Parameters

Ground-water flow codes generally use transmissivity and storage coefficient, as defined for ground-water flow, as major parameters that govern head changes produced by pumping or boundary head change stress. These values are defined differently in gas-flow simulation. The property analogous to transmissivity is the thickness-mobility product, defined as:

$$\frac{bkK_{ra}}{\mu}, \quad (2)$$

where

b is layer thickness,

k is intrinsic permeability, μm^2 ;

K_{ra} is relative permeability to air, dimensionless; and

μ is dynamic viscosity, kPa-s.

The term "relative permeability to air" refers to the fractional permeability of the medium at its prevailing water content to the permeability of the air-dry medium. For these simulations, K_{ra} is assumed equal to 1, probably a good approximation for the Topopah Spring Tuff as the air-bearing fractures are drained or nearly so. Weeks (1978) suggests that K_{ra} is on the order of 0.6 to 0.8 in well-drained porous media, thus indicating that the identified permeability of the PTn is about 30% smaller than that of the air-dried medium. Initial estimates of the thickness-mobility product were specified for the model, and the parameter estimation capabilities of Modflowp were used to determine refined estimates.

This model does not include effects of anisotropy in the horizontal plane. Typically, fracture media exhibit higher permeability parallel to the orientation of the dominant fracture set. The Modflowp code allows simulation of such anisotropy, but only by orienting the model axes parallel to the main anisotropy axes. These axes vary in direction across Drill Hole Wash, and are not parallel to

the North Ramp of the ESF. Hence, adequate model treatment of horizontal anisotropy is complicated, and is beyond the scope of these simulations.

The gas-flow model term analogous to "storage coefficient" in ground-water flow is defined as

$$\frac{b\phi_a}{P}, \quad (3)$$

where ϕ_a is air-filled porosity, dimensionless; and P is mean atmospheric pressure, in kPa.

Porosity and water-saturation data are available from an extensive suite of cores from several boreholes in the vicinity of the North Ramp, so the storage coefficient for gas flow can be independently estimated, based on matrix porosity. Because matrix porosity is generally large relative to fracture porosity, matrix porosity was assumed equal to total porosity for this model. Values used in the model are based on porosity and saturation data for borehole NRG-6, and are assigned to each layer based on the average porosity for that depth interval times (1-water saturation), that quantity divided by the mean atmospheric pressure at Yucca Mountain (85 kPa). In the absence of flow measurements, which cannot be obtained due to their small magnitude, the storage coefficient cannot be identified by modeling separately from the permeability. Consequently, no effort was made to identify storage coefficient values in the model.

Model Pressure Data

Data available for parameter estimation in the model include time series of pressure potentials observed for various monitoring stations in boreholes NRG-6, NRG-7a, and NRG#5. These data were collected at different intervals, and periods of missing data vary from borehole to borehole. The time series are additionally complicated by the fact that they are induced by continuous fluctuations in atmospheric pressure, resulting in a complicated record. To simplify these records, data used in the model are based on the sine waves best fitting the synoptic atmospheric changes, as described above. Pressures at the top of the PTn and within the tunnel (the ghbc nodes) are represented as a sine wave of

unit (1 kPa) amplitude and no phase lag. Pressure potentials at each monitoring station are represented by sine waves of equal period, but having an amplitude and phase lag equal to that determined for the borehole based on cross-spectral analysis, as listed in figures 20, 22, and 24. Each sine wave representing surface and tunnel pressure is represented by 32 equally spaced (in time) values. For the 170-hour period selected for analysis, each time step thus represents 19,125 seconds (about 5.3 hours). Data were included for each monitoring station for every other time step, resulting in 16 "measurements" per sine cycle. To allow for cyclic steady state initial conditions to be achieved, data for the observation boreholes were used only after 64 time steps.

The finite-difference grid was established to place the observation boreholes at the cell centers. However, the depth locations were variable, and the multilayer well option was used to interpolate values to the appropriate depth. In this case, all observations included "boreholes" that spanned two layers, and the weight was assigned proportional to the complement of the fractional distance from the observation point to the center of the nearer node, and the fractional distance to the nearer node was assigned as the weight for the more distant node.

Simulation of air flow due to atmospheric pressure change requires frequent updating of pressure potentials along the specified pressure and ghbc boundary nodes. Such updating was accomplished in this model by modifying the subroutine SEN1RH in Modflowp (Hill, 1992, p. 290). This subroutine was written to update heads at specified head nodes at the end of each time step, based on a table of values. The subroutine was adapted to update all pressures in the uppermost layer and in the ghbc nodes at the end of each time step, and represents a problem-specific subroutine. In general, problems involving frequent updates of heads or pressures in boundary nodes will require more specific logic than can readily be written into a general subroutine, so the above adaptation represents a needed step. Call statements to this subroutine were modified to be activated whenever a nonzero file number is provided for IUNIT(21), regardless of whether parameter estimation was specified in the model run.

This allows heads to be updated each time step in Modflow itself. The reader is referred to McDonald and Hargbaugh (1988) for details on the use of the Modflow code.

Initial Conditions

Initial conditions for a model representing effects of atmospheric pressure fluctuations on rock gas pressures at depth are complicated by the fact that atmospheric pressure is never constant for a long enough period that pressure differences with depth disappear. For the sine-wave based approach used here, we instead seek to establish a simulated cyclic steady state prior to the time interval over which we identify transport properties that match the borehole data. For typical borehole-aquifer systems, such cyclic steady state should be closely approximated after one sine cycle starting from zero initial conditions (Cooper et al., 1965, fig. 3). It was assumed that this time criterion was suitable for gas flow effects from the ESF at Yucca Mountain. The assumption was tested, however, by simulations based on parameter estimation for data for the second and third cycles as compared to data for the third and fourth cycles of the simulation. Use of data for the third and fourth cycles resulted in only slight deviations from those for the second and third cycles, and the one-cycle equilibration for cyclic steady state is adequate. However, all simulations discussed below involved four-cycle simulations with data matched only during cycles 3 and 4.

Parameter Estimation for Boreholes NRG#5, NRG-6, and NRG7

Several attempts were made at parameter estimation using Modflowp before convergence to stable parameters was obtained. The first run that converged to a solution involved analysis of measured pressures selected at three-hour intervals collected from June 30 to July 4, 1995 at NRG#5, prior to the time TBM effects were observed. Thus, in this case, the problem is actually 1D, and subject to the same limitations as those of AIRK. Actual pressures were used in this simulation because tunnel effects were suspected to have begun to appear in the data set originally described as "pretunnel effect"

data, and the truly initial data set was too short to determine a synoptic sine wave. This successful run involved three layers, two for the PTn and one for the Topopah Spring Tuff. Identified permeabilities are 0.8, 0.4, and $60 \mu\text{m}^2$ for the three layers, starting at the top of the PTn. Values for the two PTn layers are quite similar to those from the 1D AIRK determinations. That for the Topopah Spring Tuff is somewhat larger than the value of $40 \mu\text{m}^2$ returned by the AIRK search procedure, but cannot be reliably determined by either code from these data.

Once this run was made, sine-wave data from borehole NRG#5 for the period September 22-October 2, 1995, were used in an attempt to estimate T values (T is the character in Modflowp designating the transmissive term, and is used here to mean thickness-mobility product) for separate units of the Topopah Spring Tuff, keeping the PTn values fixed as those found by the three-layer simulation. These attempts, involving either two or three Topopah Spring Tuff layers, were completely unsuccessful in converging toward a solution, as increases in the permeability of one layer would be compensated by a decrease in the permeability of another. Consequently, it was concluded that the Topopah Spring Tuff should be treated as a single unit for the equivalent porous medium model.

The next attempt involved using these same data for borehole NRG#5 only to determine T and the ratio of horizontal permeability, k_H , to vertical permeability, k_V , or k_H/k_V for the Topopah Spring Tuff, keeping Ts for the PTn layers fixed. The anisotropy ratio is designated "ANIV" in Modflowp, and that term will be used to represent anisotropy in the following discussion. This attempt also failed to provide convergence. However, a plot of the sum-of-squares error (SOS) between measured and simulated pressures for the updated estimates of T and ANIV indicated that essentially identical minimum SOS values occurred for constant values of the T/ANIV ratio. These results lead to the recognition that the posed problem is similar to that of determining the permeability anisotropy ratio based on an aquifer test involving a partially penetrating production well (Weeks, 1968). For such tests, data collected from an observation well located near the production well cannot be used to determine the anisotropy ratio unless data are available on transmissivity from another source. One such source

involves the analysis of data for observation wells located sufficiently distant from the production well to be unaffected by partial penetration. This distance is given as $r > 1.5b \sqrt{\frac{k_H}{k_V}}$ (Hantush, 1961), where b is aquifer thickness. Thus, it was concluded that successful parameter estimation of both T and ANIV would require data for borehole NRG-6, which is located about 460 m from the tunnel and hence meets this distance requirement, in addition to data for borehole NRG#5 and/or borehole NRG-7a.

Once this problem was recognized, a series of simulations in which the horizontal and vertical permeability of the Topopah Spring Tuff and the isotropic permeability of the PTn were determined, using data from borehole NRG-6 alone and in conjunction with data for borehole NRG#5 and borehole NRG-7a separately, and boreholes NRG#5 and NRG-7 together. Data used were all for the 170-hour synoptic, and included data for the period over which the tunnel extended entirely through the North Ramp. Results of these simulations are given in table 6

Table 6. Summary of Modflow simulations to estimate permeabilities near boreholes NRG#5, NRG-6, and NRG7a

Borehole(s)	Topopah Spring welded unit		Paintbrush nonwelded unit
	$k_H, \mu\text{m}^2$	$k_V, \mu\text{m}^2$	$k, \mu\text{m}^2$
NRG-6	30	NA	0.90
NRG#5/NRG-6	49	94	0.54
NRG#5/NRG-6	42	80	0.7 (fixed)
NRG-6/NRG-7a	34	68	0.67
NRG#5/NRG-6/NRG-7a	56	83	0.50
NRG#5/NRG-6/NRG-7a	45	72	0.7 (fixed)

Simulation of data for borehole NRG-6 only resulted in an identified PTn k of $0.90 \mu\text{m}^2$, which is identical to that determined for the full thickness of the PTn by the AIRK simulation of pre-TBM effect data. The Topopah Spring Tuff k_H value of $30 \mu\text{m}^2$ is somewhat smaller than the k_V value of $40 \mu\text{m}^2$ returned from the AIRK program, and may represent the fact that the near-vertical orientation of major fractures should result in the Topopah Spring Tuff k_H being smaller than its k_V value.

Another concern regarding the k_H value for the Topopah Spring Tuff is that the Modflowp statistics indicate that its value is inversely correlated with the value of k for the PTn, so a smaller PTn value and larger Topopah Spring Tuff k_H would provide almost as good a match as the values returned by the program. To test the validity of the PTn k determination, a simulation was made with the tunnel removed from the model to predict pre-tunnel Topopah Spring Tuff residual amplitudes at NRG-6. Results of this simulation indicate that the residual amplitudes in the Topopah Spring Tuff would be about 0.30, agreeing almost exactly with the residual amplitude determined from the measured NRG-6 data for the pre-August 1995 period. Consequently, a plausible conclusion is that the AIRK results are correct in showing that the PTn is more permeable in the vicinity of borehole NRG-6 than it is in the vicinities of boreholes NRG#5 and NRG-7a.

Simulation of data for the NRG#5-NRG-6 pair result in substantially higher permeability of the Topopah Spring Tuff and lower permeability of the PTn than for the simulation of data for borehole NRG-6 only. The PTn permeability is about equal to the value of $0.5 \mu\text{m}^2$ determined for the full PTn thickness using AIRK, and indicates that the results of this simulation are strongly influenced by the inclusion of data for borehole NRG#5. Modflowp statistics indicate that the PTn permeability is only weakly correlated (-0.23) with the Topopah Spring Tuff permeability for this system. Because the NRG-6 only data are highly negatively correlated, a decrease in PTn permeability and increase in Topopah Spring Tuff permeability would have little effect on the overall results for matching NRG-6 data, but might significantly affect the match for NRG#5 data. Thus, the NRG#5 data dominate the parameter estimation results.

Although the parameter estimation results are dominated by data from borehole NRG#5, the permeability of the PTn appears to vary areally, and that, in the absence of varying that permeability in the model, the tunnel effects might appropriately be modeled using an areally averaged value of PTn permeability. A separate parameter estimation run was made using data for boreholes NRG#5 and

NRG-6 assuming that the PTn k was the average of the values determined for the three boreholes--0.7 μm^2 . These results indicate a Topopah Spring Tuff k_H of about 40 and a k_V of about 80 μm^2 .

Results for the NRG-6-NRG-7a simulations indicate a slightly larger value for the k_h of the Topopah Spring Tuff and a smaller value (0.67 μm^2) for the PTn. The value for the PTn is almost exactly the same as that determined for most of the PTn thickness using the AIRK program, indicating that, similarly as for the NRG#5-NRG-6 pair, parameter estimation of the PTn permeability is dominated by the data for borehole NRG-7a. Modflowp statistics show a negative correlation of -0.62 between Topopah Spring Tuff k_H and PTn k, compared to the -.81 value for the NRG-6 data, indicating that the NRG-7a data should dominate the determination.

Results for data from the NRG#5-NRG-6-NRG-7a triplet of boreholes are very similar to those for the NRG#5-NRG-6 pair, presumably because of the much lower negative correlation between the PTn k and the Topopah Spring Tuff k_H than for data either for borehole NRG-6 or for the NRG-6-NRG-7a pair. The model-determined high vertical permeability for the Topopah Spring Tuff may represent the effects of a subvertical high-permeability feature transecting the Topopah Spring Tuff near borehole NRG#5. Tunnel effects increased dramatically on September 22, which might coincide with the time at which the TBM penetrated the feature. Because anisotropy (defined as k_h/k_v) is very strongly correlated with k_h for the Topopah Spring Tuff, k_h for the Topopah Spring Tuff could easily be reduced to the value determined for borehole NRG-6 only, with anisotropy decreasing and k_v remaining about the same as the value determined using data for all three boreholes. Also, as for the NRG#5-NRG-6 data, an areal average PTn value might be more appropriate in the simulation than the one determined by the dominant NRG#5 data. Consequently, a simulation was made in which the PTn permeability was fixed at 0.7 μm^2 . The resulting identified parameters are quite similar to those for the similar assumption made for the NRG#5-NRG-6 pair, as might be expected.

Except for the parameter-estimation run using very early data for borehole NRG#5, no parameter-estimation simulations were made to determine k for the PTn using data collected before

TBM effects were observed. Results of determining k 's of the PTn from the after-tunnel data are so similar to those determined from pre-tunnel data using the 1D AIRK program that the effort did not seem warranted.

A series of model runs were made, based on the tunnel either being absent or being advanced to its position as of September 5, 1995 for comparison with various data sets. These simulations were based on the preset tunnel positions, but were conducted for a four-week period to achieve cyclic steady state, and results were compared for the final week. The run for pretunnel conditions based on best-fit parameters for post tunnel data for borehole NRG-6 only provided excellent agreement with the pre-tunnel measurements. Because the pre-tunnel Topopah Spring Tuff residual amplitudes are totally dominated by the permeability of the PTn in the model, these results indicate that the value of k identified for the PTn is indeed plausible. A prediction run was also made to determine the cyclic steady-state effects of the tunnel as it existed on September 5, 1995 on residual amplitudes in the Topopah Spring Tuff at borehole NRG-6, using parameters identified using data for NRG-6 only. This approach led to a good match (.03 increase in fractional amplitude) with an indicated increase in amplitude of 0.04 for the Topopah Spring Tuff response at borehole NRG-6 for the period July 19-October 1, 1995, relative to that determined from the February 22-July 12, 1995 data set. However, other simulations for borehole NRG#5 indicated that the simulated cyclic steady state response was larger than the observed changes at that borehole. This lack of agreement led to the recognition that this simulation approach was unrealistic, because the tunnel was being advanced by as much as 200 m a week, and steady-state conditions did not prevail.

Further attempts to test whether the model could match observed times at which tunnel effects were observed in various boreholes were made by simulating the ESF as a moving boundary, based on dividing the time interval for the period July 5-November 15, 1995 into 15 stress periods, as shown in table 7.

Table 7. Location of ESF used to simulate temporal effects of tunnel advancement

Ending Date (1995)	Day of Year	Tunnel Station, meters	Columns with Tunnel Activated
07/19	200		None
08/02	214	11+82	4
08/09	221	12+41	4-5
08/23	235	12+91	4-6
08/30	242	13+48	4-7
09/06	249	15+00	4-9
09/13	256	16+30	4-11
09/20	263	17+54	4-18
09/27	270	19+01	4-21
10/04	277	20+88	4-24
10/11	284	21+80	4-25
10/18	291	22+91	4-27
10/25	298	24+12	4-34
11/01	305	25+48	4-37
11/15	319	25+79	4-38

For this simulation, properties used were those based on parameter estimation using data for all three boreholes, but with the PTn permeability set to $0.7 \mu\text{m}^2$. Pressures at one probe tapping the Topopah Spring Tuff at each borehole (probe 7, borehole NRG#5, probe 5, NRG-6, and probe 5, UZ#4 NRG-7a) were simulated based on boundary node pressures specified as a sine wave of exact 7-day period starting on July 5 with an amplitude of 1.0.

Results (fig. 29) indicate that simulated responses for boreholes NRG#5 and NRG-6 began to show subtle TBM effects on about September 5, and a significant increase in amplitude was simulated for borehole NRG#5 between September 12 and 15, in agreement with the date picked of Sept. 14 when the event was first observed (Rousseau et al. 1996). Simulated TBM effects for borehole NRG#5 continued to increase until late October, whereupon their magnitude was constant. Simulated TBM

effects in borehole NRG-6 increase quite slowly, and no clear-cut increase can be attributed to a given date. Nonetheless, the increase in amplitude between Sept. 26 and Sept. 30 is somewhat larger than those for previous periods, and agrees reasonably well with the date of Oct. 1 originally picked from borehole data. The simulated amplitude response in borehole NRG-7a shows a dramatic increase between Oct. 17 and Oct. 20, slightly sooner than the picked date of Oct. 21 from data for when effects were first observed. Overall, dates picked as representing those when TBM effects were first observed agree well with simulated results based on model-identified properties. In fact, considering that the simulated tunnel was advanced only weekly, compared to a more incremental daily advance by the tunnel itself, the agreement is as good as can be expected.

Figure 29. Figure 29 near here.

Parameter Estimation for Boreholes UZ#4 and UZ#5

Boreholes UZ#4 and UZ#5 are located north of the North Ramp in Pagany Wash. Both boreholes were drilled through the PTn a short distance into the Topopah Spring Tuff. The boreholes are located about 40 m apart, with borehole UZ#4 being located in the center of the wash channel, and UZ#5 located on the hillslope south of the channel. These boreholes were stemmed shortly before the ESF was extended into the Topopah Spring Tuff. Pressures are being measured at eight stations in each borehole. For borehole UZ#4, the shallowest station is at the base of the channel alluvium, the second at the base of the Tiva Canyon Tuff, the next five stations are located at various contacts among subunits of the PTn, with probe 7 being located at the very base of the unit. Probe 8 is in the uppermost part of the Topopah Spring Tuff. Borehole UZ#5 differs in that there is no alluvium, and the first probe is at the base of the Tiva Canyon Tuff.

Results of one-dimensional AIRK simulations of the data for UZ#4 and UZ#5 are ambiguous. The top part of the Tiva Canyon Tuff shows somewhat lower permeability here than at some other

locations, and most of the atmospheric pressure change becomes damped in the very upper part of the PTn in each borehole. Because of this damping, estimates of k for the lower layers are unreliable. Based on the assumption that minimum permeabilities could be found that would still reproduce the data, Kwicklis (Rousseau, 1996) used the AIRK program to determine permeabilities of the various lower subunits of the PTn to range from 1 to $10 \mu\text{m}^2$, with the uppermost bedded unit having a permeability of about $0.2 \mu\text{m}^2$. However, tunnel effects resulted in substantial pressure response in the Topopah Spring Tuff, whereas the response in the bottom PTn probe in each borehole was quite subdued. Consequently, the lowermost unit of the PTn may also have a low permeability to air. The intervening layers might equally well have large or small permeability, as far as can be determined from the data.

The observed response to the TBM in boreholes UZ#4 and UZ#5, based on the 170-hour synoptic for the period August 13-November 27, 1995 was simulated for each borehole separately and for the two boreholes combined. For the simulation, the locations of the boreholes were mirror-imaged across the ESF trace into the NRG#5/NRG-6/NRG-7a model domain. Data from the spectral analysis for probes A, C, D, and F for each borehole (figures 20, 22, and 24) were selected for use in the analysis. Data for probes A and B are nearly identical, and the probes are vertically separated only a short distance. The probes C, D, and E tapping the PTn also show similar response, so one was eliminated. Parameter estimation was originally attempted for the data for borehole UZ#4 for one Topopah Spring Tuff and two PTn layers, based on results of Kwicklis' AIRK determinations (Kwicklis, 1996). However, with tunnel effects included, parameter estimates of permeabilities for the two PTn layers were almost identical, so the layers were combined for the results tabulated below. The tunnel was modeled as extending the full length of the model.

Results of these simulations are shown in table 8.

Table 8. Summary of Modflowp simulations to estimate permeabilities near boreholes UZ#4 and UZ#5

Borehole(s)	Permeability, μm^2	
	Topopah Spring Tuff	PTn
UZ#4	800	0.22
UZ#5	2,200	0.23
UZ#4 and UZ#5	1,100	0.23

Permeability values for the Topopah Spring Tuff are very large, and likely represent the effects of a fault zone extending from Station 12+65 in the ESF northward to the near vicinity of the two boreholes. In regard to whether the model plausibly represents the fault, it can be argued that, with the tunnel extending the length of the model, it is for all intents and purposes, a cross-sectional model, particularly if the breccia zone is highly permeable but the slip plane of the fault is a low-permeability barrier. In these circumstances, the pressure response propagated along the highly permeable zone would be isolated from the less fractured Topopah Spring Tuffs to the west of the fault trace. Hence, the model may reasonably represent the system. The large difference between permeabilities determined for the two boreholes could be accounted for by relatively small differences in width of more typical Topopah Spring Tuff rock separating the fault zone from the boreholes, and/or in differences in the effectiveness of the small-permeability barrier created by the fault.

Summary of Parameter Estimation Results

Results of the separate simulations for the NRG-5—NRG-6—NRG-7a boreholes and for the UZ#4-UZ#5 boreholes are contradictory, and illustrate some of the problems encountered in using a porous media model to simulate effects of major discrete features that have quite different permeabilities than those of the rest of the system. The results indicate that a local portion of the repository block might be satisfactorily simulated by a porous-media model when data are available for

calibration, but the use of parameters identified for the local system might provide quite erroneous results if applied to the repository block as a whole. As an example, the good agreement between simulated and observed results for data from boreholes NRG-5—NRG-6—NRG-7a indicates that the presence of highly conductive faults and of partial flow barriers that divide the Topopah Spring Tuff into more permeable compartments are not necessarily important in describing the overall behavior of air movement through that part of Yucca Mountain immediately south of the North Ramp of the ESF. However, the permeability values identified for these rocks would completely fail to simulate the tunnel-induced effects determined for boreholes UZ#4 and UZ#5. Conversely, results of parameter identification for these boreholes would be totally inappropriate for the area south of the tunnel.

The results of this study indicate that, although local portions of Yucca Mountain can be satisfactorily modeled without regard to the location of faults, a repository-scale model should include major faults as features of large permeability and/or as partial flow barriers, as indicated by borehole data. Thus, despite the apparent success of the equivalent porous medium approach to the simulation of the system south of the North Ramp, a fully successful larger-scale model should include greater heterogeneity.

GAS-PHASE CIRCULATION AT YUCCA MOUNTAIN CREST

The potential importance of gas-phase circulation through the fractured rocks comprising Yucca Mountain was first confirmed by the observation of substantial rock gas exhaust from two open boreholes located on Yucca Mountain Crest. This circulation has been previously described and/or summarized by Weeks (1987), Thorstenson et al., (1990), Weeks (1993), Thorstenson, (1993), Thorstenson et al., (1995), and Thorstenson et al. (1996a). The following discussion summarizes those previous descriptions.

Physical Processes

Gas-phase circulation at Yucca Mountain Crest undoubtedly occurs both in the presence and absence of open boreholes, but our understanding of such circulation has been developed almost entirely from measurements made in borehole UZ-6s and by short term measurements of flow in borehole UZ-6. This understanding has been greatly augmented by data collected on gas chemistry in these boreholes and in a series of boreholes drilled to provide access for neutron logging, hereafter referred to as "neutron holes", that are only open over a short interval, as described by Thorstenson et al. (1990, 1995, 1996a, 1996b). Boreholes UZ-6, UZ-6s and three of the neutron holes, N-93, N-94, and N-95, are located very near Yucca Mountain Crest on Highway Ridge (fig. 30). Six other neutron holes (N-71-76) are located on Broken Limb Ridge. The washes separating the ridges also serve as flow divides for gas-phase circulation, and the two ridges thus form separate flow systems, as outlined on fig. 30. Gas-phase flow in the absence of open boreholes is too slow to be measured, and its presence and magnitude must be inferred from interpretations and inferences based on open-borehole flow and temperature measurements and from chemistry data for both open boreholes and the neutron holes.

Figure 30. Figure 30 near here.

Gas-phase circulation through unsaturated material in hilly terrain arises from three separate weather-related phenomena, including barometric pumping, thermosyphon pumping and windpumping. The mechanisms by which these processes generate flow, both in the presence and absence of open boreholes is briefly described below, followed by an assessment of the relative magnitudes of the effects based on analyses of flow measurements made in borehole UZ-6s.

Barometric Pumping

Barometric pumping occurs in any borehole open to permeable materials in the unsaturated zone, and results from changes in atmospheric pressure. Barometric pumping in open boreholes has been observed by many investigators working in areas of volcanic terrain, but is little noted in the literature. Ferris et al. (1962, p. 84) very briefly describes the phenomenon, and Barraclough et al. (1967) and Purtyman et al. (1974) describe flow measurements made in wells tapping the Snake River Plain Basalt at the Idaho National Engineering Laboratory and the Bandelier Tuff at the Los Alamos National Laboratory, respectively. Recent interest in the phenomenon centers on its potential for removing volatile organic contaminants from the unsaturated zone (Rohay et al., 1993, Phelan et al., 1995).

Barometrically-induced flow in open boreholes arises from the fact that pressure changes are transmitted instantaneously down the borehole, but only with time lag and attenuation through the unsaturated zone, resulting in a pressure imbalance at the borehole-unsaturated zone interface. The magnitude and duration of barometrically induced borehole fluxes depends both on the permeability and porosity of the materials extending from depth to land surface and on the depth of the unsaturated zone. These factors in turn determine the duration of the time lag before cross-formational air movement equalizes pressure at depth with that of the atmosphere. For a shallow well tapping materials of high permeability throughout, lag would be short and attenuation small, resulting in small effects, and the air flow would be dependent on barometric changes occurring in the previous hour or two. If instead a layer of low permeability isolates a high-permeability zone at depth from the atmosphere, barometric effects are large, and the well responds to changes in barometric pressure for days afterward. However, barometric pressure fluctuates about a mean, so that the cumulative effects of barometric pumping over an extended period of time result in zero net flux to or from the borehole. Their main effect is to exchange rock gas with air at depth in the formation, resulting in substantial mixing of the borehole gases.

Barometric pumping also occurs in the absence of open boreholes. Atmospheric pressure changes at land surface result in air movement into or from the unsaturated zone in response to compression of unsaturated zone gas as atmospheric pressure increases or to expansion of the unsaturated zone gas as atmospheric pressure declines. Buckingham (1904) analyzed barometric pumping based on the assumption that air enters or leaves the unsaturated zone by piston displacement, and concluded that soil-gas transport would be limited to approximately the top 1% of the unsaturated zone thickness and hence was not a significant transport mechanism. Massmann and Farrier (1992) extended Buckingham's analysis to include effects of dispersion during air movement into or from the unsaturated zone, and showed that transport would occur to greater depth, but that barometric pumping remained a relatively minor transport mechanism.

Nilson et al. (1991), in response to observations of rapid transport of gaseous radionuclides from rubble chimneys of underground nuclear explosions to land surface, developed a theory for barometric pumping in vertically fractured porous media that accounts for rates of transport many times greater than could be provided by gaseous diffusion, caused by deep vertical penetration of a barometric pulse in the fractures that allows horizontal diffusion of the tracer into the porous fractured rock matrix. Not all of the diffused tracer is discharged in the following exhaust cycle of flow from the fracture, and the tracer is thus "ratcheted" down its concentration gradient. As a test of that theory, Nilson et al. (1992) conducted a field experiment on Pahute Mesa on the Nevada Test Site by injecting large quantities (45 kg each) of sulfur hexafluoride (SF_6) and Freon F13B1 (CBrF_3) into a collapse chimney from an underground nuclear test that extends from depth to about 300 m below land surface. Large concentrations of both tracers (1,000 to 10,000 parts per trillion by volume (pptv)) were detected in fractures exposed at land surface within about three months of tracer emplacement.

Although barometric pumping occurs in cycles of no more than a few days, and does not result in net exchange of gases between atmosphere and rock gas, the deep penetration of air into fractures induced by barometric pumping may result in relatively rapid mixing of atmospheric trace-gas

constituents with unsaturated-zone gas, resulting in "young" tracer ages for the rock gas in the Tiva Canyon Tuff wherever the formation outcrops in hilly terrain. Barometric pumping also likely results in significant penetration to depth of trace gases in the vicinity of the Topopah Spring Tuff outcrop in Solitario Canyon. In other areas, however, barometric pumping in the Topopah Spring Tuff will be quite limited due to the capping effect of the PTn. Except where fractured, barometric pumping will also be quite limited in the PTn.

Thermosyphon Pumping

Thermosyphon pumping occurs in wells in hilly terrain that are open through a section of the unsaturated zone and results from temperature-induced density differences between atmospheric air and the rock gas. Briefly, a thermosyphon is considered to have two distinct limbs—a cooler downcast limb and a warmer upcast limb, with a heat source maintaining the temperature differences between the limbs. The temperature-induced density difference between the limbs induces flow from the colder to the warmer limb. In the case of Yucca Mountain Crest, the downcast limb in winter consists of air extending from the hillside fractured rock outcrop to the altitude of the near-crest well head or fracture, and the upcast limb extends from the outcrop through the fracture network and borehole to the near-crest wellhead or fracture. In winter, the thermosyphon behaves in its normal mode, with cold atmospheric air entering the mountain along hillside outcrops, becoming heated from the rock due to geothermal heat and heat stored in the rock, and discharging from open boreholes or fractures in the vicinity of the mountain crest. In summer, the thermosyphon reverses, and hot atmospheric air enters the near-crest open boreholes or outcrop fractures, is cooled by the rock mass, and discharges from the hillside outcrops.

The magnitude of the pressure potential that produces thermosyphon pumping, based on the assumption that the gas in each limb is isothermal, is given by the equation (Sanford, 1982; Weeks, 1987):

$$\Delta P = P_1 \left[\exp\left(\frac{-g\Delta z}{R_A T_{RV}}\right) - \exp\left(\frac{-g\Delta z}{R_A T_{AV}}\right) \right] \quad (4)$$

where

ΔP = pressure difference at wellhead, Pascals;

P_1 = atmospheric pressure at wellhead altitude,

g = acceleration due to gravity, $m\ s^{-2}$;

Δz = altitude difference from outcrop to wellhead or point of discharge, m;

R_A = air-specific gas constant, $J\cdot kg^{-1}K^{-1}$; and T_{RV} and

T_{AV} = virtual temperatures in K of rock gas and air, respectively. Virtual temperature is defined as the temperature that dry air must have to be of the same density as the humid air at ambient conditions.

At Yucca Mountain Crest, the wintertime thermosyphon effect results in air entering the Topopah Spring Tuff outcrops near the base of Solitario Canyon and exiting near the Topopah Spring Tuff-PTn contact, creating a circulation cell that extends some distance beneath Yucca Mountain Crest, but is limited by the fact that no eastern outcrop of the Topopah Spring Tuff for this fault block exists. The thermally induced pressure potential is larger in the Topopah Spring Tuff than in the PTn or the Tiva Canyon Tuff resulting in air "leaking" across the PTn into the Tiva Canyon Tuff. The largest and most pronounced thermally-induced flow cells occur in the Tiva Canyon Tuff, with air entering the Tiva Canyon Tuff outcrops in Solitario Canyon and in the east-flowing washes, and discharging near the crest beneath the less permeable caprock and upper cliff microunits. Less pronounced circulation cells of reversed direction occur in summer, resulting in enhanced mixing of air and rock gas.

Windpumping

Windpumping as applied to boreholes tapping the unsaturated zone in hilly terrain was first described by Woodcock (1987). Colbeck (1989) noted that wind should induce airflow through snow dunes, and termed such airflow "windpumping". Cunningham and Waddington (1994) made

measurements of the pressure potential produced by wind at the surface of snow dunes in Antarctica, confirming the results of flume studies by Vanoni and Hwang (1967). Briefly, wind striking the side of a hill or other topographic feature creates a higher than ambient pressure due to a drag effect, while wind over the crest of the feature results in a lower than ambient pressure due to an airfoil or lift effect. In the presence of a borehole or open fracture near the hill crest, this pressure difference will result in airflow moving into the hillside exposure of permeable rocks and out the borehole or fracture. For relatively smooth topographic surfaces, the pressure potential developed by wind would be described by the Bernoulli equation (Vanoni and Hwang, 1967; Colbeck, 1989):

$$\Delta P = C_D \rho u^2 \quad (5)$$

where

C_D is a combined drag and lift coefficient, dimensionless;

ρ = air density, kg m^{-3} ; and

u is wind speed at an unobstructed height, m s^{-1} . As described below, however, the Bernoulli equation must be modified to account for "boundary layer separation" (Schlichting, 1968) in complex terrain.

Windpumping at Yucca Mountain mainly affects the Tiva Canyon Tuff, as the Topopah Spring Tuff outcrop in Solitario Canyon is sheltered from the wind by Jet Ridge. Effects of windpumping through the Tiva Canyon Tuff are hypothesized to be substantial, based on the regression analyses of flow from borehole UZ-6s (described below), which indicated that about 40% of the net flow measured from borehole UZ-6s was induced by such effects. Windpumping is superimposed on thermosyphon effects and on barometric pumping, and likely results in even more mixing of rock gas and air than would occur in its absence.

In summary, gas-phase circulation through the unsaturated zone in hilly terrain is governed by three weather-related phenomena—barometric pressure changes, air temperature and relative humidity

variations, and wind speed and direction. The relative magnitudes of these various effects depends on the topographic situation and on the stratigraphy, structure, and permeability of the unsaturated materials.

Physical Measurements

Quantitative analyses of the effects of the physical processes causing gas-phase circulation at Yucca Mountain is based on measurements of flow, temperature, and relative humidity in open boreholes made concurrently with measurements of atmospheric pressure changes, air temperature and relative humidity, and wind speed and direction. Flow records suitable for analysis were obtained only from borehole UZ-6s, as that borehole was open throughout the PTn, but was filled in above the top of the Topopah Spring Tuff. Flow data for borehole UZ-6 are complicated by effects of hole construction and by the fact that flow from and to the Topopah Spring Tuff is more completely dominated by barometric pumping than is flow in the Tiva Canyon Tuff. The fact that the borehole taps both formations also greatly complicates analysis of flow records. The neutron holes are open only over a very short interval, and do not provide data particularly suitable for determining the magnitude of various contributing factors.

Measurements in UZ-6s

Surface Airflow Measurements at Borehole UZ-6s

The main source of airflow data at Yucca Mountain Crest includes average hourly air-discharge velocity at borehole UZ-6s measured for 4,748 hours during the period November 1988 to August 1989 (Weeks, 1993), and 15-minute average velocities measured for 6,100 hours during the period May 1993 to March 1994. Borehole UZ-6s is located only about 12 m from the cliffs overlooking the east side of Solitario Canyon, and is ideally situated to be maximally affected by thermal and wind effects, and,

because barometric pressure can equilibrate with rock gas pressure in the vicinity of the borehole both by vertical and horizontal exchange, to be minimally affected by barometric pressure changes. In addition, the hole construction is quite simple, the borehole is open throughout the thickness of the Tiva Canyon Tuff, but is filled in to above the top of the Topopah Spring Tuff-PTn contact. The borehole was drilled with an Odex system to a depth of 150.2 m using a 212-mm bit, and cored to a total depth of 158.2 m. The borehole penetrated 124 m of densely welded Tiva Canyon Tuff, 23 m of the PTn, and 11 m of densely welded Topopah Spring Tuff (Loskot, 1993). The casing, except for a 1-m section, was pulled, and the borehole caved or filled back to a depth of 136.6 m; thus the hole is open through almost the entire section of the densely welded Tiva Canyon Tuff and is bottomed in the PTn.

Flow measurements were made using a hot-wire anemometer, which measures vertical mass flow velocity, but does not distinguish flow direction. Particularly in summer, flow direction in borehole UZ-6s reverses frequently, so simultaneous measurements of flow velocity were made using a propeller anemometer that generates a positive electric signal for exhaust and a negative signal for borehole intake. Readings of flow were taken every 5 seconds, and the hot-wire anemometer signal conditioned to have the same signal as the propeller anemometer. In addition to average flow for the period, average positive and negative flows were recorded. For the May 1993-March 1994 record, maximum exhaust velocity for a 15-minute interval was 8.02 m/s, recorded on December 12, and maximum intake velocity was 3.61 m/s, measured on June 16. The number of flow reversals was also recorded for each measurement interval. The maximum number of reversals measured in a 15-minute interval was 72, and the total number for the period of record was 55,736, nearly all of which occurred during the summer months. Very frequent flow reversals have also been observed at cave entrances (Lewis, 1991), and is attributed in the speleological literature to high-frequency low-amplitude barometric pressure changes. However, wind effects, as described above, are undoubtedly also partly responsible, due to the gusty nature of wind velocity and the fact that wind effects counteract thermosyphon effects in summer, when most of the reversals occur.

Flow Measurements at Depth

The distribution of flow with depth was determined using a propeller anemometer that was lowered to selected depths, chosen from caliper logs as locations where the borehole was uniform in diameter. The reading was allowed to stabilize, and the voltage signal was recorded. The process was continued until a depth was reached that no flow was measured, whereupon flow was measured at the same stations as the anemometer was withdrawn from the hole. During each visit, the anemometer was calibrated by making a number of simultaneous measurements with the hot wire anemometer, and developing a calibration by regression. The data are non-qualified according to Yucca Mountain Project quality assurance procedures, but provide useful supporting data for interpretation of chemistry data, as described by Thorstenson et al., (1990, fig. 3); Thorstenson et al, (1995, fig. 3). The data also provide useful supporting data for Modflow modeling of airflow through borehole UZ-6s, as described below.

Counting upward logs separately from downward logs, a total of 25 flow logs were obtained, including 23 during periods of borehole exhaust and 2 during periods of borehole intake. Of these logs, about equal numbers were made for surface flow velocities of greater than 3 m/s, 2-3 m/s, and less than 2 m/s. Data for each of these classes were plotted separately, although all plots are of the fraction of surface flow measured at a given depth. These plots were made to test the hypothesis that flow contribution with depth varies with surface flow velocity. Other plots were made based on whether atmospheric pressure was rising or falling during the period the logs were obtained to check the hypothesis that flow contribution with depth varies with the relative magnitude of different driving forces. These plots instead indicated that, within the precision of the readings, all logs are similar. Hence, a composite log, based on data from all 25 logs was prepared to provide comparative data on flow contributions with depth in the borehole. These data indicate that half the flow enters the borehole in the top 20 m, and 80% in the top 40 m.

Surface Temperature and Relative Humidity Measurements

Temperature of the air exiting and entering borehole UZ-6s was measured at a depth of 1 m below the top of the casing whenever flow measurements were made. Measurements in summer were made using a thermistor and a humidity probe, but during winter, water continually condenses from the nearly continuous exhaust that occurs, and the probes became inoperative. Thus, in winter, measurements were made with dry-bulb and wet-bulb thermocouples. These measurements indicated that winter air exhaust from the borehole was nearly constant at 17 °C, and was water-vapor saturated. In summer, temperatures during periods of continuous intake were typically in the 30-35 °C range, and the recorded relative humidity was about 0.1. (The humidity probe failed its post-measurement calibration thus the data are non-qualified, but they qualitatively show wet vs. dry conditions. Its minimum reading is about 0.1, indicating that the intake air was very dry.) During summer periods when the exhaust velocity was at least 1 m/s, temperatures ranged from 18-20 °C, and the relative humidity was about 1. During periods of flow reversal, temperature and relative humidity ranged between these values.

Measurements of Temperature at Depth

Temperatures were measured at depth by lowering a bundle of nine thermocouples downhole ending at depths of 1 to 80 m and recording temperatures hourly for the period Jan. 22 to Feb 17, 1992. These records indicate that temperatures are nearly isothermal with depth as well as with time. Average temperature for this period is plotted vs. depth in fig. 31. Note that the entire temperature range is less than 1 °C. Also note that the warmest temperatures occur in the top 20 m, the same zone from which about 50% of the flow enters the borehole.

Figure 31. Figure 31 near here.

Measurements In Borehole UZ-6s

Borehole UZ-6 was drilled in 1984 to a depth of 575 m using a reverse-air vacuum drilling. Rocks penetrated by UZ-6 include 123 m of densely welded Tiva Canyon Tuff, 25 m of the PTn, 275 m of densely welded Topopah Spring Tuff, 90 m of the Calico Hills Formation, and 60 m of the Prow Pass member of the Crater Flat Tuff (Whitfield et al., 1993).

Borehole UZ-6 is located at Yucca Mountain Crest, and is subject to the effects of the barometer and of temperature and wind. However, flow phenomena at the borehole are complicated by its construction, shown in figure 32. Although the annular space is completely interconnected with the inner casing, the flow characteristics of the two zones are quite different, and it is common, particularly in winter, to observe atmospheric air entering the inner casing at the same time rock gas is exhausting from the annulus.

Figure 32. Figure 32 near here.

The annular space, extending from outside the bottom of the inner casing to land surface, is dominated by thermal and wind effects, and shows a nearly continuous exhaust from November through April. Spot measurements in the 3-inch pipe nipple indicate that flow velocity is commonly 5-6 m/s in winter, about twice that measured simultaneously in borehole UZ-6s. (Because the diameter of the pipe in which the measurements are made is less than half that of borehole UZ-6s, the volumetric flow rate would be about 40% of that in borehole UZ-6s.) Although flow velocities have not been continuously recorded in the annulus, shut-in pressures were monitored from January 22 to February 17 and from August 28 to September 8, 1993. A regression analysis of the winter data indicated that changes in barometric pressure occurring more than 75 minutes before a given annulus pressure reading had no effect on the reading. Thus, the system memory at the top of the annulus for atmospheric pressure change is only about an hour, resulting in barometric effects being a minor component of those

affecting flow in the annulus. Average shut-in pressure in winter was 23.7 Pa, and in summer, -0.3 Pa. Average air temperatures for the same two periods, based on records obtained at USGS weather station 4, located at Yucca Mountain Crest about 600 m southwest of well UZ-6, was 5.85°C for the winter record and 27.0°C for the summer record.

The inner casing provides the main access to borehole UZ-6, and the terms will be used interchangeably below. Flow and pressure are much more influenced by barometric pressure than is the annulus, and borehole UZ-6 typically shows diurnal reversals in flow in winter in response to barometric pressure changes. These large effects result from the fact that rock gas pressure in the highly fractured rocks near the base of the Topopah Spring Tuff are isolated from the atmosphere by the overlying Topopah Spring Tuff and by the PTn, resulting in pressure changes at that depth lagging far behind that in the atmosphere. The combination of high permeability of the lower nonlithophysal unit of the Topopah Spring Tuff and large pressure differentials results in large flows into or from the borehole to the depth of the lower nonlithophysal unit. Spot measurements of flow velocity in borehole UZ-6 while open to the atmosphere indicate that velocities may reach values of $\pm 2 \text{ m s}^{-1}$ on occasion, resulting in air exchanges of as much as $0.4 \text{ m}^3 \text{ s}^{-1}$. These flows are so large that they mask the smaller but more continuous thermosyphon effects that result in substantial wintertime inflow of air from the Topopah Spring Tuff into the Tiva Canyon Tuff at the borehole, as inferred from chemistry and shut-in pressure data.

Repeated flow surveys were made in UZ-6 using a cup anemometer housed in a 127 mm ID Plexiglass pipe with an outside-mounted aircraft inner tube that acted as an inflatable packer to force the entire flow through the tube. These surveys indicated that flow decreased to about half its surface value fairly gradually from a depth of about 150 m to about 365 m, but the remaining half was lost in the next 40 m. This 40-m interval includes a highly fractured interval of Topopah Spring Tuff (Whitfield, Cope, and Loskot, 1993, fig. 9). No measurable flow was noted in the partly welded to nonwelded tuffs below that interval, despite the fact that numerous readings were taken at those depths.

These measurements indicate that the entire thickness of the Topopah Spring Tuff takes part in gas circulation at Yucca Mountain Crest, providing a large reservoir of rock gas.

Although insufficient flow record is available to determine net fluxes on a seasonal basis from UZ-6, the shut-in pressures collected in 1993 showed that the average downhole pressure was 49.4 Pa in winter and -14.0 Pa in summer. These measurements indicate that, even under shut-in conditions, an average upward pressure potential gradient exists in winter between the bottom of the casing and the top of the annular space. In summer, a downward pressure gradient exists, indicating that a seasonal loss of rock gas should occur from the Tiva Canyon Tuff into the Topopah Spring Tuff. In addition, regression analyses indicate that shut-in pressure differences are affected by barometric pressure changes occurring at least 40 hours previously; thus the borehole indeed has a long "memory" of pressure change.

Measurements in Neutron Holes

The neutron holes should be affected by topographic, wind, and barometric effects, but since they are open only for a thickness of about 0.5 m, most show minimal flow. Spot readings of flow in the neutron holes on the UZ-6 pad have been made on numerous occasions. Flow velocity in N94 is typically about half that in borehole UZ-6s, despite its short open interval, perhaps indicating that the open section of this hole penetrates an open fracture. Boreholes N-93 and N-95 show steady upward flow in winter, but the flow velocities are on the order of 10% of those in borehole UZ-6s. Only a few spot measurements of flow have been made in the N-70 series boreholes, all located in the Broken Limb Ridge flow system, and only one of these exhibits measurable flow—N-74. That borehole exhibits flow velocities on the order of 20% of that of borehole UZ-6s. The N-70 series boreholes are situated such that they should exhaust during winter, so the lack of measurable flow from them must result from the fact that they are open only through relatively low-permeability rocks. The N-70 series boreholes are in

a separate flow system from that including boreholes UZ-6 and UZ-6s, and provide chemistry data on a natural system that is not affected by the presence of open boreholes.

Weather Records

As noted above, flow from or to open boreholes is dependent on three weather phenomena, and barometric, air temperature and relative humidity, and wind speed and direction data are required to analyze the flow data. Barometric pressure was recorded as part of this study, as records were not available during the full period of record from either the USGS or NWS stations. Data on air temperature and relative humidity were taken from USGS weather station WX4, located about 200 m northeast of well UZ-6s until 1990, and about 200 m south of the borehole after that date. Records are complete for this station during the time interval that UZ-6s flow records were obtained. Data on wind speed and direction measured at a height of 10 m were taken from the NWS MEDA-24 weather station, located 20 m north of borehole UZ-6s, as the records from the 3-m tower for the USGS station were affected by nearby topography. Missing record for the MEDA station were taken from the SAIC Yucca Mountain station, located 2 km north of the borehole, as those data were also taken from a 10-m tower. For periods when wind records were missing for both these stations, values were taken from the USGS WX4 station.

Analysis of Flow Data from Borehole UZ-6s

Flow data were analyzed by regression analyses to determine the relative magnitude of barometric pumping, thermosyphon, and windpumping effects on the total flow, as described by Weeks (1993), and as summarized below. These analyses were made based on the assumption that the flow generated by each weather process can be represented by an effective pressure potential multiplied by a linear proportionality factor.

Application of this concept is complicated by the fact that pressure losses due to flow-friction effects occur in borehole UZ-6s that result in flow velocity varying nonlinearly with pressure drop, requiring a correction. These friction effects were corrected for based on the following analysis. At Reynolds numbers of about 10^4 - 10^5 , typical of those for velocities measured at borehole UZ-6s, friction losses are proportional to the flow velocity raised to the 1.75 power, as originally noted by Blasius (Streeter, 1962, p. 217-218). For the borehole geometry and flow distribution, the theoretical flow velocity in the absence of friction losses, V_{WLC} , is related to the measured velocity, V , (in m/s) by the equation (Weeks, 1993)

$$V_{WLC} = V + 0.25V^{1.75} \quad (6)$$

For the regression analyses, all measured average flow velocities were converted to well-loss corrected values using eq. 4.

For each weather process, the linear-regression coefficients have a physical basis that can be used to select a proper form for the regression equation. Barometric pumping results from barometric changes occurring over the recent past, and may have a component due to leakage from the PTn that is related to the difference between ambient pressure and the mean pressure. Hence, effects of barometric pumping on flow velocity were assumed to be represented by an equation of form:

$$v_{LC} = a_0(P_0 - \bar{P}) + a_1(P_0 - P_1) + a_2(P_1 - P_2) + a_3(P_2 - P_3) + \quad (7)$$

where

P_0 is the pressure measured at the end of the current period, kPa;

\bar{P} is mean pressure,

P_1 is pressure measured at the beginning of the period, and

P_2 is pressure measured at the beginning of the previous interval. Various trials based on this equation

indicated that, compromising between goodness of fit and use of a minimum number of

prediction variables, flow from the borehole in response to barometric pressure changes, in units of kPa, may be computed from the equation:

$$w_{LC}(BP) = -9.81(P_0 - P_2) - 0.313(P_0 - \bar{P}), \quad (8)$$

where

P_0 =pressure at end of hour;

P_2 =pressure two hours previous; and

\bar{P} =mean pressure. Thus, almost all of the barometrically induced flow from borehole UZ-6s results from pressure changes occurring no more than two hours previously.

Initially, windpumping effects were assumed to be represented by a form of the Bernoulli equation, based on flume and other studies (Vanoni and Hwang, 1967)

$$V_{wLC}(WP) = b_0 u^2, \quad (9)$$

where b_0 depended on whether wind was from the east or the west, and

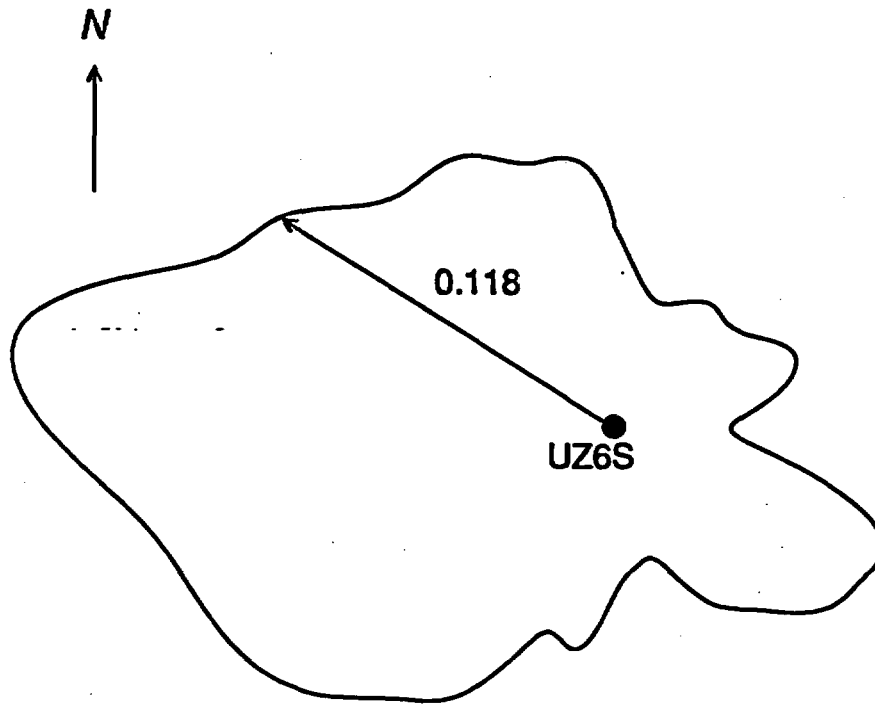
u is wind speed, m/s, measured at a height of 10 m at the MEDA24 weather station. However, it became clear that wind effects were quite sensitive to wind direction, and that the exponent 2 in the above equation gave a much poorer fit than a value of 1 in some, but not all cases. Because of the irregular shape of Yucca Mountain Crest, and the sharp break in slope on the western side of the crest, the Bernoulli equation does not necessarily describe wind effects on the pressure distribution over the mountain. Moreover, the nature of the topography encountered, and hence the magnitude of the drag coefficient, varies greatly with wind direction. Consequently, flow velocity records were separated according to 20° sectors in 10° increments, allowing for 36 overlapping sectors, from which the wind blew during that period, and regression analyses were made to relate flow velocity to wind speed, u , for trial exponent values, n , of 1, 1.5, and 2. For wind direction from the southeast or northeast, the Bernoulli equation ($n=2$) gave the best regression fit, while effects of wind from the west are best

described as being linearly dependent on wind speed ($n=1$). For intermediate wind directions, and for the record as a whole, the best match between measured and computed flow velocities were obtained using $u^{1.5}$. Consequently, the expression used to estimate wind-generated flow from borehole UZ-6s, based on the desirability of estimating flow using only one wind function regardless of wind direction is (Weeks, 1993):

$$V_{WLC}(WP) = g(\theta) u^{1.5} \quad (10)$$

where

$g(\theta)$ is a direction-dependent wind influence function ranging from about $0.18 \text{ (m/s)}^{-0.5}$ for winds from the west to about $0.039 \text{ (m/s)}^{-0.5}$ for winds from the east; and u is wind speed in m/s.



This sketch shows the shape of the wind influence function. For wind coming from a given direction, the magnitude of the function is given by the vector extending from borehole UZ-6s to the

function boundary. For example, if the wind were coming from the west-northwest, the function $g(\theta)$ would have the value 0.118.

Effects of virtual temperature on flow from borehole UZ-6s should be described by eq. 2, as the air column in the borehole is indeed nearly isothermal (fig. 31), and altitude differences are small enough that the atmospheric adiabatic lapse rate is unimportant, as noted by Weeks (1987). Virtual temperature may be computed from the equation (Montieth, 1973, p. 7) $T_v = T \left(1 + (1 - \epsilon) \frac{e}{P} \right)$, where $\epsilon = M_w/M_A$, or 0.622, and e is vapor pressure, in kPa. Vapor pressure of water-vapor saturated air was computed using a sixth order polynomial (Lowe, 1976). For rock gas, the air was assumed water-vapor saturated, and was assigned a virtual temperature of 20 °C, corresponding to a gas temperature of 17.4 °C at the altitude of Yucca Mountain. To determine the virtual temperature of air, the vapor pressure was computed as that for water saturated air times relative humidity as a decimal fraction.

It is clear from the form of equation 2 that the pressure potential varies nonlinearly with temperature. However, temperature effects may be approximately linearized about that of the virtual temperature of the rock gas by the equation: $T_c = [20^\circ\text{C} - T_{AV}] \times \left[\frac{293.2}{273.2 + T_{AV}} \right]$ where T_c is linearized temperature. In this form temperature-dependent flow velocity should be zero at a virtual air temperature of 20 °C.

The regressions of flow against changes in atmospheric pressure and against wind speed provided useful guidance on the nature of the final regression equation to be used, but the final analyses were made by multiple regression of well-loss-corrected flow velocity as the dependent variable against the two pressure terms and the wind speed raised to the 1.5 power as multiplied by the previously determined wind-influence function. This analysis resulted in the equation (Weeks, 1993):

$$V_{WLC} = 0.523 - 0.313(P_0 - P) - 9.81(P_0 - P_2) - 0.204T_c + g(\theta) u^{1.5}$$

Theoretically, the intercept for this equation should be zero, rather than 0.523, as no flow should be generated when the atmospheric pressure is at its mean value and has not changed in the last two

hours. Also, flow induced by windpumping should be zero under calm conditions. Thus, if the intercept is attributed to temperature effects, flow would be zero at a T_V of 22.5 °C, rather than the value of 20 °C indicated by borehole temperature data. Nonetheless, the value is substantially less than the T_V of 23.8 °C determined to result in zero flow before wind effects were recognized (Thorstenson et al., 1990). The offset may arise and may arise at least in part from a too-crude estimate of wind effects.

To provide a visual check of how well temperature effects were determined by this equation, well-loss corrected flow velocities due to temperature effects only ($V_{WLC}(T)$) were computed from the equation:

$$V_{WLC}(T) = V_{WLC} - \left[0.523 - 0.313(P_0 - P) + (-9.81(P_0 - P_2)) + g(\theta) u^{1.5} \right] \quad (11)$$

Daily averages of $V_{WLC}(T)$ were computed to minimize errors in estimation of barometric effects, and those averages plotted against the daily average value of T_C , as shown in fig. 33. The match is quite good, and the results convincing that temperature effects are responsible for much of the observed flow from the borehole. The problem of the intercept not being zero at a T_V of 20 °C is clearly illustrated.

Figure 33. Figure 33 near here.

Continuous weather records for 1988 were also used in equation 8 to compute flow from borehole UZ-6s throughout an annual cycle. Discharge, Q , in m^3/s of air at ambient conditions was computed from the velocity data using the equation:

$$Q = \pi r_c^2 V \times 0.80 \times P_r / P \times T / T \quad (12)$$

For these computations, r_c , the radius of the casing in which the measurements are made, is 0.0925 m, the factor 0.8 represents a correction for the fact that the flow velocity measurement was measured at

a point at the center of the casing. In the range of Reynolds numbers of 10^4 - 10^5 , typical for air flow in borehole UZ-6s, the center velocity is 1.25 times the average velocity (Bird et al., 1960, p. 155, eq. 5.1-3,4). P_r and T_r are the reference pressure and temperature at which the hot-wire anemometer, which measures mass flow velocity, is calibrated (1 atmosphere and 294.3 K) and P and T are ambient pressure and temperature, assumed for these computations to be 0.85 atmosphere and 290.2 K. These pressure and temperature terms result in a multiplier of 1.16.

This analysis, taken from Weeks (1993), has been adjusted downward by 0.13 to correct for an error in casing radius used in the prior calculations. In the absence of well losses, borehole UZ-6s would have shown a net discharge of about 1,700,000 m^3 for the year, including about 1,200,000 m^3 due to temperature effects and 500,000 m^3 due to wind effects. Values for actual flow velocity were computed by solving for V in Eq. 4 from computed hourly values of V_{WLC} using an iterative technique. These values were converted to discharge and summed by month, as listed in table 9. Some values differ by 0.1 from the sums given due to rounding.

Table 9. Summary of analyses of air flow from borehole UZ-6s

Month	Air Flow from Borehole UZ-6s, $10^5 m^3$		
	Thermal	Wind	Total
JAN	1.6	0.3	1.9
FEB	1.2	0.3	1.5
MAR	1.0	0.4	1.4
APR	0.9	0.3	1.2
MAY	0.4	0.5	1.0
JUN	-0.2	0.5	0.4
JUL	-0.6	0.4	-0.2
AUG	-0.3	0.3	0.0
SEP	0.0	0.3	0.3
OCT	0.2	0.3	0.5
NOV	1.1	0.3	1.5
DEC	1.5	0.3	1.7
ANNUAL	6.8	4.2	11.0

These computations indicate that the annual flow is about 1,100,000 m³, including 680,000 m³ due to temperature and 420,000 m³ due to wind. Most of this flow occurs during the winter exhaust period extending from November through April. For that period, thermal drive resulted in the exhaust of 730,000 m³ and wind pumping of 190,000 m³, for a total exhaust of 930,000 m³. Wind effects are important on an annual basis because they are always positive, whereas those of temperature become negative in summer. Moreover, when the thermal and wind effects cancel or nearly so, there is little correction for well-loss effects, causing the computed results to appear to be more significant than would be the case if well losses were absent.

Total flow for the intervals from July 1986 through March 1994 during which borehole UZ-6s was open were computed to be about 5,000,000 m³, based on the assumption that monthly averages computed for 1988 applied to all months during which the borehole was open.

Sources of Cross-Bed Flow to Borehole UZ-6s

Interpretations of gas chemistry as described by Thorstenson et al. (1995) indicate that a substantial fraction of the gas exhausted from borehole UZ-6s is derived from a source of lower than atmospheric CFCs presumably derived by upward leakage through the PTn and by cross-formational leakage through borehole UZ-6. The physical plausibility of this circulation and confirmation that the majority of the cross-bed flow was occurring through borehole UZ-6 was checked using permeability estimates derived from this study.

Cross-Bed Leakage Through the PTn

An estimate of upward leakage across the PTn from the Topopah Spring Tuff can be made based on estimates of the vertical permeability to air of the PTn. Although permeability estimates are not available for the immediate vicinity of boreholes UZ-6 and UZ-6s, determinations of the PTn air permeability based on use of the AIRK program are available, as listed above, for borehole SD-7.

located east of the boreholes on Highway Ridge, and for boreholes in the vicinity of the North Ramp of the ESF. These analyses indicate that the average full-thickness permeability of the unit ranges from 0.2 to 1.0 μm^2 , and for borehole SD-7, the borehole nearest Yucca Mountain Crest on Highway Ridge, the permeability is 0.4 μm^2 . This value was used with other estimates of terms in Darcy's Law to estimate the flux across the PTn due to thermosyphon effects. For the SD-7 air k value of $4 \times 10^{-13} \text{ m}^2$; a wintertime thermally-induced pressure gradient, dP/dz , of 0.525 Pa/m (corresponding to a virtual temperature difference between rock gas and air of 15 °C); a dynamic viscosity of air, μ , of 1.8×10^{-5} Pa-s, and an area, A , contributing flow, presumably derived by upward leakage through the to borehole UZ-6s of 700,000 m^2 , application of Darcy's Law: $Q = \frac{AkdP}{\mu dz}$, indicates that the flow contribution is about $1.0 \times 10^{-2} \text{ m}^3/\text{s}$, or about 20% of the flow from borehole UZ-6s under the same thermal regime. Thorstenson and others, (1995), estimated leakage to be $6.4 \times 10^{-3} \text{ m}^3/\text{s}$ assuming $k=0.2 \mu\text{m}^2$ based only on Drill Hole Wash PTn permeability data. The area of 700,000 m^2 is that for the Modflow model area as shown in fig. 30. The model results indicate that the area actually contributing flow to borehole UZ-6s is substantially smaller than the modeled area, and upward leakage through the PTn probably contributes no more than a few per cent to the flux from borehole UZ-6s.

Cross-Formational Flow Through Borehole UZ-6

Cross-formational flow through borehole UZ-6 is plausible, because the upper 150 m section of the Topopah Spring Tuff unit outcrops along the eastern flank of Solitario Canyon. Altitude of the outcrop ranges from 1,275 m at the Solitario Canyon fault to 1,387 m at the Topopah Spring Tuff-PTN contact, well below the UZ-6 wellhead altitude of 1,504 m. For a borehole located at a distance a from a linear line source (such as the Solitario Canyon outcrop), the flux Q , in m^3/s , is given by the equation (Rorabaugh, 1956, p. 121):

$$Q = \frac{2\pi kb\Delta P}{\mu} / \ln\left(\frac{2a}{r_w}\right), \quad (13)$$

where

b is formation thickness,

ΔP is the pressure potential difference between the borehole and the line source,

r_w is the borehole radius, and

other terms are as previously defined.

For a 15°C virtual temperature difference between formation gas and the atmosphere, and an altitude difference between the midpoint of the outcrop and the UZ-6 wellhead of 173 m, ΔP is about 90 Pa. However, when borehole UZ-6 is shut in, air discharges into the annulus, which has a higher pressure potential than the atmosphere. Presumably, that pressure is represented by the average of the shut-in pressures for the annulus and deep casing in borehole UZ-6. This pressure potential, as measured in February 1993, is about 36 Pa, and the pressure difference driving flow during that period would be 90-36, or 54 Pa. Thus, for a horizontal k for the Topopah Spring Tuff of $5 \times 10^{-11} \text{ m}^2$, as determined from the North Ramp Modflow model, a formation thickness of 275 m, a distance a of 400 m determined from the geologic map (Scott and Bonk, 1984), and a borehole radius of 0.2 m, $Q=0.03 \text{ m}^3/\text{s}$, about half that of borehole UZ-6s for a similar thermal drive. Using preliminary estimates of Topopah Spring Tuff permeability, Thorstenson, et al (1995) computed Q to be $0.055 \text{ m}^3/\text{s}$. Hence, physical considerations indicate that a major fraction of the flow from the Topopah Spring Tuff to the Tiva Canyon Tuff occurs through borehole UZ-6, and leakage through the PTn provides a minor component.

Gas Chemistry Interpretations

Physical data allow interpretation of the processes resulting in gas phase circulation through open boreholes, but do not allow effects caused by the presence of the boreholes to be separated from those occurring under natural conditions. These may be inferred instead from gas chemistry data, as described in detail by Thorstenson et al. (1995, 1996a, 1996b). These interpretations rely heavily on

concentrations of CFCs (chlorofluorocarbons), and on $^{14}\text{CO}_2$ activities in gas sampled from the various boreholes. Both the CFCs and the ^{14}C are present due to Man's activities, with well-documented histories of their presence in the atmosphere. Hence, they represent excellent tracers of the movement of air into the subsurface.

Natural System Flow

Thorstenson et al. (1996b, in preparation) have extensively evaluated the use of CFC and $^{14}\text{CO}_2$ data to interpret gas-phase circulation, including comparison of various flow models and mixing models to determine gas residence time and effective water saturation. Only those aspects of the interpretations that bear on the modeling of the Highway Ridge system are repeated here.

The natural system represented by data from the N70 series boreholes has been referred to as the Broken Limb Ridge system (fig. 30) by Thorstenson et al. (1996b). The assumption is made that air flow into that system becomes well-mixed with the resident rock gas on a time scale of months because of barometric pumping through vertical fractures, seasonal reversals in thermosyphon pumping, and highly variable effects of windpumping. Under these conditions, rock gas concentrations may be interpreted using the well-known box model (Imboden and Lerman, 1971). Briefly, the concentration in the initially tracer-free reservoir of volume V due to input of inert carrier gas at flux rate Q , the gas having a tracer of species i with concentration C_{oi} , is given by the solution, for the appropriate boundary conditions, of the differential equation (Perry, 1963; Imboden and Lerman, 1971):

$$\frac{d}{dt}C_i(1 + rKd_i) = (C_{oi} - C_i)\frac{Q}{V} \quad (14)$$

where

r is the ratio of water-filled to air-filled pore space and

Kd_i is the gas-liquid partitioning coefficient of species i .

The term rK_d accounts for the amount of tracer dissolving into a static liquid phase as tracer-tagged air enters the reservoir. The inverse of the ratio of flow rate to reservoir volume, V/Q , represents the mean residence time of the carrier gas within the reservoir, commonly symbolized τ , T. Assuming that tracer is added at time $t=0$, the concentration within the reservoir at time t is given by the equation:

$$C_i(t) = C_{oi} \left[1 - \exp\left(-\frac{t}{\tau(1+rK_d)}\right) \right] \quad (15)$$

Concentration of tracer i in the reservoir (C_i) as a result of steady input of gas with a continuously changing concentration may be computed by representing the concentration history as a series of equally-spaced (in time) step changes. Under this assumption, convolution may be applied to equation 2, and the concentration is given by the equation:

$$C_i(nt) = \sum_{n=1}^{nt} \Delta C_{oi_n} \left[1 - \exp\left(-\frac{\Delta t(n-0.5-nt)}{\tau'}\right) \right] \quad (16)$$

$(\Delta C_{oi})_n$ = change in concentration in the atmosphere between time step n and step $(n-1)$, assumed here to occur instantaneously at the midpoint of the time step, ML^{-3} ; $\tau'_i = \tau(1+rK_d)_i$, T; and Δt is the length of the time step, T. The term τ' is the species residence time.

That model was applied to data for the N-70's neutron holes to develop box-model residence times for each of three CFC species (CFC-11, CFC-12, and CFC-113) and for $^{14}CO_2$, as described in detail by Thorstenson et al., (1996). (Use of the box model to compute $^{14}CO_2$ residence times is complicated by effects of radioactive decay and isotopic fractionation of plant uptake of the root-respired CO_2 that is the main soil source. The reader is referred to Thorstenson et al. (1996b) for details of this analysis). Species residence times were computed for each compound, based on the history of the concentration of that compound in the atmosphere, using equation 15 or its equivalent for a decaying species. Values of τ_i for species with different K_d 's may be used to determine values for r and for τ , the air residence time (Thorstenson et al., 1996b). Results of the analyses indicate that, despite

uncertainties in the data, air residence time for the Broken Ridge system is fairly narrowly constrained to range from 1 to 4 years, with the best estimate to be about 2 years.

The UZ-6/UZ-6s Local System

Thorstenson et al. (1996a) have interpreted flow contributions in the UZ6/UZ-6s system by assuming that Tiva Canyon Tuff gas composition in the absence of open boreholes is represented by the average CFC and CO₂ concentration for the N70 series neutron holes. The chemistry of gas exhausting from borehole UZ-6s was assumed to represent an instantaneous mixture of this Tiva Canyon Tuff gas, gas from UZ-6 having the concentrations of the trace gases measured in that borehole, and an atmospheric component resulting from enhanced circulation induced by the presence of borehole UZ-6s that is not represented in the N-70 gas chemistry. Concentrations of each of the three measured CFC species and of CO₂ were used in a system of simultaneous equations that indicate that rock gas discharge from borehole UZ-6s is apportioned:

56% Tiva Canyon rock gas, 37% borehole UZ-6 gas, and 7% atmosphere.

The gas chemistry results also show insight on flow paths through Highway Ridge, at least in the vicinity of boreholes UZ-6 and UZ-6s, which appear to define a local flow system, as outlined in figure 30. Of the three neutron holes sampled on the UZ-6 pad, boreholes N-93 and N-94 show CFC and radiocarbon chemistry very similar to that of the N-70 series of boreholes, and appear to lie outside the local UZ6/UZ-6s system. Borehole N-95, on the other hand, is quite substantially depleted in all three measured CFC species, and has a significantly lower (and declining with time) radiocarbon activity, despite the fact that the borehole is shallower than all the other neutron holes, being only about 7 m deep. Thus, borehole N-95 appears to lie within the local flow system and the CFC concentrations are presumably effected by upward leakage. Results for borehole N93 are not surprising, because the borehole is to the east and down dip from borehole UZ-6, so wintertime up dip migration of Topopah Spring Tuff gas from borehole UZ-6 should be away from that well. Borehole N-94, however, is up dip

from borehole UZ--6 and is only about 30 m distant. Any concept of flow based on uniform flow properties of the Tiva Canyon Tuff would result in that borehole being in the local system. Thus, the chemistry for this borehole suggests that the local UZ6/UZ-6s system is affected by preferential pathways, presumably resulting from a fault traversing Highway Ridge from the upper reach of Ghost Dance Wash into the Solitario Canyon that is not included in the model, and a second fault extending from the flank of Ghost Dance Wash to the vicinity of borehole UZ-6.

UZ6-UZ6s Tracer Test

To support the interpretations based on the chemistry data above, a convergent tracer test was conducted in April, 1995. Borehole UZ-6s, which continually exhausts formation gas during the winter months, was used as the pumping well. Borehole UZ-6, which alternates from exhausting and intaking, was used as the injection well. Neutron holes N-94 and N-95 were used as intermediate observation wells (figure 30). The test was designed as follows: One 244 m long tube and one 107 m long tube were lowered into borehole UZ-6 and the borehole was sealed at the surface to prevent the exhalation of formation gasses into the atmosphere. The 244 m long tube was open below the PTn and was used to inject SF6 tracer gas into the borehole while it was exhaling from the Topopah Spring Tuffs. The tracer gas then mixed with the upward flowing formation gas and entered the formation through the Tiva Canyon Tuff after passing through the PTn, which in this borehole spans the depth of 82 to 150 m. The 107 m long tube was used to monitor the tracer gas concentration as it actually entered the formation. Sampling tubes were installed in borehole UZ-6s at depths of 6, 12, 18, 30, 61, 107, 122, and 131 m. Peristaltic pumps were connected to each sampling tube and operated continuously to sample the airstream from borehole UZ-6s. The neutron holes N-94 and N-95 were sealed at the surface and each equipped with a single sampling tube and peristaltic pump and operated similarly to UZ-6s. After all of the sampling tubes were installed and the pumps were turned on, The injection well was observed until it began to exhale. Depending on the season and barometric conditions, UZ-6 begins to exhale about

noon and exhalation increases until about 15:00, after which the exhalation decreases until the flow reverses in the evening. Another cycle of exhalation generally occurs around 1 or 2 am. Injection began at 12:32 on March 30, 1995 and continued until 16:32 at the following rates:

March 30

Time	Rate	Volume
12:32 until 13:32	25 cc/min	1.5 liters
13:32 until 14:32	50 cc/min	3.0 liters
14:32 until 16:32	75 cc/min	9.0 liters

A second injection was conducted on March 31, using the following rate:

March 31

Time	Rate	Volume
13:30 until 15:50	125 cc/min	17.5 liters

The actual concentration of tracer entering the Tiva Canyon Tuff was monitored through the 350 foot tube and is displayed on figure 34. Samples were also collected from a tube inserted into the top of the casing to monitor the amount of tracer that did not enter the Tiva Canyon Tuff. Those samples had tracer concentrations at background levels (about .002 ppm) throughout the testing while the borehole was sealed and verified that the tracer entered the formation as planned. Figure 34 shows the SF6 concentration in UZ-6, N-95, and the 20, 40, and 60 foot zones in UZ-6s. Tracer was not detected in N-94 or in any of the deeper zones in UZ-6s throughout the duration of the test. The injection rates reported above resulted in 2 separate peaks in UZ-6 of 4.5 and 7.3 ppm respectively. Because of the procedure of mixing the tracer in the borehole the injection "slugs" are more diffuse than would be ideal, but for the purpose of the following discussion the midpoint of each injection peak in UZ-6 was used to estimate the first arrival and peak arrival times at the monitoring boreholes. Because this test was designed to take advantage of the natural flow between these boreholes, there was no way to maintain a steady flow rate. When natural reversals occurred in UZ-6, the tracer in the vicinity of the

injection hole was probably pulled back toward the borehole to some unknown extent. Additionally, the flow rate through the mountain is effected by diurnal variations in barometric pressure which added another variable controlling tracer movement. This intermittent flow pattern resulted in fluctuations in tracer concentration in the observation holes as reflected on figure 34. The first tracer injection reached its peak concentration in UZ-6 after 5.2 hours. The first detected arrival of tracer at N-95, 65 m distant from UZ-6, was at 31.2 hours after injection began. Thus the fastest travel time between UZ-6 and N-95 is 26 hours. The first detection of tracer in UZ-6s occurred in the 20 foot sampling zone 48 hours after the test began, thus, the fastest travel time between UZ-6 and UZ-6s is 42.8 hours. The 40 and 60 foot zones in UZ-6s had arrival times between 48 and 50 hours. Because of interference from the first injection, no first arrival can be detected for the second injection. Interpretation of the travel time for the peak concentration is complicated by the variable flow pattern described above. Also, the results seem to indicate that 24 hours between injections was not sufficient to prevent interference between the 2 injections. Ideally the injections would have been conducted with different tracers but because of permitting restrictions at the NTS only one tracer was available. By visual inspection, the peak concentration of SF6 in N-95 can be estimated as having occurred at about 84 hours after the test began or about 79 hours after the first injection and about 56 hours after the second injection. In the 20 foot zone of UZ-6s, the peak arrival of SF6 can be estimated as having occurred at about 137 hours after the test began, or about 132 hours after the first injection and about 109 hours after the second injection. Because only one peak is inferable from the available data and the recognition that the peak arrival from the first injection may have been masked by the presence of tracer from the second injection, we can only use these peak arrival times as bounding estimates. The results of the tracer test verify that substantial flow occurs between the Topopah Spring Tuff in borehole UZ-6 and the Tiva Canyon Tuff in borehole UZ-6s, as interpreted from the gas chemistry data discussed above. The first arrival of tracer at N-95 occurred 26 hours after the first injection. This results in an estimated travel rate of about 60 m/day. If the estimated peak arrival is attributed to the first injection, the calculated travel rate of the

tracer plume is about 20 m/day, whereas, if the peak arrival is attributed to the second injection the rate of travel of the tracer plume is about 28 m/day. The first arrival at UZ-6s occurred about 43 hours after the first injection, which results in an estimated travel rate of 53 m/day. If the estimated peak arrival is attributed to the first injection, the calculated travel rate of the tracer plume is 17 m/day, whereas, if the peak arrival is attributed to the second injection the rate of travel of the tracer plume is 21 m/day. The lower peak concentration observed in UZ-6s as compared to that of N-95 can be attributed to mixing of tracer free gas exhausting from the lower zones in the borehole with tracer laden gas from the upper zones and diluting the concentration of the tracer in the upper part of the borehole.

Figure 34. Figure 34 near here.

Modflow Modelling of Thermally Driven Air Flow in the UZ-6/UZ-6s System

A 3-D model of the Tiva Canyon member of the Paintbrush Tuff for the Highway Ridge flow system was formulated, based on the Modflowp version (Hill, 1992) of the Modflow code (McDonald and Harbaugh, 1988). In particular, the model was used to assess the permeability of the Tiva Canyon Tuff required to produce the measured flow from borehole UZ-6s based on thermal drive, to determine the maximum permeability that the caprock might have and still allow the measured flow to be induced, to assess the physical plausibility of the indicated contribution of flow occurring from borehole UZ-6, as postulated by Thorstenson et al. (1995), and to simulate the tracer test that was conducted to further test this hypothesis.

Use of a model that does not include temperature and/or density effects to simulate thermosiphon-generated air flow appears on its face to be ill-conceived. For this modeling effort, it is assumed that the thermal mass of the rocks comprising Yucca Mountain is sufficiently large as to be unaffected by air flow through them. This assumption seems valid based on the fact that air temperatures measured in the wintertime exhaust from borehole UZ-6s have remained essentially

constant from 1986, when first measured, through March 1994. In addition, ρC_p , the volumetric specific capacity at constant pressure is $1,000 \text{ J(Joules)/m}^3$ for air and $2,000,000 \text{ J/m}^3$ for densely welded tuff.

Conceptual Model

As discussed above, large volumes of rock gas exhaust have been measured from borehole UZ-6s, arising from thermosyphon and wind effects. Despite this large measured net exhaust, which amounts to a volume many times the available pore space, gas CO_2 chemistry for borehole UZ-6s, both in terms of partial pressure and in terms of isotopic composition, as extensively tabulated by Thorstenson et al., (1995) changed very little over a 5-year period. The $\delta^{13}\text{C}$ composition of the gas, averaging about -17.5% , strongly indicates a soil source for the sampled CO_2 , but the soil exposure along the flank of Solitario Canyon, the most obvious source of the exhausted gas, is limited. Thus, it appeared that much of the gas must be derived from updip migration from the eastern flank of the mountain. Other concepts developed from the flow measurements include the conclusions that the Tcul (upper lithophysal unit of the Tiva Canyon Tuff) must be very permeable, as about 80% of the exhausted air enters the borehole from that unit. In addition, the Tcuc (upper cliff) and Tccr (caprock) units must provide a less permeable cap to the Tcul. Otherwise, thermosyphon-driven gas flow would exhaust from fractures in those units without becoming focussed through borehole UZ-6s. Finally, Thorstenson et al. (1995) interpreted CFC data collected from boreholes UZ-6s and UZ-6 to indicate that about one third of the flow from UZ-6s was captured from rock gas moving upward from the Topopah Spring Tuff through borehole UZ-6. That flow presumably enters the Tiva Canyon Tuff from the annulus between the UZ-6 casing and the Tiva Canyon Tuff, and moves updip by the thermosyphon effect to exhaust at borehole UZ-6s. These hypotheses are amenable to testing using a numerical model to simulate gas flow.

Model Structure

The finite-difference grid for this problem consists of 40 rows oriented parallel to Yucca Mountain Crest ridge, 50 columns perpendicular to the ridge, and 13 layers, including 11 layers representing the units underlying the Tcuc, and two layers representing the Tcuc and Tccr-combined. The western extent of the model is the PTn-Tiva Canyon Tuff outcrop in Solitario Canyon. All outcrop nodes are designated as specified head, so each layer includes specified head nodes in its outcrop area on the flank of Solitario Canyon and throughout the remainder of the area wherever a layer outcrops. For this airflow model, valleys or washes represent no flow boundaries, because maximum or minimum pressure potentials are induced by the thermosyphon density effects along these features. The UZ-6s model is bounded on the south by Ghost Dance Wash (fig. 30), and on the north by an unnamed wash located 480 m from the Ghost Dance Wash. The eastern boundary was arbitrarily selected at a break in slope 1300 m east of the PTn-Tiva Canyon Tuff outcrop in Solitario Canyon. The northern boundary wash is trending southeast in the eastern part of the model area, so the model pinches in width to the east.

Areal extent and thickness of each layer was determined by a complicated process required to maintain some simplicity to the model structure while still preserving the mapped locations and altitudes of the Tcul-Tcuc outcrop, as mapped by Scott and Bonk (1984). Because the Tcuc and Tccr represent the "cap" of the model, errors in the position or altitude of that contact could result in spurious flow features. Briefly, the west edge of the model (the Tiva Canyon Tuff-PTn contact) was assumed to be straight and of constant altitude at 1404 m, representing simplification of the actual contact. The break in slope at the crest was assumed to be at the center of row 31, with each cell having its mapped altitude. Between row 1 and the row including the west Tcul-Tcuc contact, altitudes were linearly interpolated between 1404 and the outcrop altitude, and for the rows between that contact and row 31, linearly interpolated between the outcrop altitude and the crest altitude. The altitude of the base of the model (the top of the PTn) was computed from the distance from the edge of the model to the center of

the relevant column by subtracting that distance times the tangent of the formation dip of 6.13° , as required to match the altitude of the PTn-Tiva Canyon Tuff contact in borehole UZ-6s. Thicknesses of the 11 layers representing the more permeable section of the Tiva Canyon Tuff were separately determined for the western and eastern contacts of the Tcuc-Tcul contact by subtracting the dip-extrapolated altitude of the PTn top at the position of each contact from the Tcuc-Tcul contact altitude and dividing by 11. Thicknesses are approximately 10 m. For the model region between the western and eastern contacts of the Tcul-Tcuc, altitudes of the Tcul top were computed by linear interpolation, and thicknesses varied accordingly. West and east of the west and east Tcul-Tcuc contacts, all layer thicknesses were set equal to the values computed for the respective Tcuc-Tcul contacts. Layers 1 and 2, representing the Tcuc and Tccr units, exist only between the western and eastern mapped Tcul-Tcuc contacts. Layer 2 thickness is the altitude of the node minus the altitude of the top of layer 3, but no more than the thickness of the underlying layers. Layer 1 exists wherever layer 2 is at its maximum thickness, but its top is still below land-surface altitude of the node. Layer 1 accounts for that remaining thickness.

A Fortran program was written to determine layer codes for the model. For a given layer, the altitude at its base and at its top are computed for each nodal position. If the bottom of the layer is above the altitude of the node, the layer is absent, and assigned a code of 0 to indicate that it is inactive. If the land surface altitude of the node is between the bottom and top altitudes for that layer at that node, the layer outcrops, and is assigned a value of -1 to indicate that it is a specified head node. If the top of the layer is below the nodal altitude, the node is active, and is assigned the layer number.

Node spacing is variable, and was selected so that the nodal position of borehole UZ-6s would have an area of 0.04 m, approximating its actual dimensions. Nodal spacing was increased in all directions from the well, to a maximum spacing of 12 m width in columns representing the Solitario Canyon flank outcrops, and to a maximum of 150 m at the eastern edge of the model.

Borehole UZ-6s is simulated by specifying each layer at its row, column location as a general head boundary node (McDonald and Harbaugh, 1988 p. 11-1—11-5). Use of this option allows separate accounting for flux from or to each layer. However, no flow losses are accounted for, so calibration is made to flows computed based on well-loss-corrected velocity. As for the North Ramp tunnel model, the ghbc conductances were adjusted upward until the simulated pressures in the ghbc-designated nodes were within a few hundredths of a Pascal of zero.

Borehole UZ-6 was not originally included in this model, because its thermosyphon contribution of Topopah Spring Tuff gas to the Tiva Canyon Tuff had not yet been recognized. However, the chemistry-based conclusion that about 37% of the gas discharged from borehole UZ-6s was derived from that source could be tested for physical plausibility by including the borehole in the model. Node spacing was revised to include the borehole at the center of a 10 m X 10 m node, and hypothetical flows from the borehole were input to the model using the Modflow well option. For this input, flows in each layer were specified as being proportional to the fraction of the total Tiva Canyon Tuff permeability included in that layer.

Model Pressure Potential Data

This preliminary model has been used only in steady-state mode to address questions concerning thermosyphon effects, based on observations made at borehole UZ-6s. Consequently, the main effort regarding model inputs concerns pressure potentials generated by density differences between node centers on outcrop and Yucca Mountain Crest. Input files for Modflow specifying the initial or steady-state head at each boundary node were created using a Fortran program. Data specified for this program include interactively entered reference altitude, and rock gas and air virtual temperatures. A file that includes the altitude of each node, entered by row and column is also required. Pressures are computed by subtracting each nodal altitude from that for borehole UZ-6s and entering that value as Δz in

equation 2. The reference pressure, P_1 , was computed using the equation developed for the Standard Atmosphere (List, 1949):

$$P_1 = P_0 \left(1 - \left(\frac{\gamma}{288.16} \right) Z \right)^{M_a g / \gamma R} \quad (17)$$

where

P_0 is sea-level pressure, 101,325 Pa;

γ is lapse rate, 0.0065 K/m for the Standard Atmosphere;

288.16 is the sea-level reference temperature, K;

Z is borehole UZ-6s altitude in meters,

M_a is molecular weight of dry air, 0.028966 kg/g-mole,

g is acceleration due to gravity, 9.80665 m/s²; and

R is the ideal gas law constant, 8.31432 J/g-mole K.s

Steady-State Calibration

The model was calibrated to determine the isotropic permeability that would provide the best fit between temperature-induced flow for a virtual temperature difference of 15 °C, or 0.08 m³/s. In addition to matching total flow, profiles of fractional simulated flow vs. depth were computed and compared to the profile developed for the composite flow logs. The permeability of each layer was varied by trial and error until the composite flow log for borehole UZ-6s was reasonably reproduced, as shown in fig. 35. The permeabilities that provided this fit are listed in table 10.

Figure 35. Figure 35 near here.

These permeabilities represent values for the Tiva Canyon Tuff, and are very large. However, it would be impossible for the borehole to exhaust so strongly unless the rocks were extremely permeable. The values are similar to those returned for the vertical permeability to air of the Tiva Canyon Tuff by

application of the AIRK program, and may thus be typical for the Tiva Canyon Tuff. It should be noted that the permeability of the caprock could be larger, based on flow simulations only, without significantly affecting the flow or flow distribution. However, simulation runs that made use of particle tracking to determine whether flow from borehole UZ-6 would reach borehole UZ-6s indicated that, for larger caprock permeability values, particles entering the Tiva Canyon Tuff by flow from borehole UZ-6 would exit from the caprock, rather than reaching borehole UZ-6s.

Table 10. Summary of permeability determinations for Tiva Canyon Tuff near Borehole UZ6s

Layer number	Permeability, μm^2
1-2	3.6
3-4	6700
5	710
6	290
7	710
8-13	210

Once simulated flow to borehole UZ-6s and its distribution with depth were matched to observations, the model was used to determine total flow, both with and without borehole UZ-6s. Steady-state flow with borehole UZ-6s in place was $1.8 \text{ m}^3/\text{s}$, so borehole UZ-6s was responsible for the discharge of only about 4.4% of the total simulated flow. Such a large total flow through the system seems large. If the annual thermosyphon flow of $700,000 \text{ m}^3$ estimated for borehole UZ-6s were similarly proportional to total flux through the mountain, that flux would be about $16,000,000 \text{ m}^3$, or about four pore volumes. This is nearly ten times the estimate of annual exchange of about 0.5 pore volumes estimated for Broken Limb Ridge, based on the 2-year residence time determined from the trace-gas chemistry data. This is a serious mismatch, as the chemistry-based estimate appears to be accurate within a factor of +/- two, as described by Thorstenson, et al (1996b).

The interpretation of flow contributions to borehole UZ-6s based on chemistry data indicate that the presence of the borehole has increased flow only moderately more than would occur in the natural system. This chemistry-based conclusion is supported by simulations that indicate that the total flow is only about 1% less with UZ-6s shut in than when the borehole is open. Simulated flow induced by the open borehole is about 22% of its discharge. Hence, the presence of the borehole is unlikely to result in the large total flows.

Effects of flow from borehole UZ-6 into the Tiva Canyon Tuff were also simulated. For this simulation, flow equal to 37% of the discharge from borehole UZ-6s, as simulated without borehole UZ-6, or 0.03 was introduced to the system at the location of borehole UZ-6 using the well option in Modflow. Inclusion of this flow reduced inflow from the outcrop nodes by 0.008 m³/s, increased outflow from borehole UZ-6s by 0.0009 m³/s, and increased outflow to the outcrops by 0.022 m³/s. Thus, the added input had little effect on the overall budget and essentially none on the discharge from borehole UZ-6s. Particle tracking, described below, indicates that essentially all of the flow from borehole UZ-6 tracked into borehole UZ-6s at this discharge rate, so the overall budget effects represent diversion of Tiva Canyon Tuff gas around the local UZ-6/UZ-6s flow system.

One result of making all outcrop nodes specified head cells with different heads is to simulate rapid movement into a lower layer node and out an adjacent upper layer node. Whether such flow actually occurs is questionable. These simulation effects warrant further investigation. Another possible source of the discrepancy involves the fact that Highway Ridge is traversed by a fault extending from the upper reach of Ghost Dance Wash into the Solitario Canyon that is not included in the model. This fault may have caused rocks in the vicinity of borehole UZ-6s to be highly permeable, producing focused flow that is not represented in the constant-property model. The inadequacy of the model in this regard is also demonstrated by the failure of the model to realistically simulate results of the UZ6/UZ-6s tracer test, described below.

Borehole UZ-6s Simulation

Once the model was calibrated, a simulation was made to determine the source of the discharged air, based on the assumption that borehole UZ-6 was not present. For this simulation, the point of origin for simulated discharge from borehole UZ-6s was determined by backward particle tracking. Using the Modpath program (Pollock, 1994), a post-processing package to evaluate output from the Modflow code. Sequential Modpath runs were made for a given Modflow steady-state simulation output to determine paths for flow into individual layers. These results indicate that nearly all the flow entering layers 3 and 4 (fig. 36) which account for 50% of the discharge, comes from air entering outcrops in the first wash to the north of borehole UZ-6s. For layers 5-7, about half the simulated flow is derived from the northeast wash, a few percent from Ghost Dance Wash, and the remainder from the Solitario Canyon outcrop. For layers 9-13, most of the flow (90%+) is derived from outcrops in Solitario Canyon. However, since most of the flow enters the borehole at shallow depth, more than half the simulated flow is derived from the wash north of the borehole. The simulations show very little contribution of flow from the Ghost Dance Wash. This is likely a result of assigning constant properties to each layer, and the fault-related preferential flow paths probably result in larger contributions from the Ghost Dance Wash to the real system than are simulated by this preliminary model.

Figure 36. Figure 36 near here.

Boreholes UZ-8/UZ6s Simulation

As described above, the hypothesis that a substantial portion of the air exhausting from borehole UZ-6s was tested by performing a tracer test in which SF₆ was released into the Topopah Spring Tuff in borehole UZ-6 while it was exhausting by barometric pumping and the tracer was periodically sampled for in boreholes N-94, N-95, and UZ-6s. This test was simulated before it was performed by adding 2% of the previously simulated exhaust of borehole UZ-6s, or 0.0016 m³/s of air, as input at the borehole

UZ-6 location. Timed forward particle tracking, based on the permeabilities given in the above table, indicated that the peak concentration of the tracer should reach borehole N-94 in one day and borehole UZ-6s in slightly less than 5 days (Fig. 37). The simulated particle paths lay to the south of the borehole N-95 location, and indicated that tracer would not be found in that borehole.

Figure 37. Figure 37 near here.

These results are partly similar and partly dissimilar to those of the tracer test. The nearly 5-day peak arrival time for borehole UZ-6s is well in line with the 4.5-5.5 estimated peak arrival time. The fact that the simulation shows arrival of tracer in borehole N-94, but not in borehole N-95, is contradictory both to gas-chemistry interpretations and to the results of the tracer test. For the model to mimic the indicated true flow path, variable permeability would need to be included. Presumably, the mapped fault extending from the upstream end of Ghost Dance Wash across Yucca Mountain Crest and the fault extending from the flank of Ghost Dance Wash toward borehole UZ-6 provide preferential pathways for air flow and rapid transport.

CONCLUSIONS

The computed phase lags and residual amplitudes of the in situ pressure data indicate that individual lithostratigraphic units can be conveniently grouped into four distinct pneumatic systems: (1) the Tiva Canyon welded tuffs; (2) the Paintbrush Group nonwelded units that include the crystal-poor vitric base of the Tiva Canyon Tuff, the Yucca Mountain and Pah Canyon Tuffs (with associated bedded tuffs), and the crystal-rich top of the Topopah Spring Tuff; (3) the Topopah Spring lithophysal and nonlithophysal welded units; and (4) the pre-Topopah Spring bedded tuff, the nonwelded tuffs of the Calico Hills Formation, and the pre-Calico Hills Formation bedded tuff.

Pneumatic pressure records for instrument stations within the Tiva Canyon welded unit display very little attenuation and lag of the synoptic pressure signal, which indicates large bulk permeability and abundant interconnection of fractures. These observations are confirmed by simulation results from the borehole UZ6s model, which indicates that the permeability of different subunits within the Tiva Canyon welded unit range from hundreds to thousands of mm^2 . Although the largest of these values likely represent fault effects, the values are similar to those determined from one-dimensional analysis of pressure responses measured in boreholes NRG-5 and SD-7.

Examination of the pneumatic pressure data from instrument stations located within and across various subunits of the PTn indicates that the pressure attenuation and lag of these subunits differ from one location to another, and that the composite thickness of the PTn is probably insufficient as a sole indicator to account for differences in the magnitude of the residual amplitude and phase lag of the synoptic pressure signal transmitted across this unit. However, results of one-dimensional model simulations using the AIRK code indicate that average bulk permeability of the full thickness of the PTn ranges between 0.2 and 1 mm^2 at boreholes NRG-5, NRG-6, NRG-7a, SD-7, and SD-9. These data indicate that the PTn permeability varies by a factor of five over the part of the repository area included in this study.

Pressure data from instrument stations located in the Topopah Spring lithophysal and nonlithophysal welded tuffs exhibit negligible attenuation and lag once the pneumatic pressure signals enter those units. Pressure signals appear to be transmitted nearly instantaneously throughout the entire Topopah Spring section at most of the borehole sites, indicating that the fractures within the Topopah Spring Tuff are very permeable and highly interconnected within both the lithophysal and nonlithophysal subunits over much of the area. However, pressure signals differ at depth from those higher in the Topopah Spring Tuff at boreholes NRG#5 and SD-12, indicating the presence of less permeable rocks within the section at those sites. Results derived from the North Ramp simulation model also indicate that the fractures within the Topopah Spring Tuff are very permeable and highly

interconnected, as the bulk horizontal permeability of the Topopah Spring Tuffs were determined to fall within the 30 to 60 mm² range in the vicinity of boreholes NRG-5, NRG-6, and NRG-7a, and the vertical permeability in the 70-100 mm² range. The North Ramp model results are also consistent with one-dimensional AIRK simulation results, which indicate that the vertical permeability of the Topopah Spring Tuffs, although not reliably determined, must be larger than about 20 mm².

The pressure record at three station where pressures are monitored below perched-water zones indicates that essentially all of the synoptic barometric signal is attenuated. This is consistent with the idea that a perched-water zone or highly saturated zone would have extremely low permeability to air and would effectively bar the downward propagation of the surface barometric signal.

Despite the relative success of the North Ramp model in simulating the magnitude and timing of effects of the North Ramp tunnel, pressure data for several wells appear to be affected by faults that are not included in the model. Of the 8 boreholes with discretized pressure records discussed in this report, 5 (NRG-5, NRG-6, SD-12, UZ-7a, and SD-7) are interpreted as having been affected by the presence of the Drill Hole Wash Fault or the Ghost Dance Fault both before and after the onset of ESF excavation effects. The ESF excavation effects of 2 others (UZ-4 and UZ-5) were initiated when the ESF intersected another fault connecting it pneumatically to those boreholes. These data emphasize the fact that a simple layered model that does not include detailed pneumatic characterization of faults and major fractures may fail to adequately represent the effects of many of the important pneumatic pathways that exist in the vicinity of the proposed repository. Thus, even though the North Ramp model provides parameter estimates that appear to be suitable for a general simulation model of repository performance, the potential for effects of extremely permeable features provided by faults needs to be included in such models.

Time constraints have prevented simulation of the effects of the main drift on pressures in the Topopah Spring Tuff at boreholes located near its trace. Results of this North Ramp model are sufficiently encouraging to indicate that such a model should be developed.

Modeling results for the Highway Ridge flow system are similar to those of the North Ramp model in that both encouraging results and discrepancies with observations occur. The model predicted the peak arrival time for the convergent tracer test between boreholes UZ-6 and UZ-6s well, but failed to accurately predict flow direction. Also, model results indicated that natural circulation through the Tiva Canyon Tuff comprising Highway Ridge was on the order of 4 pore volumes annually, nearly ten times larger than the chemistry-based estimate of about 0.5 pore volumes per year, as determined by Thorstenson et al. (1996b). As with the North Ramp model, results are sufficiently encouraging to indicate that further model development is warranted.

The fact that thermosyphon movement of air occurs from the Topopah Spring Tuff to the Tiva Canyon Tuff through borehole UZ-6 indicates that no significant permeability barriers exist in the Topopah Spring Tuff between the Topopah Spring Tuff outcrop in Solitario Canyon and the borehole, a distance of about 400 m. These findings indicate that heat generated by waste emplacement in the Topopah Spring Tuff would likely result in gas-phase circulation cells between the repository and the outcrop that would discharge heat, moisture, and $^{14}\text{CO}_2$ to the atmosphere. The fact that the indicated volume of thermosyphon circulation is well-calculated using the permeability inferred from pressure responses to the North Ramp tunnel provides further confidence that such values might be useful in a general porous-media-based model to simulate repository performance.

The fact that gas enters the Tiva Canyon Tuff through the opening in the PTn created by the presence of borehole UZ-6 can be identified from CFC chemistry data, as demonstrated by Thorstenson et al. (1995, 1996a, 1996b) and confirmed by tracer test results, is an important conclusion. These results indicate that CFCs should be measured in previously unsampled neutron holes on Yucca Mountain Crest and in the various lined and stemmed boreholes. Such data can be used to determine the air residence time in the Tiva Canyon Tuff and might identify localities where the PTn is breached, allowing freer air circulation between the Topopah Spring Tuff and the Tiva Canyon Tuff.

REFERENCES

- Barracough, J.T., Teasdale, W.E., Robertson, J.B., and Jensen, R.G., 1967, Hydrology of the National Reactor Testing Station, Idaho: U.S. Geol. Survey Open File Report, 95 p.
- Bird, R.B., W.E. Stewart, and E.N. Lightfoot, 1960, Transport phenomena, McGraw-Hill, New York, p. 154-155.
- Buckingham, Edgar, 1904, Contributions to our knowledge of the aeration of soils: U. S. Dept Agric. Soils Bull. 25, 52 p.
- Carslaw, H.S., and Jaeger, J.C., 1959, Conduction of heat in solids: London, Oxford Univ. Press, p. 59, fig. 12.
- Colbeck, S.C., 1989, Air movement in snow due to windpumping: Jour. of Glaciology, v. 35, p. 209-213.
- Cooper, H.H., Bredehoeft, J.D., Papadopoulos, I.S., and Bennett, R.R., 1965, The response of well-aquifer systems to seismic waves: Jour. Geophys. Research, v. 70, no. 16, p. 3915-3926.
- Cunningham, J., and Waddington, E.D., 1993, Air flow and dry deposition of non-sea salt sulfate in polar firn: paleoclimate implications: Atmospheric Environment, v. 27A, p. 2943-2956.
- Ferris, J.G., Knowles, D.B., Brown, R.H., and Stallman, R.W., 1962, Theory of aquifer tests: U.S. Geological Survey Water-Supply Paper 1536E, p. 84
- Hantush, M.S., 1991, Drawdown around a partially penetrating well: Am. Soc. Civil Eng. Proc., v. 87, no. HY5, p. 171-195.
- Hill, M.C., 1992, A computer program (Modflowp) for estimating parameters of a transient, three-dimensional, ground-water flow model using nonlinear regression: U.S. Geol. Survey Open-File Report 91-484, 358 p.
- Imboden, D. M., and Lerman, A., 1978, Chemical models of lakes, in Lerman, A., Lakes: Chemistry; Geology; Physics: Springer-Verlag, New York, p. 343-346.
- Lewis, W.C., 1991, Atmospheric pressure changes and cave airflow: a review: National Speleological Society Bull., June, p. 1-12.
- List, R. J., Smithsonian Meteorological Tables, Sixth ed., Smithsonian Institution Press, Washington, D. C., 527 pp., 1949.

- Loscot, C.L., 1993, Geohydrologic data for test hole USW UZ-6s, Yucca Mountain area, Nye County, Nevada: U.S. Geological Survey Open-File Report 93-60, 25p.
- Lowe, P. R. 1976, An approximate polynomial for the computation of saturation vapor pressure: *Jour. Applied Meteorology*, v. 16, no. 1, p 100-103.
- Massmann, Joel, and Farrier, D. F., 1992, Effects of atmospheric pressures on gas transport in the vadose zone: *Water Resour. Res.*, v. 28, no. 3, p. 777-791.
- McDonald, M.G., and Harbaugh, A.W., 1988, A modular three-dimensional finite-difference ground-water flow model: U.S. Geol. Survey Tech. of Water-Resources Investigations, Book 6, Ch. A1, 586 p.
- Montieth, J.L., 1973, Principles, of environmental physics: Edward Arnold, London, p. 7
- Nilson, R.H., Peterson, E.W., Lie, K.H., Burkhard, N.R., And Hearst, J.R., 1991, Atmospheric pumping: A mechanism causing vertical transport of contaminated gases through fractured porous media: *Jour. Geophys. Res.*, v. 96, No. B13, p. 21,933-21,948.
- Nilson, R. H., McKinnis, W.B., Lagus, P.L., Hearst, J.R., Burkhard, N.R., and Smith, C.F., 1992, Field measurements of tracer gas transport induced by barometric pumping: Amer. Nuclear Soc. High-Level Radioactive Waste Conference Proceedings, Las Vegas, Nevada, p. 710-716.
- Perry, J.H., ed., 1963, Perry's Chemical Engineers Handbook, 4th edition, McGraw-Hill, p. 14-20.
- Phelan, J.M., Reavis, B. and Cheng, W.C., 1995, Passive soil venting at the chemical waste landfill site at Sandia National Laboratories, Albuquerque, New Mexico: Sandia Report SAND95-0776, UC-602, 35 p.
- Pollock, D. W., 1994, User's guide for Modpath/Modpath-plot, Version 3: U.S. Geol. Survey Open-File Report 94-464, variously paged.
- Purtyman, W.D., Koopman, F.C., Barr, S., and Clements, W.E., 1974, Air volume and energy transfer through test holes and atmospheric pressure effects on the main aquifer: Los Alamos Laboratory Informal Report LA-5725-MS, 14 p.

- Rohay, Virginia, Rossabi, Joe, Brian Looney, Richard Cameron, and Brian Peters, 1993, Well venting and application of passive soil vapor extraction at Hanford and Savannah River: Westinghouse, Hanford Company, WHC-SA-2064-FP, p. 815-818.
- Rorabaugh, M.I., 1956, Ground water in northeastern Louisville, Kentucky: U.S. Geological Survey Water-Supply Paper 1360-B, p. 122.
- Sanford, R.L., 1982, Natural ventilation in Hartman, H.L., ed., Mine ventilation and air conditioning: Wiley Interscience, New York, p 239-253.
- Schlichting, Hermann, 1968, Boundary-layer theory, McGraw-Hill, New York, 744 p.
- Spengler, R.W., Byres, F.M., and Warner, J.B., 1981, Stratigraphy and Structure of Volcanic Rocks in Drill Hole USW-G1, Yucca Mountain, Nevada: U.S. Geological Survey Open-File Report 81-1349, 50 p.
- Streeter, V.L., 1962, Fluid mechanics: McGraw-Hill, New York, p. 217.
- Thorstensen, D.C., Weeks, E.P., Haas, Herbert, and Woodward, J.C., 1990, Physical and chemical characteristics of topographically affected airflow in an open borehole at Yucca Mountain, Nevada: Focus 89 Proceedings on Nuclear Waste Isolation in the Unsaturated Zone, American Nuclear Society, p. 256-270.
- Thorstenson, D.C., 1993, Composition and CO₂ isotope signature of gases from borehole USW UZ-6, Yucca Mountain, Nevada: U.S. Nuclear Regulatory Commission Report NUREG/CP-0049, p. 184-188.
- Thorstenson, D.C., Haas, Herbert, Peters, C.A., and Yang, I.C., 1995, The reactions and transport of CO₂ and its C-isotopes in the unsaturated zone at the crest of Yucca Mountain: U.S. Geol. Survey Admin. Report, 66 p.
- Thorstenson, D.C., Weeks, E.P., Haas, Herbert, Woodward, J.C., and Peters, C.A., 1996a, The chemistry of unsaturated zone gases sampled in open boreholes at the crest of Yucca Mountain, Nevada-Data and basic concepts of chemical and physical processes in the mountain: Water Resour. Research, ms. in preparation, 61 p.
- Thorstenson, D.C., Weeks, E.P., Busenberg, E., and Plummer, L.N., 1996b, Application of chlorofluorocarbon tracers in an advectively dominated unsaturated-zone gas flow system at Yucca Mountain, Nevada, Water Resources Res., in preparation, xx p.

- Vanoni, V.A., and Hwang, L.S., 1967, Relation between bedforms and friction in streams: *Jour. Hyd. Div. Am. Soc. Civil Engineers*, v 93, no. HY3, p. 121-144.
- Weeks, E.P., 1968, Determining the ratio of horizontal to vertical permeability by aquifer-test analysis: *Water Resour. Res.*, v. 5, no. 1, 196-214.
- Weeks, E.P., 1978, Field determination of the vertical permeability to air: *U.S. Geol. Survey Prof. Paper 1058*, 41 p.
- Weeks, E.P., 1987, Effect of topography on gas flow in unsaturated fractured rock—concepts and observations: in *Flow and transport through unsaturated fractured rock*, Evans, D.D. and Nicholas, T.J., eds., *Geophysical Monograph 42*, Am. Geophys. Union, Washington, D.C., p. 165-170
- Weeks, E. P., 1993, Does the wind blow through Yucca Mountain: *U.S. Nuclear Regulatory Commission Report NUREG/CP-0049*, p. 43-53.
- Whitfield, M.S., Cope, C.M. and Loskot, C.L., 1993, Borehole and geohydrologic data for test hole USW UZ-6, Yucca Mountain area, Nye County, Nevada: *U.S. Geological Survey Open-File Report 92-28*, 36 p.
- Woodcock, A.H., 1987, Mountain breathing revisited—the hyperventilation of a volcano cinder cone: *Bulletin American Meteorology Society*, v. 68, no. 2, p. 125-130.

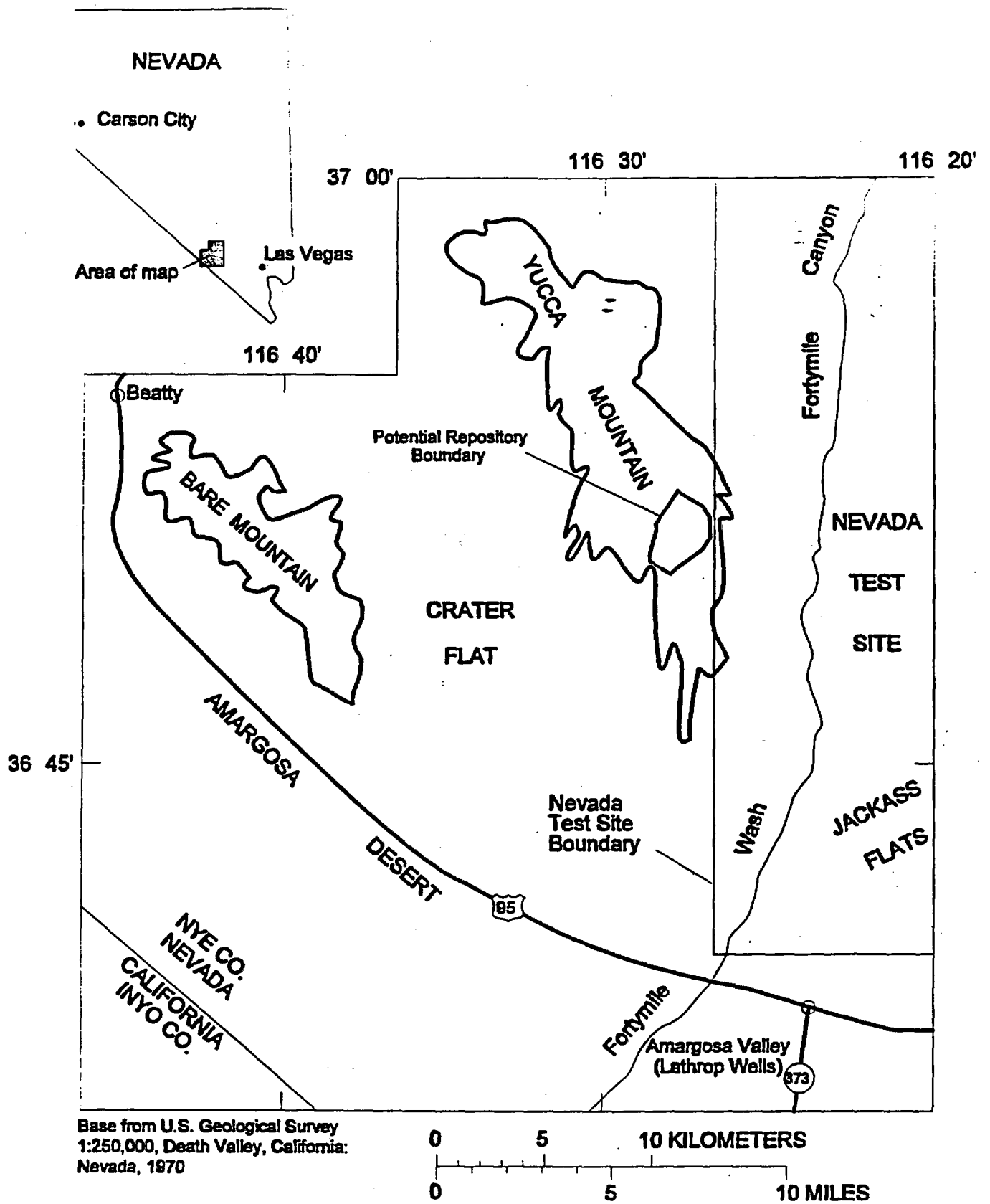


Figure 1. Location of study area.

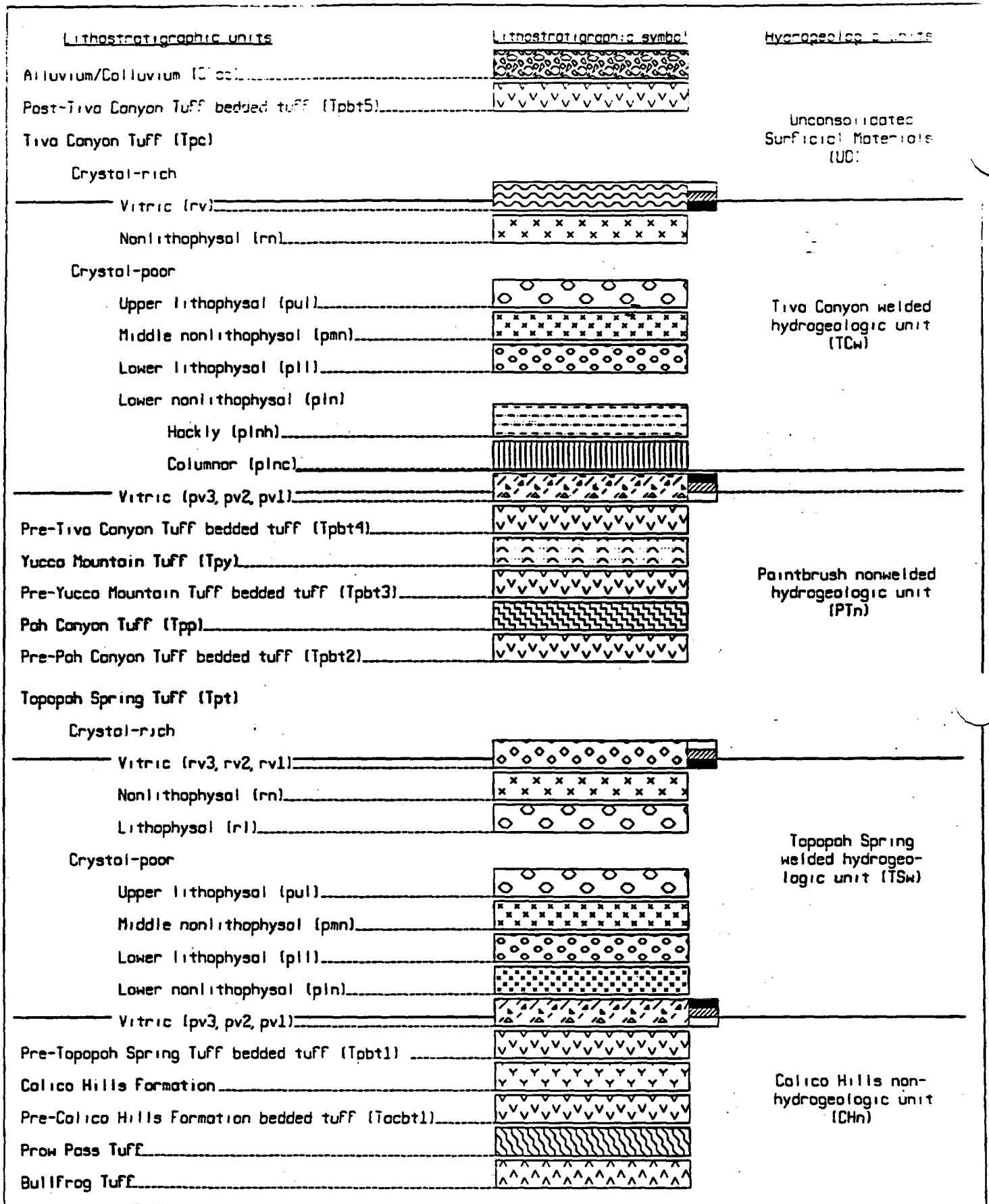
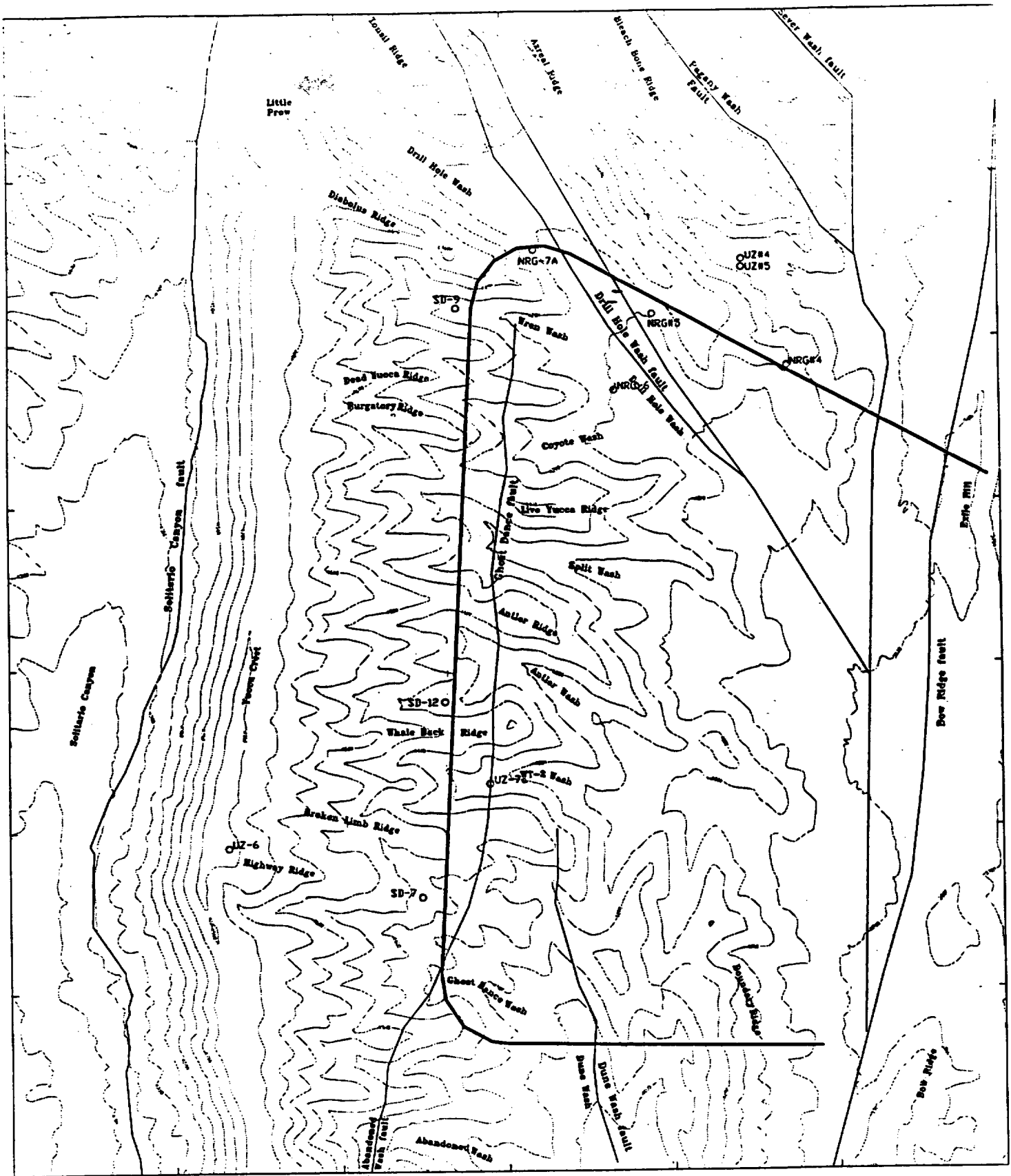


Figure 2. Lithostratigraphic and hydrogeologic units in the Yucca Mountain Area.



150 0 150 300 450 600 METERS

○ Borehole Name
 — Fault
 — Exploratory Studies Facility

Figure 3. Borehole locations and Trace of the Exploratory Studies Facility

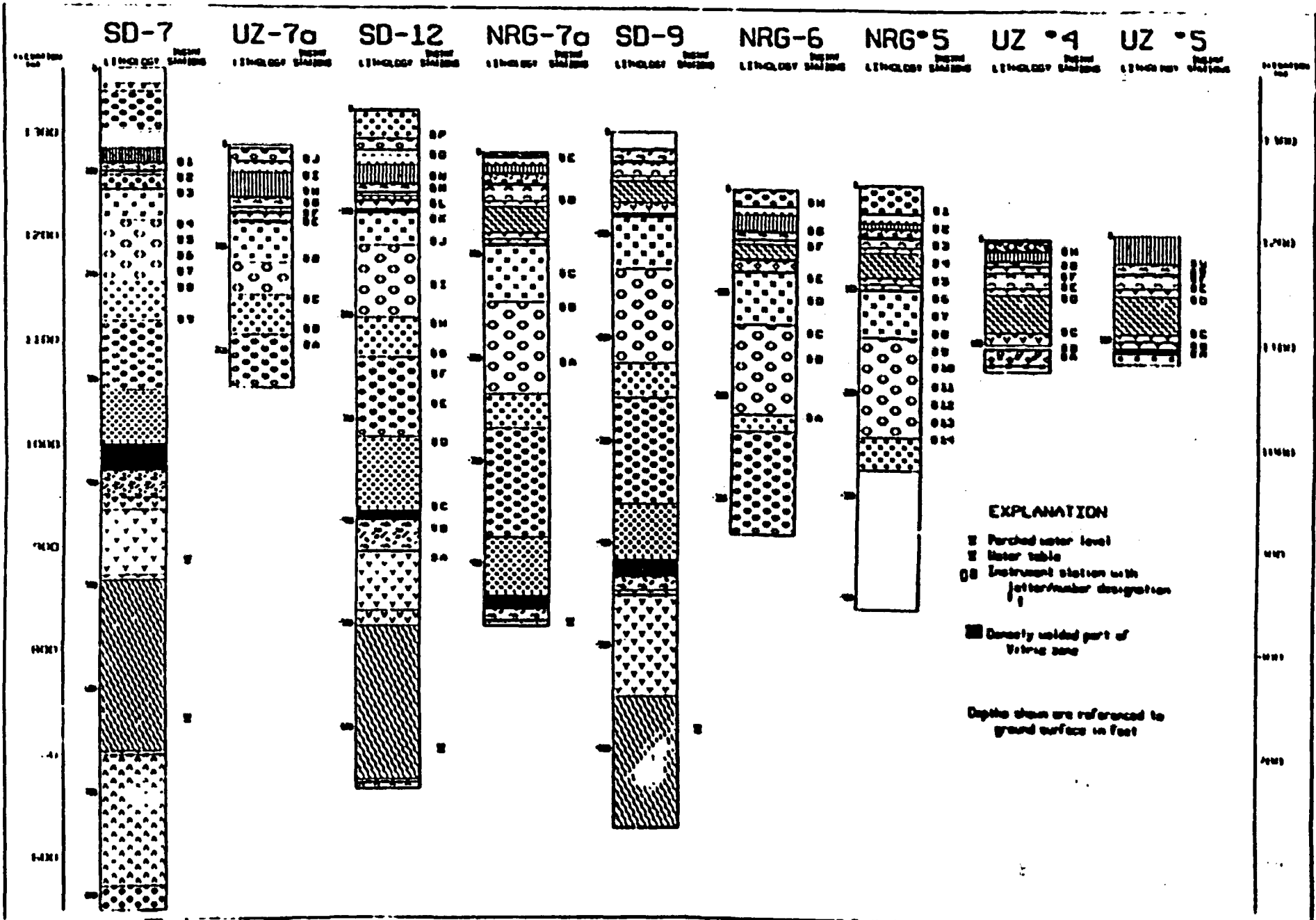


Figure 4. Stratigraphy and monitoring locations of instrumented boreholes.

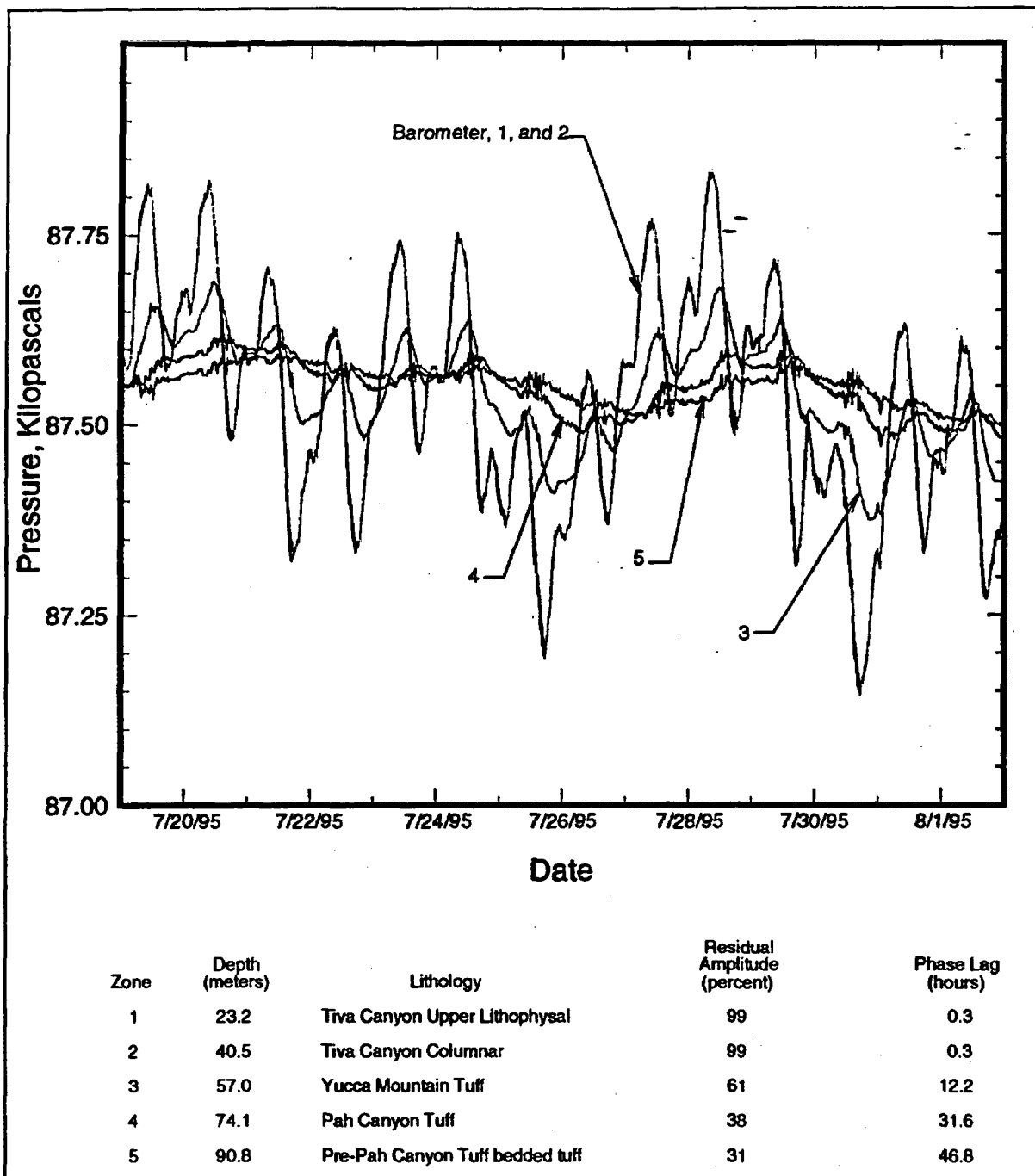


Figure 5a. Pressure record and the results of cross-spectral analysis on data from borehole UE-25 NRG#5 prior to the effects of ESF excavation.

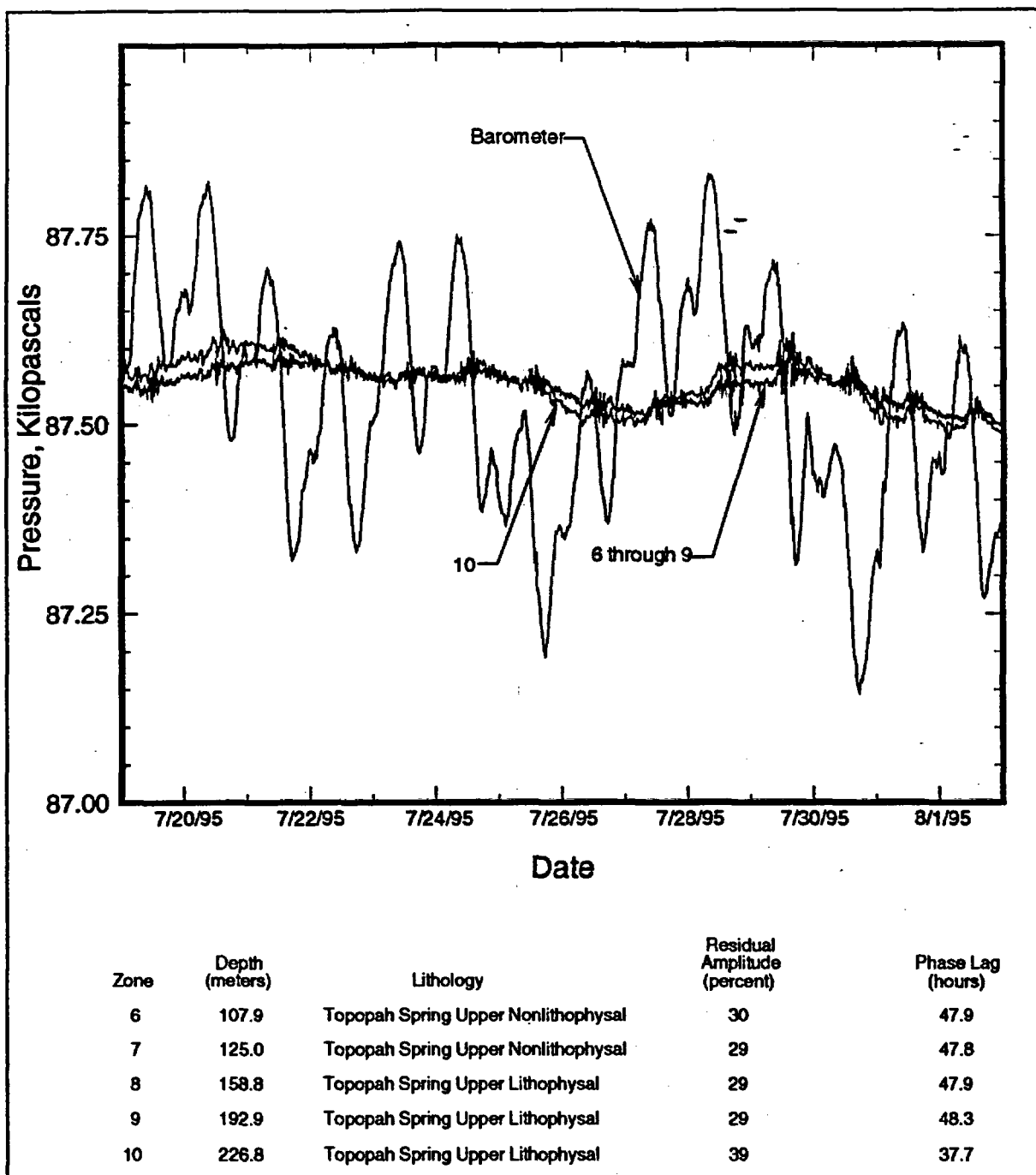


Figure 5b. Pressure record and the results of cross-spectral analysis on data from borehole UE-25 NRG#5 prior to the effects of ESF excavation.

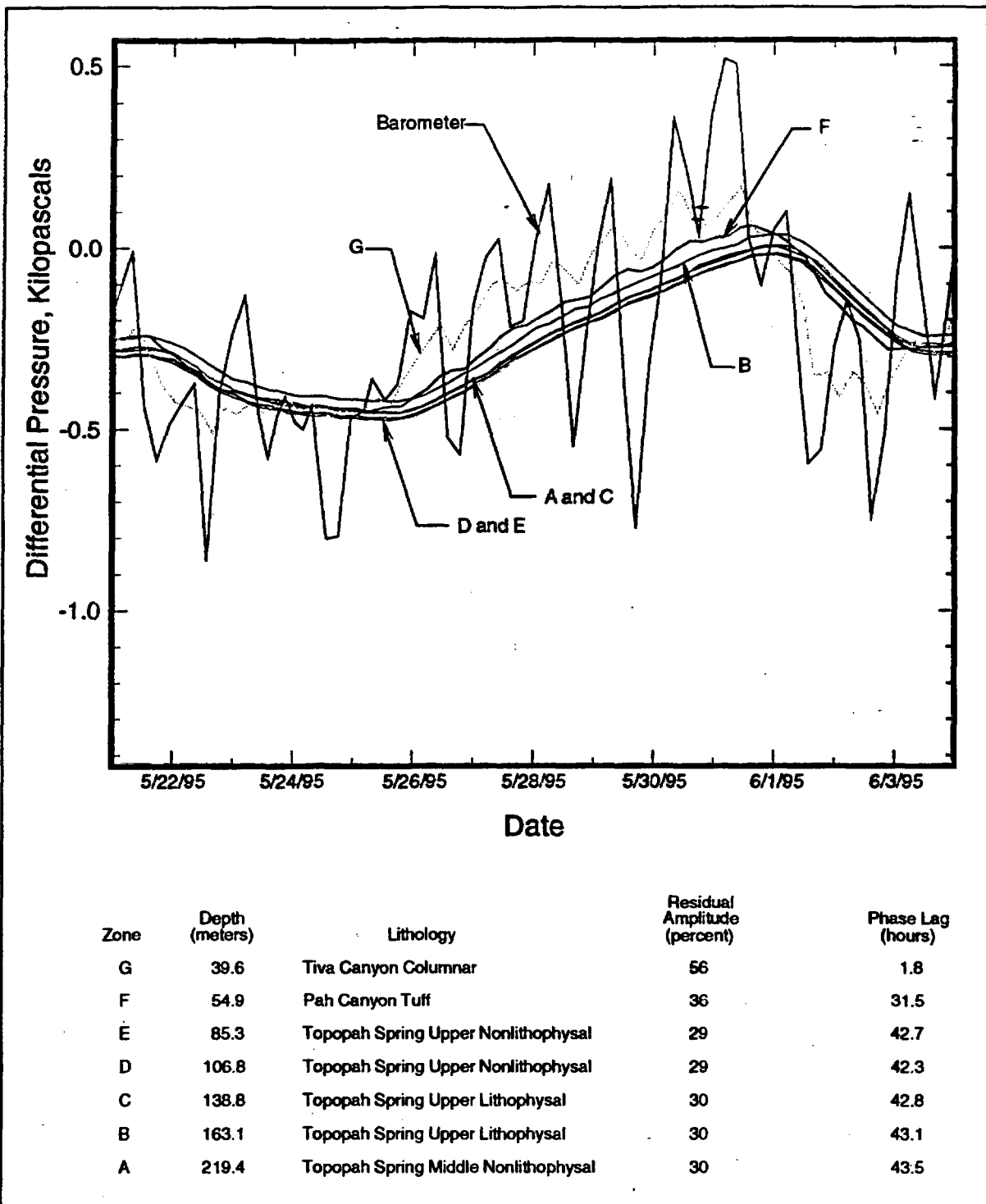


Figure 6. Pressure record and the results of cross-spectral analysis on data from borehole USW NRG-6 prior to the effects of ESF excavation.

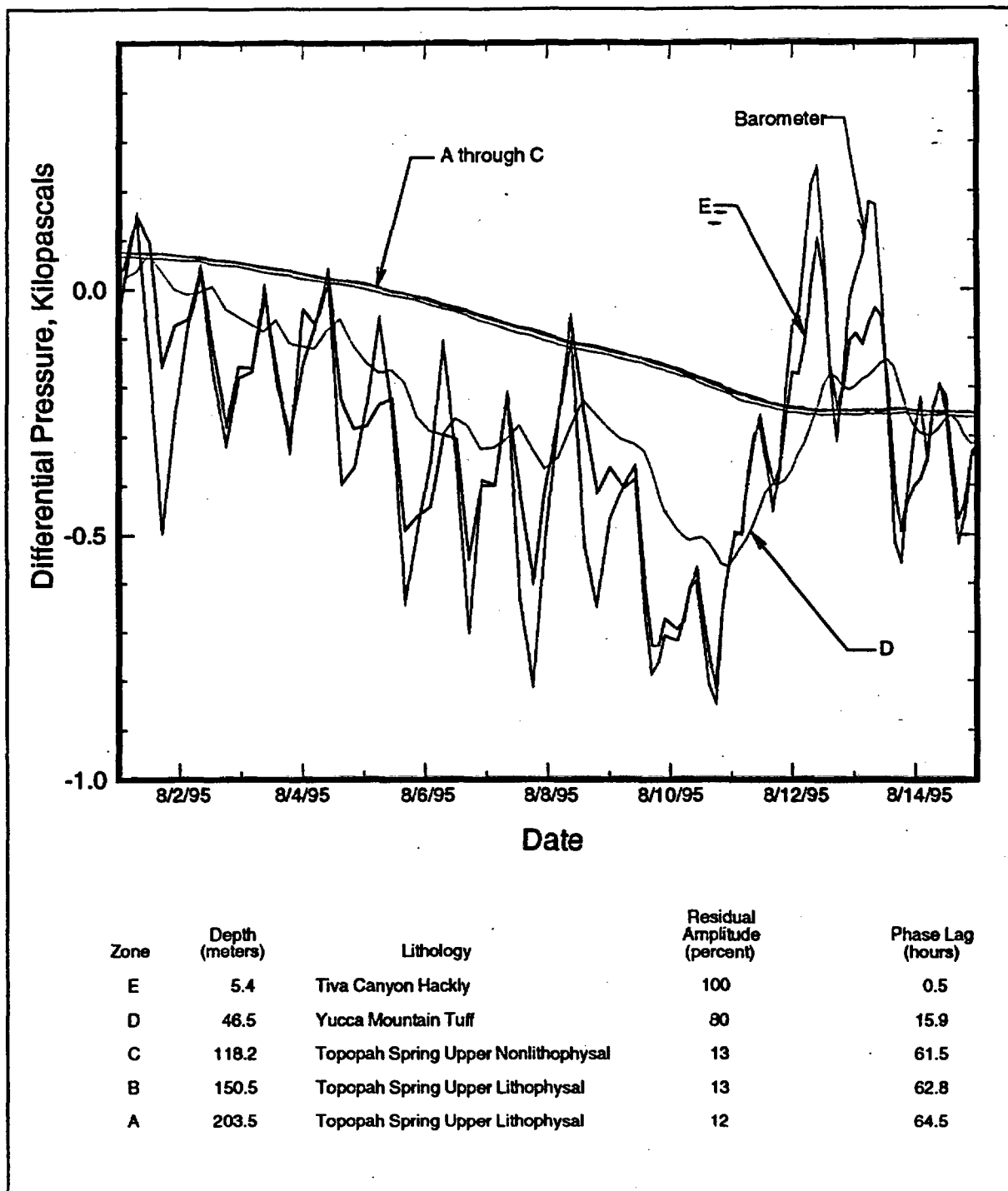
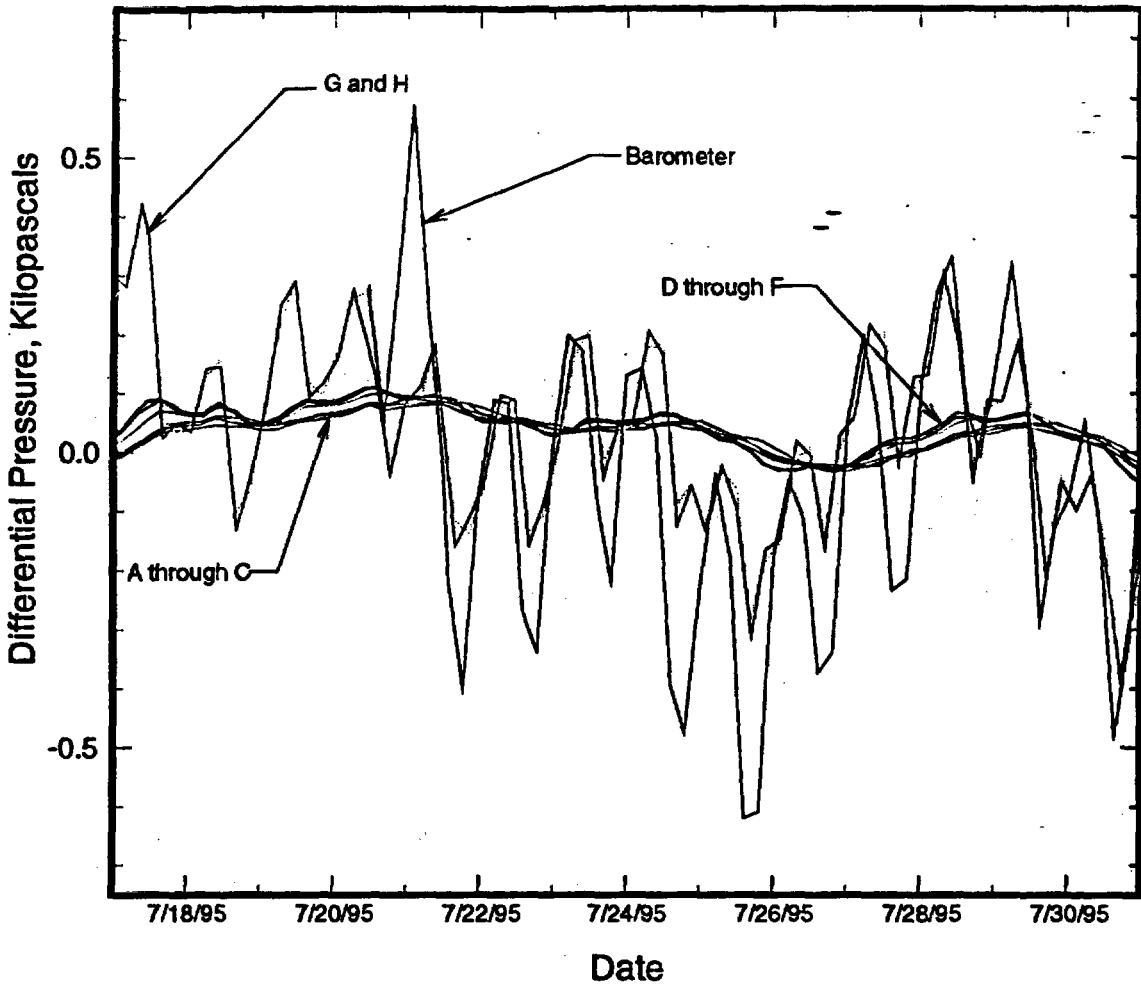


Figure 7. Pressure record and the results of cross-spectral analysis on data from borehole USW NRG-7a prior to the effects of ESF excavation.



Zone	Depth (meters)	Lithology	Residual Amplitude (percent)	Phase Lag (hours)
H	11.1	Alluvium/Colluvium	N/A	N/A
G	24.5	Tiva Canyon Crystal-Poor Vitric	N/A	N/A
F	35.2	Yucca Mountain Tuff	21	15.9
E	45.0	Yucca Mountain Tuff	21	16.5
D	55.9	Pah Canyon Tuff	21	20.3
C	88.2	Pah Canyon Tuff	16	26.5
B	104.1	Topopah Spring Crystal-Rich Vitric	15	23.7
A	112.0	Topopah Spring Upper Nonlithophysal	16	22.9

N/A = Not analyzed

Figure 8. Pressure record and the results of cross-spectral analysis on data from borehole UE-25 UZ#4 prior to the effects of ESF excavation.

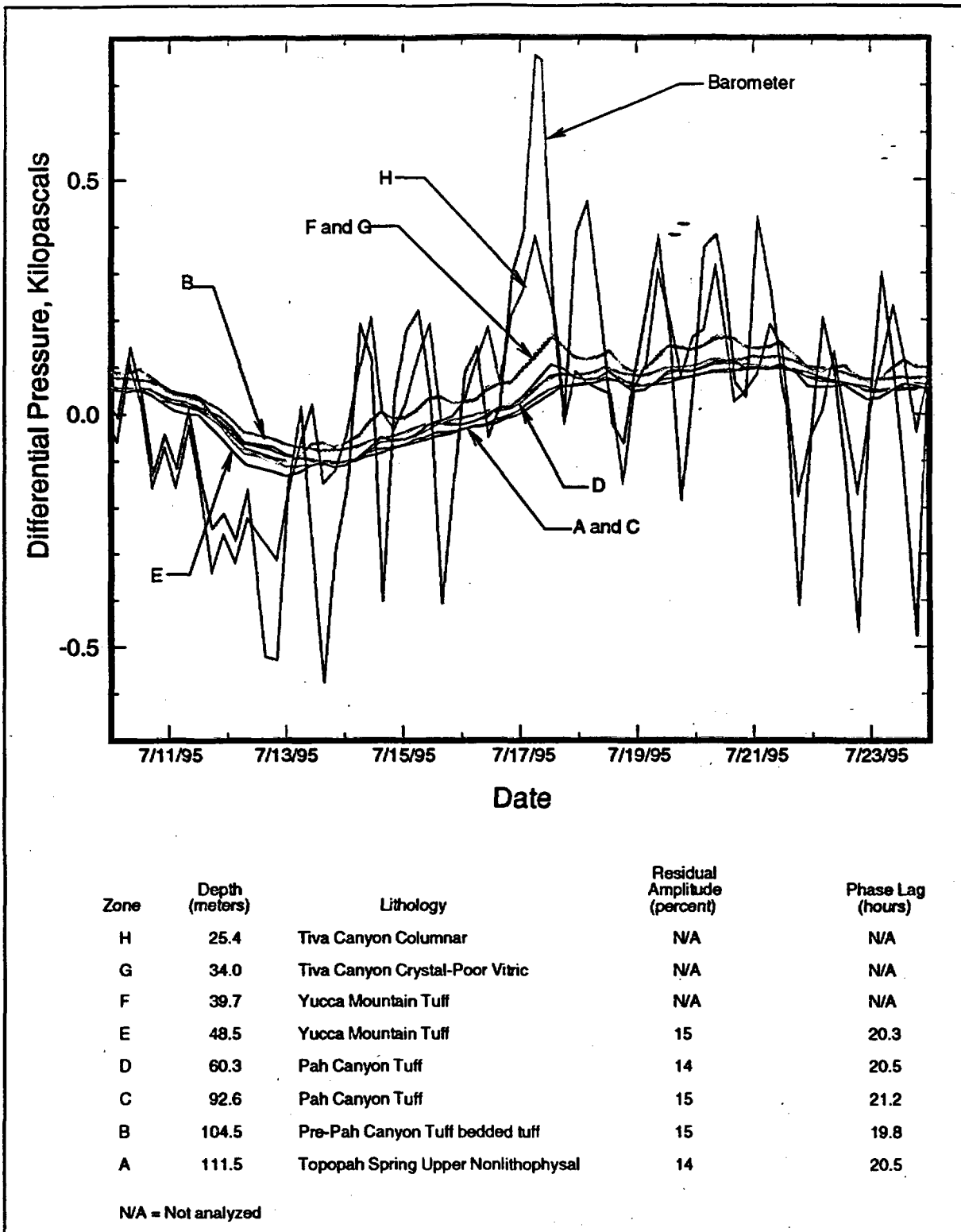


Figure 9. Pressure record and the results of cross-spectral analysis on data from borehole UE-25 UZ#5 prior to the effects of ESF excavation.

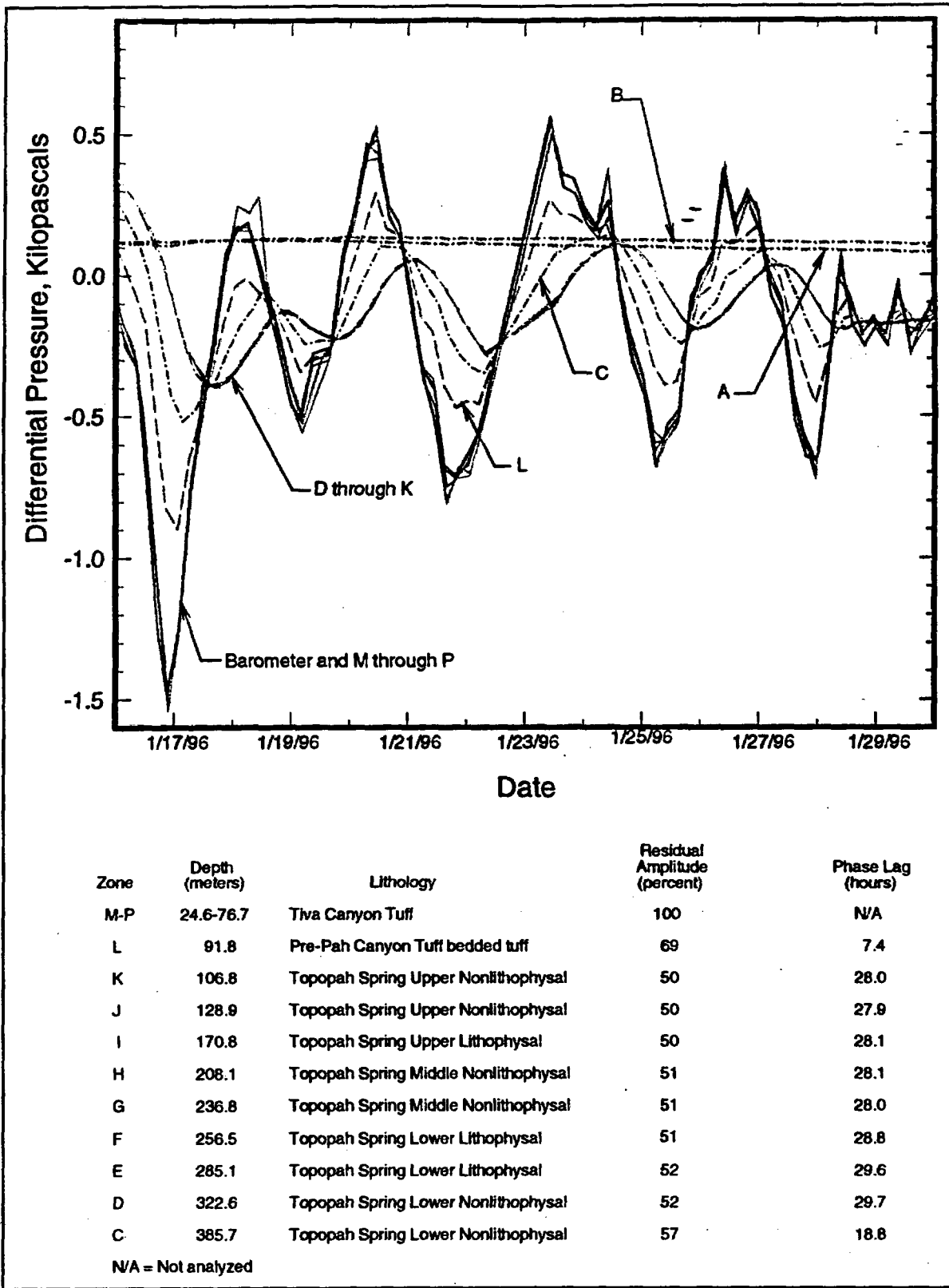


Figure 10. Pressure record and the results of cross-spectral analysis on data from borehole USW SD-12 prior to the effects of ESF excavation.

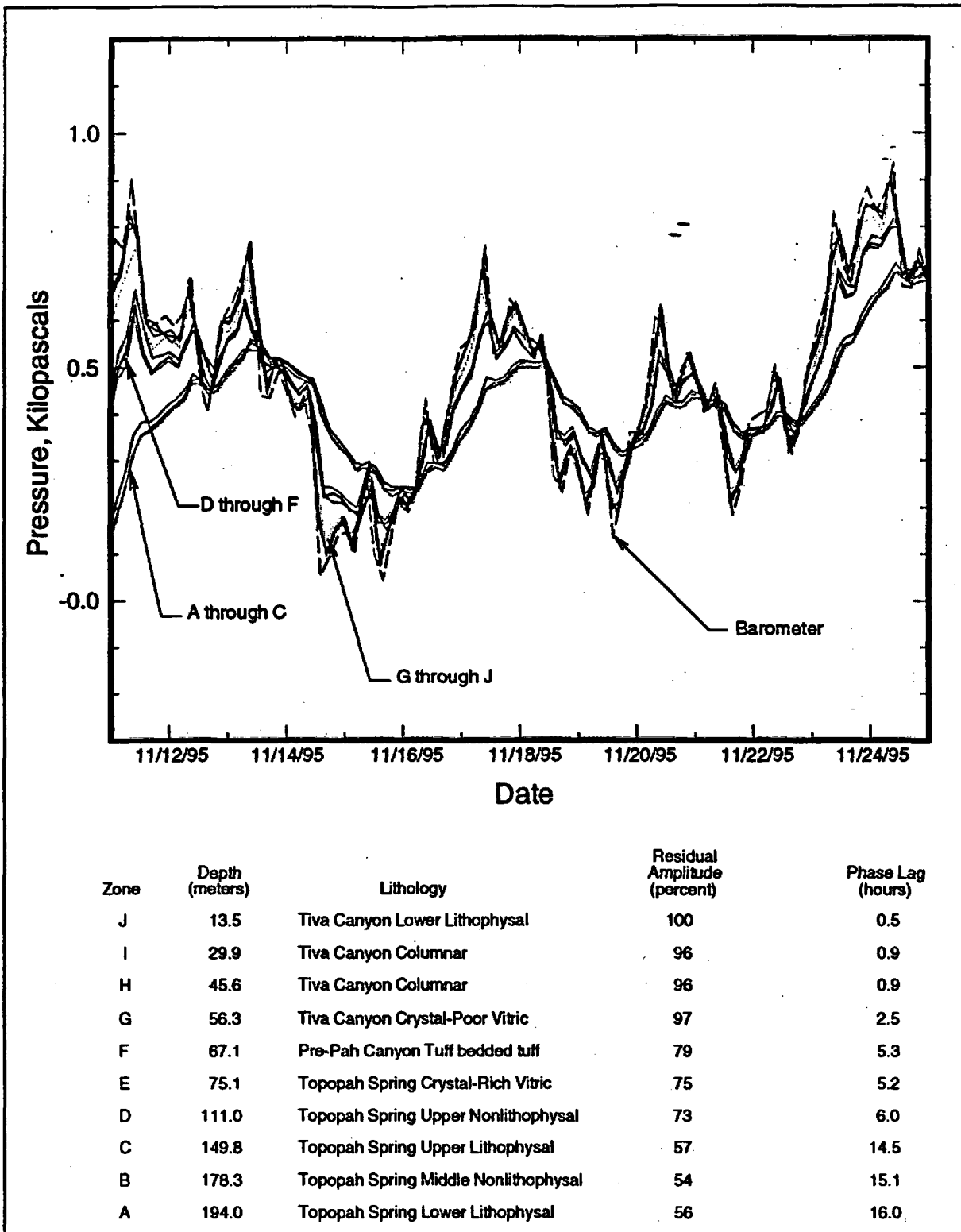


Figure 11. Pressure record and the results of cross-spectral analysis on data from borehole USW UZ-7a prior to the effects of ESF excavation.

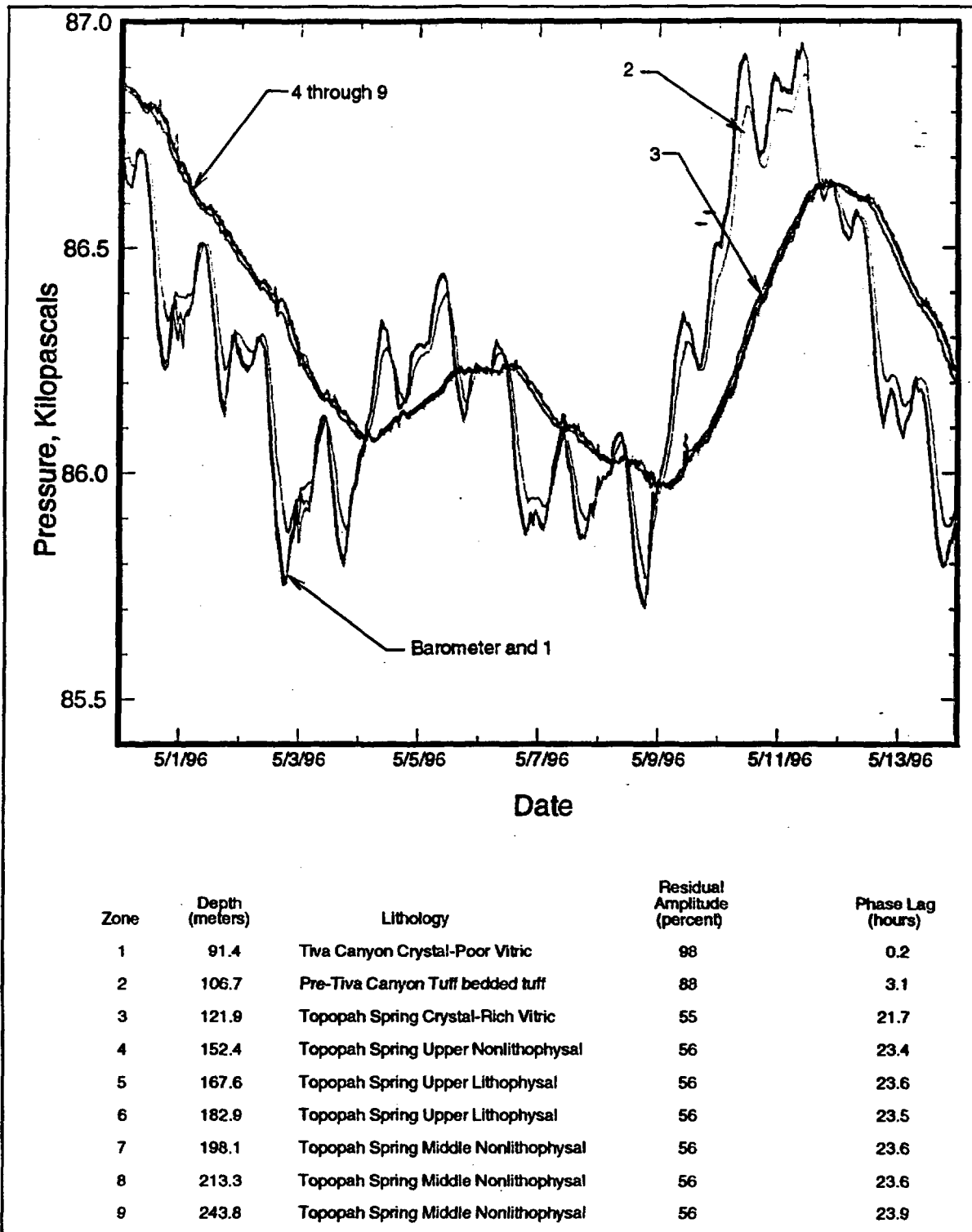


Figure 12. Pressure record and the results of cross-spectral analysis on data from borehole USW SD-7 prior to the effects of ESF excavation.

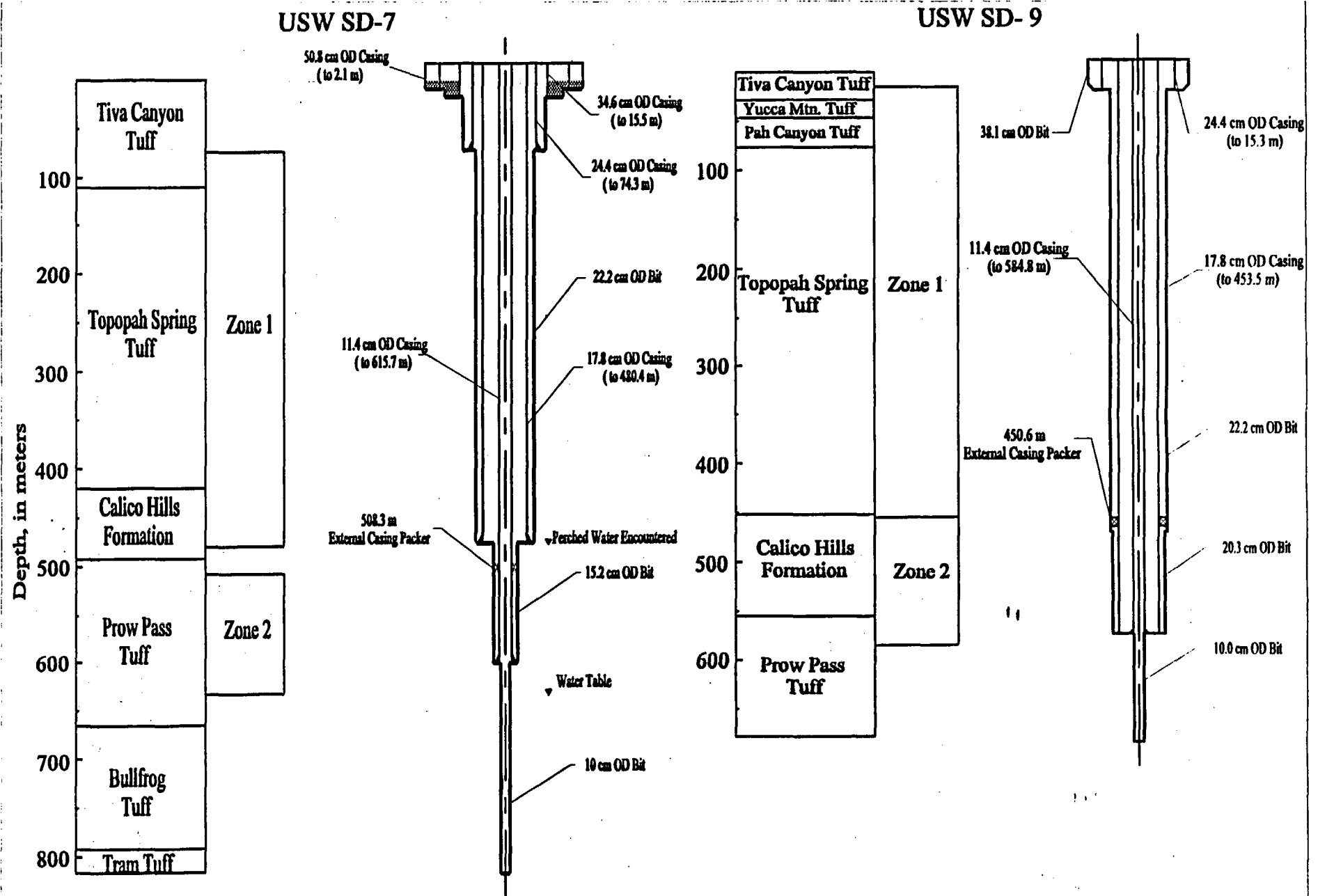


Figure 13. Casing configuration and monitoring zones at boreholes USW SD-9 and USW SD-7.

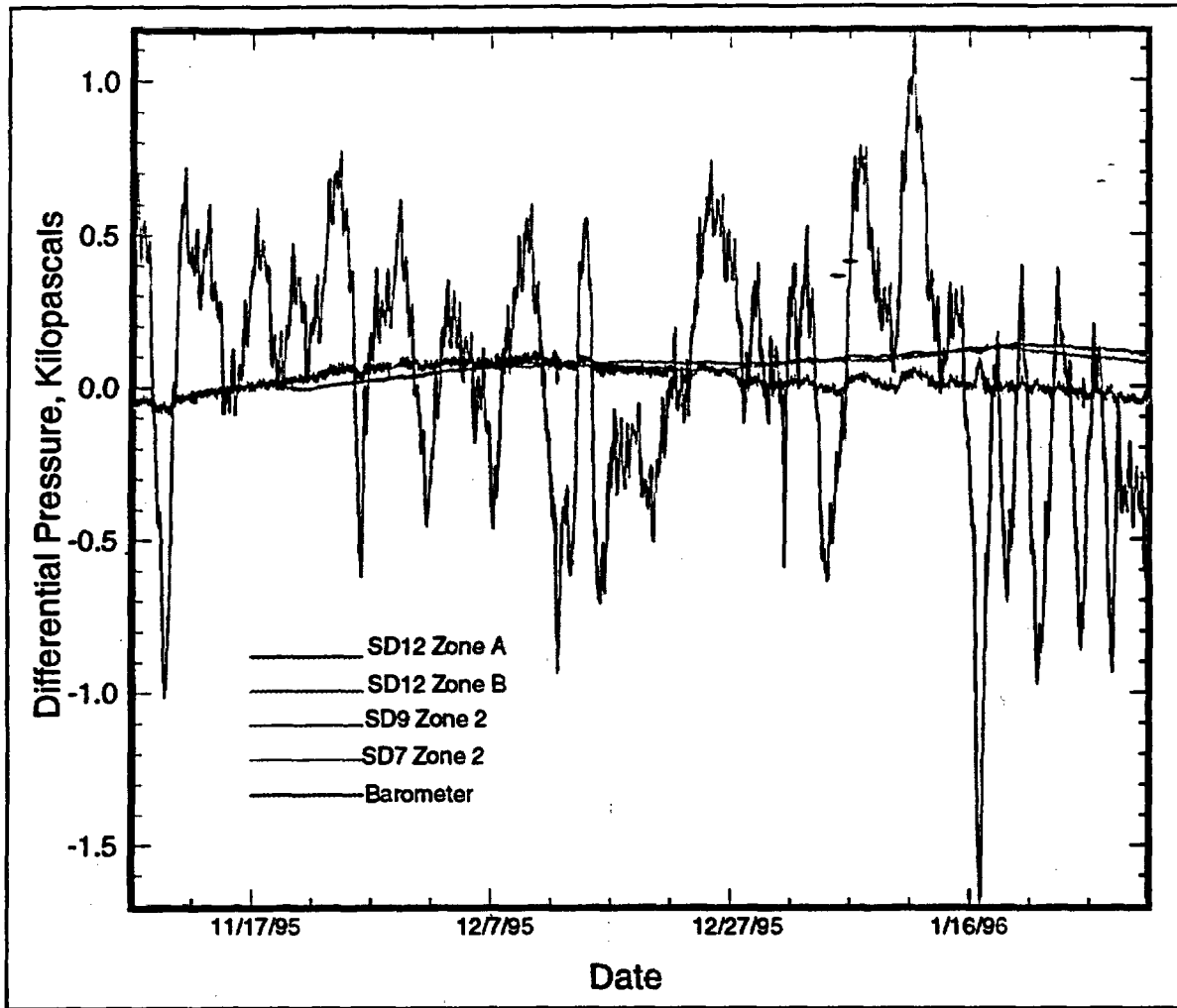


Figure 14. Pressure record from monitoring stations below perched water.

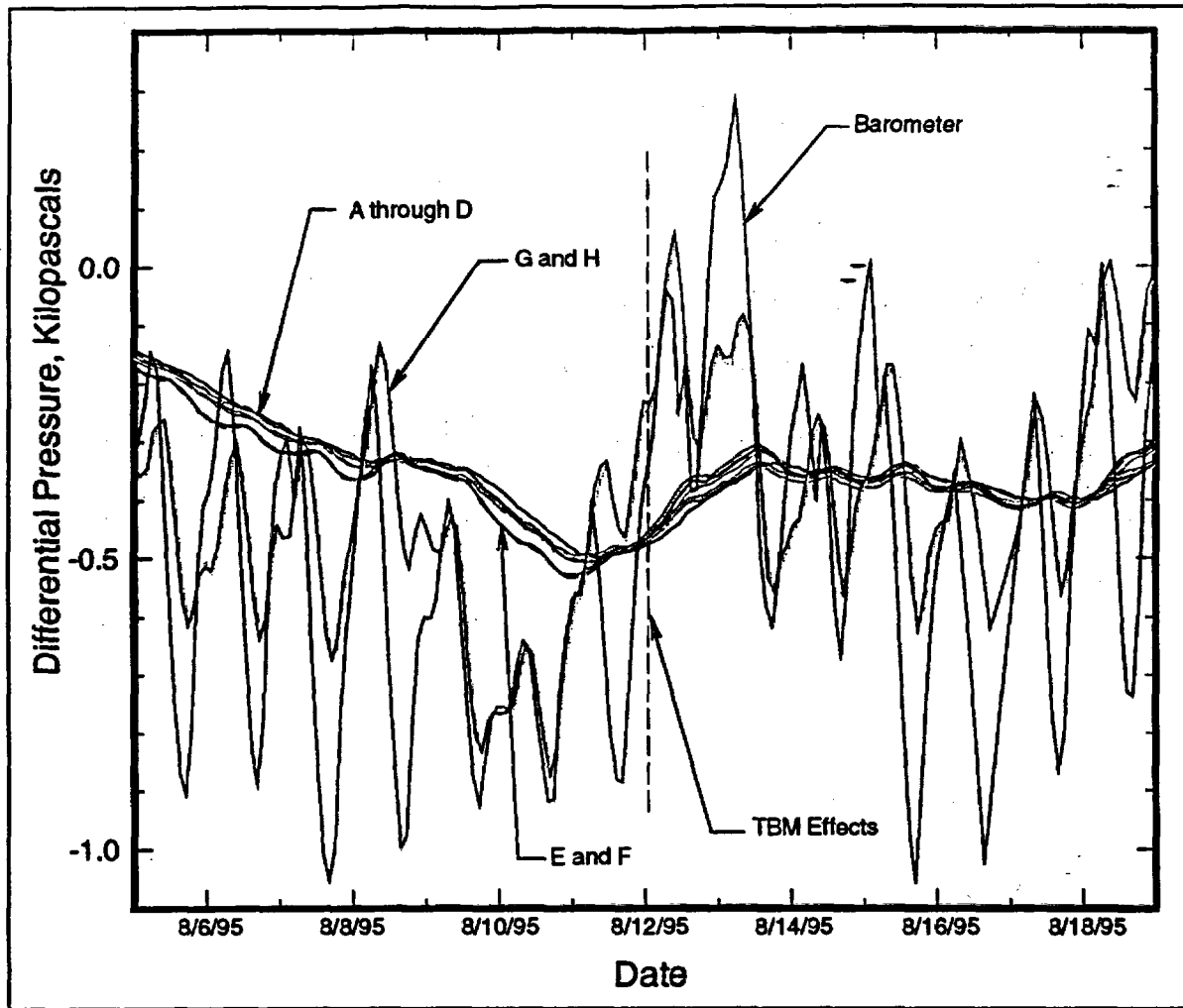


Figure 15. Selected onset of the effects of ESF excavation on pneumatic pressures at borehole UE-25 UZ#4.

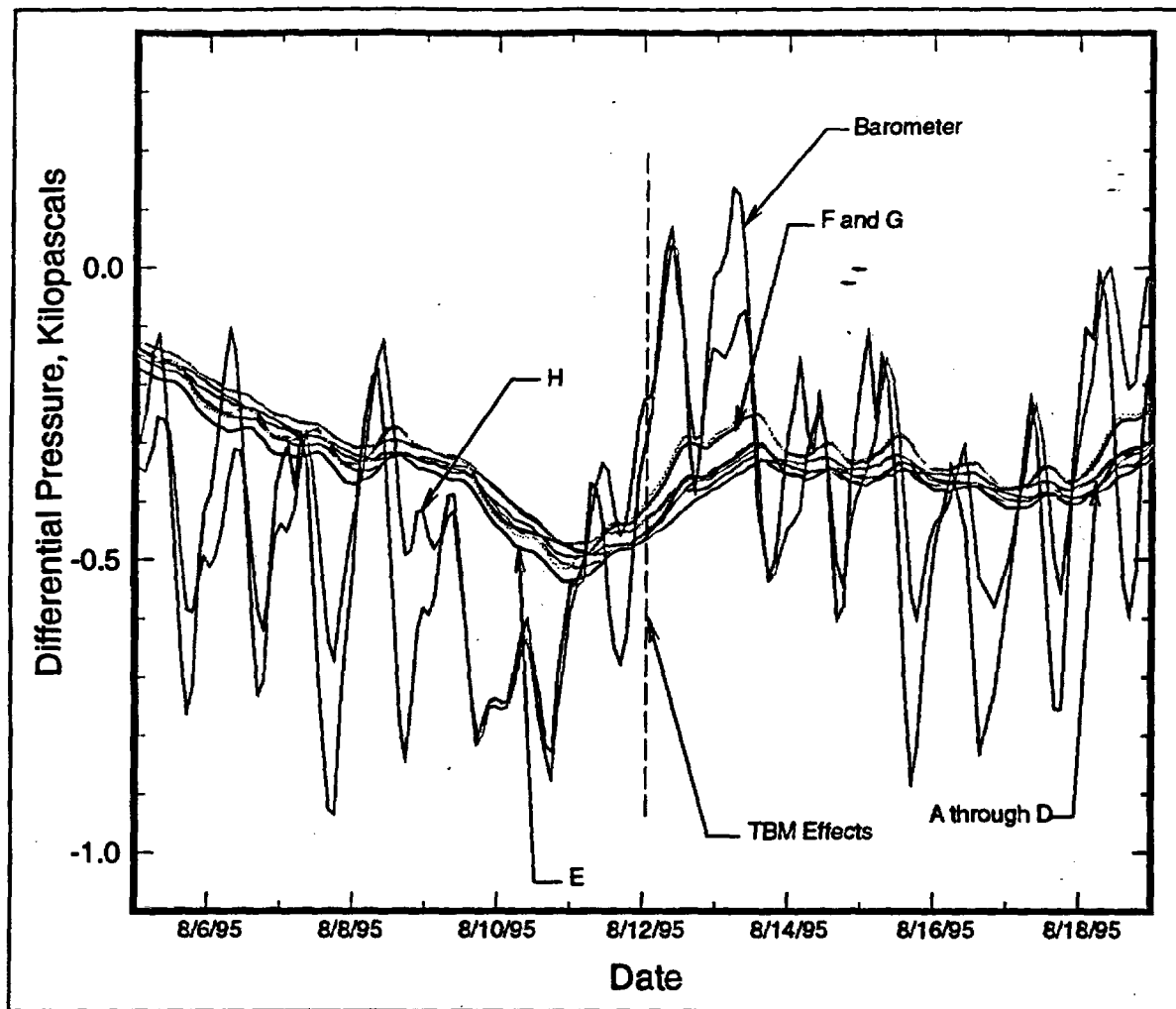


Figure 16. Selected onset of the effects of ESF excavation on pneumatic pressures at borehole UE-25 UZ#5.

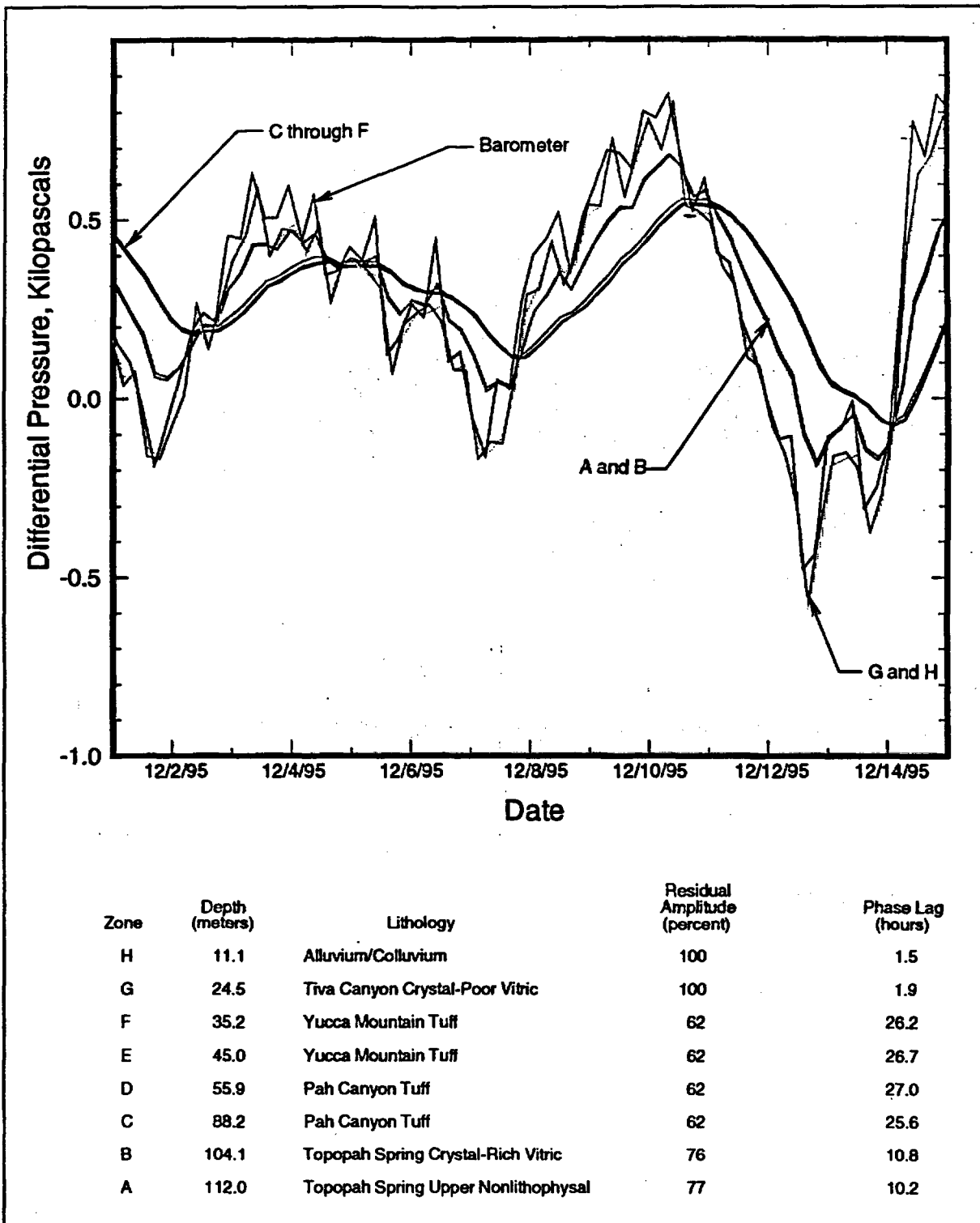


Figure 17. Pressure record and the results of cross-spectral analysis on data from borehole UE-25 UZ#4 after the effects of ESF excavation.

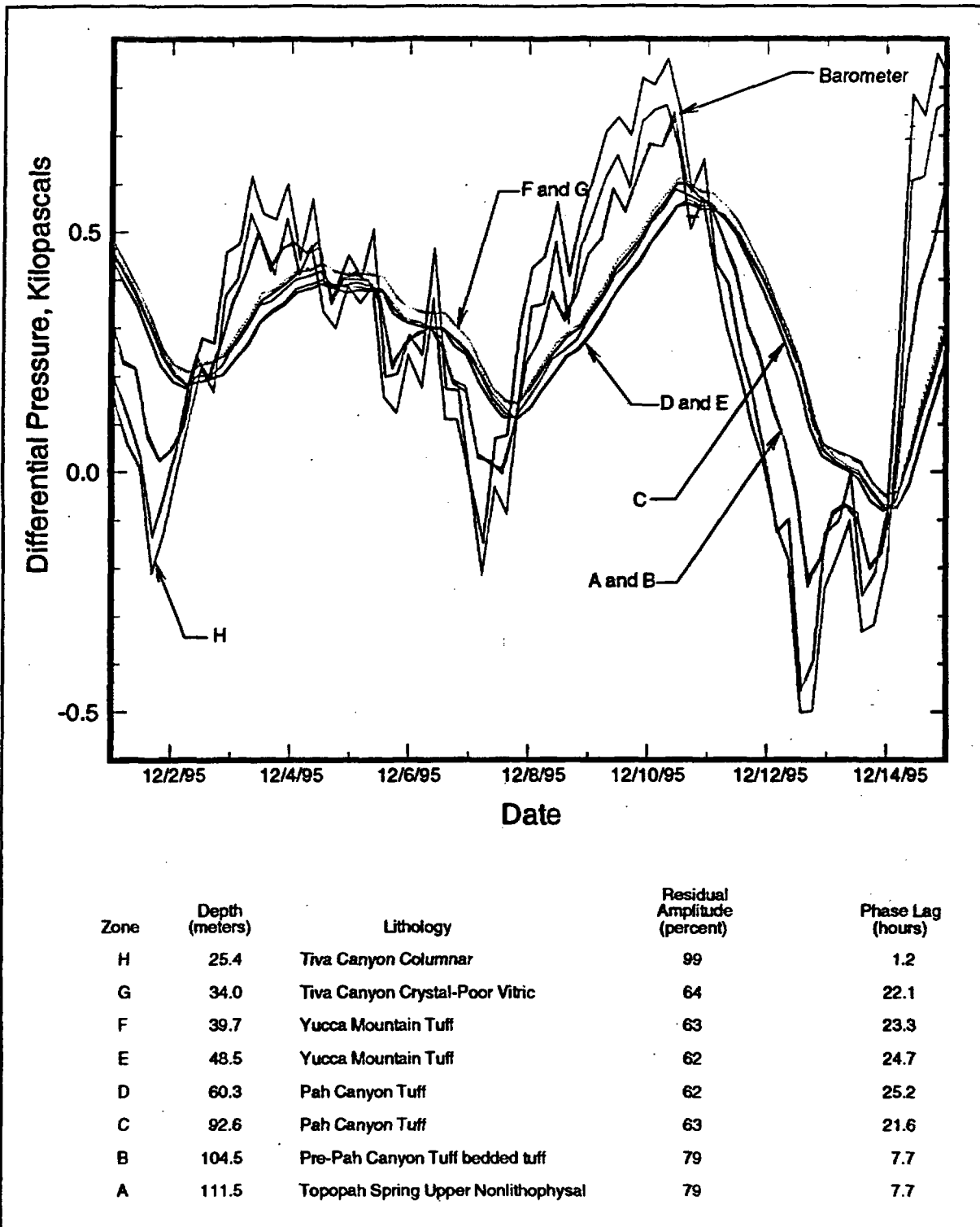


Figure 18. Pressure record and the results of cross-spectral analysis on data from borehole UE-25 UZ#5 after the effects of ESF excavation.

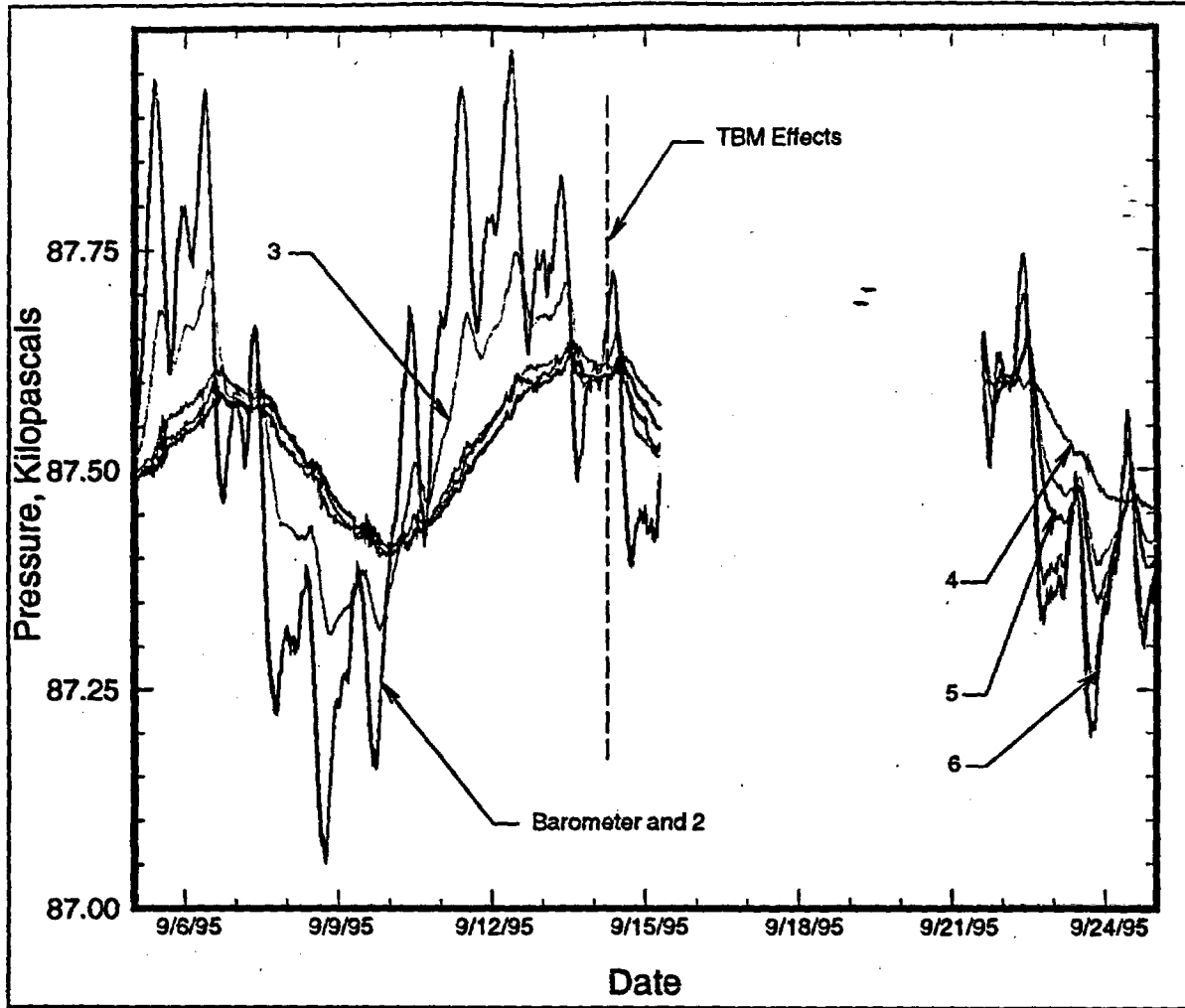


Figure 19a. Selected onset of the effects of ESF excavation on pneumatic pressures at borehole UE-25 NRG#5.

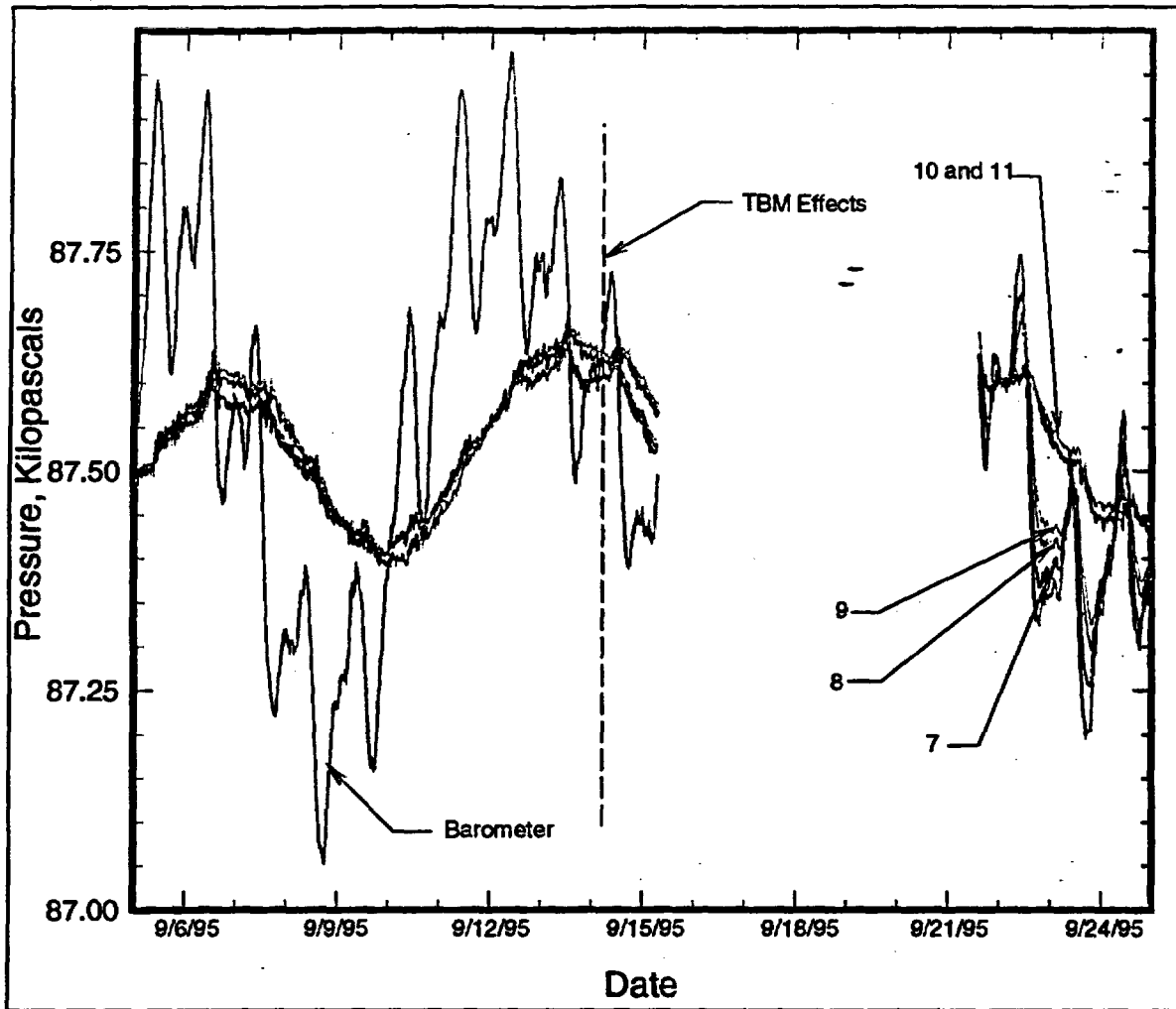


Figure 19b. Selected onset of the effects of ESF excavation on pneumatic pressures at borehole UE-25 NRG#5.

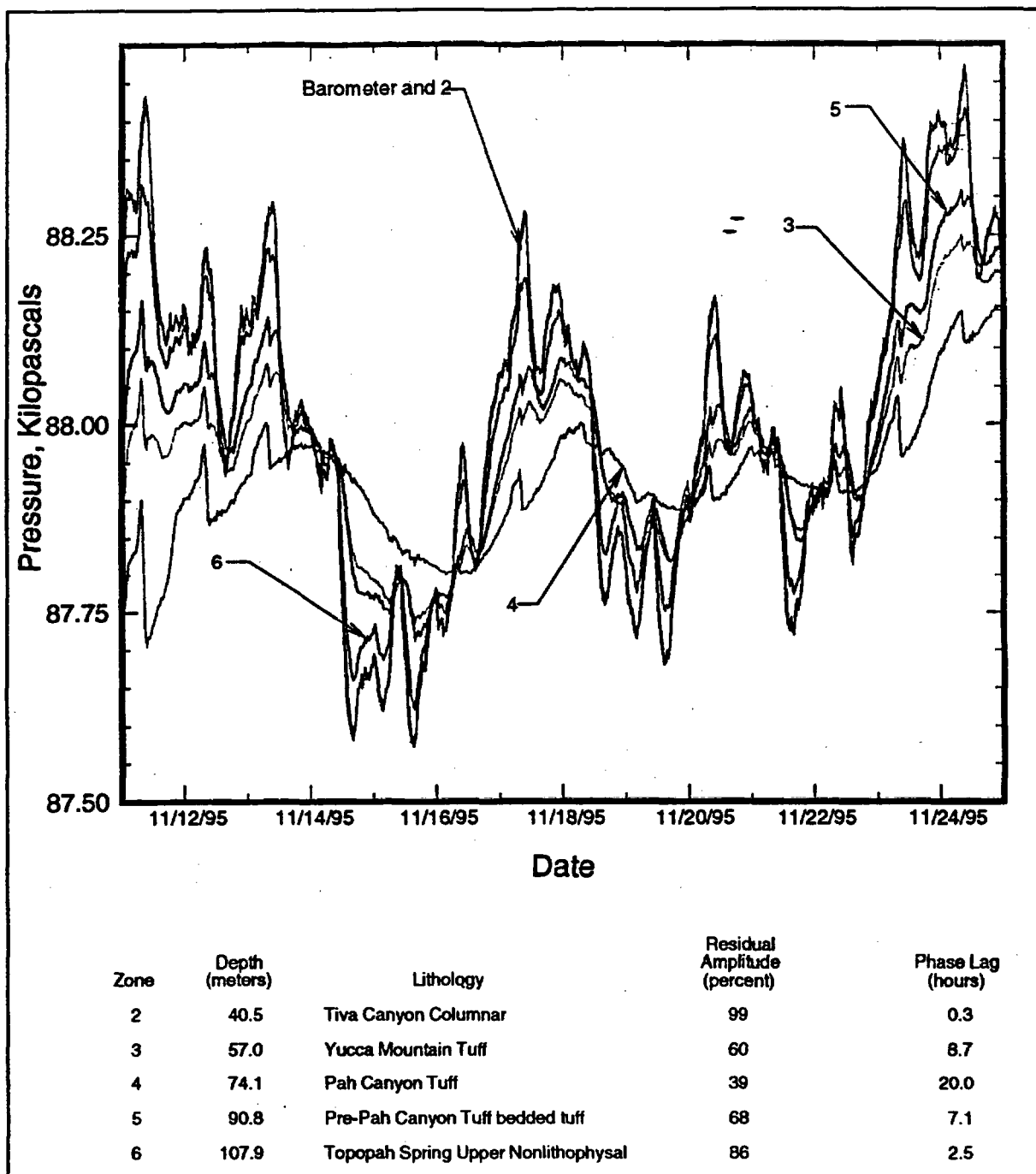


Figure 20a. Pressure record and the results of cross-spectral analysis on data from borehole UE-25 NRG#5 after the effects of ESF excavation.

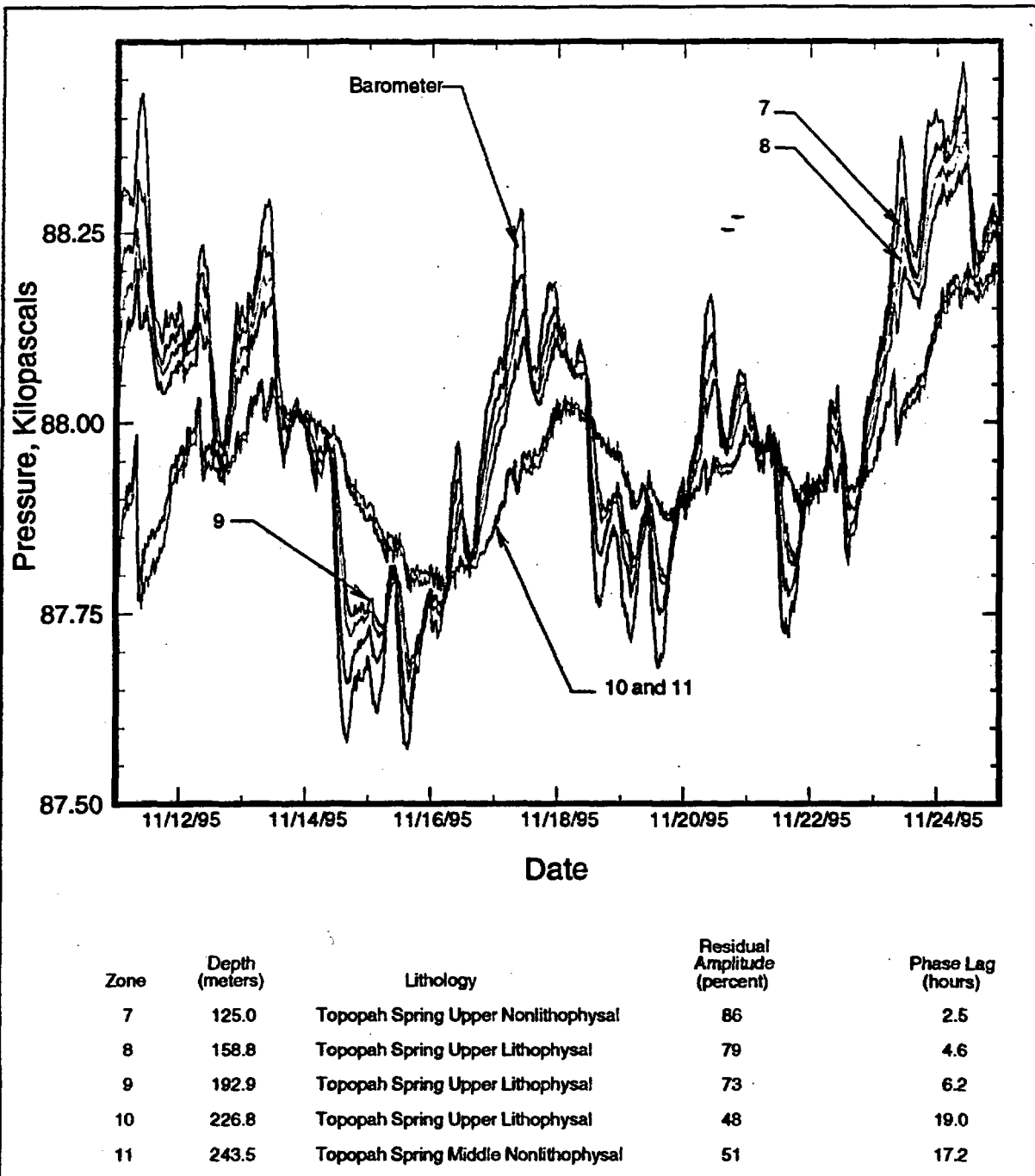


Figure 20b. Pressure record and the results of cross-spectral analysis on data from borehole UE-25 NRG#5 after the effects of ESF excavation.

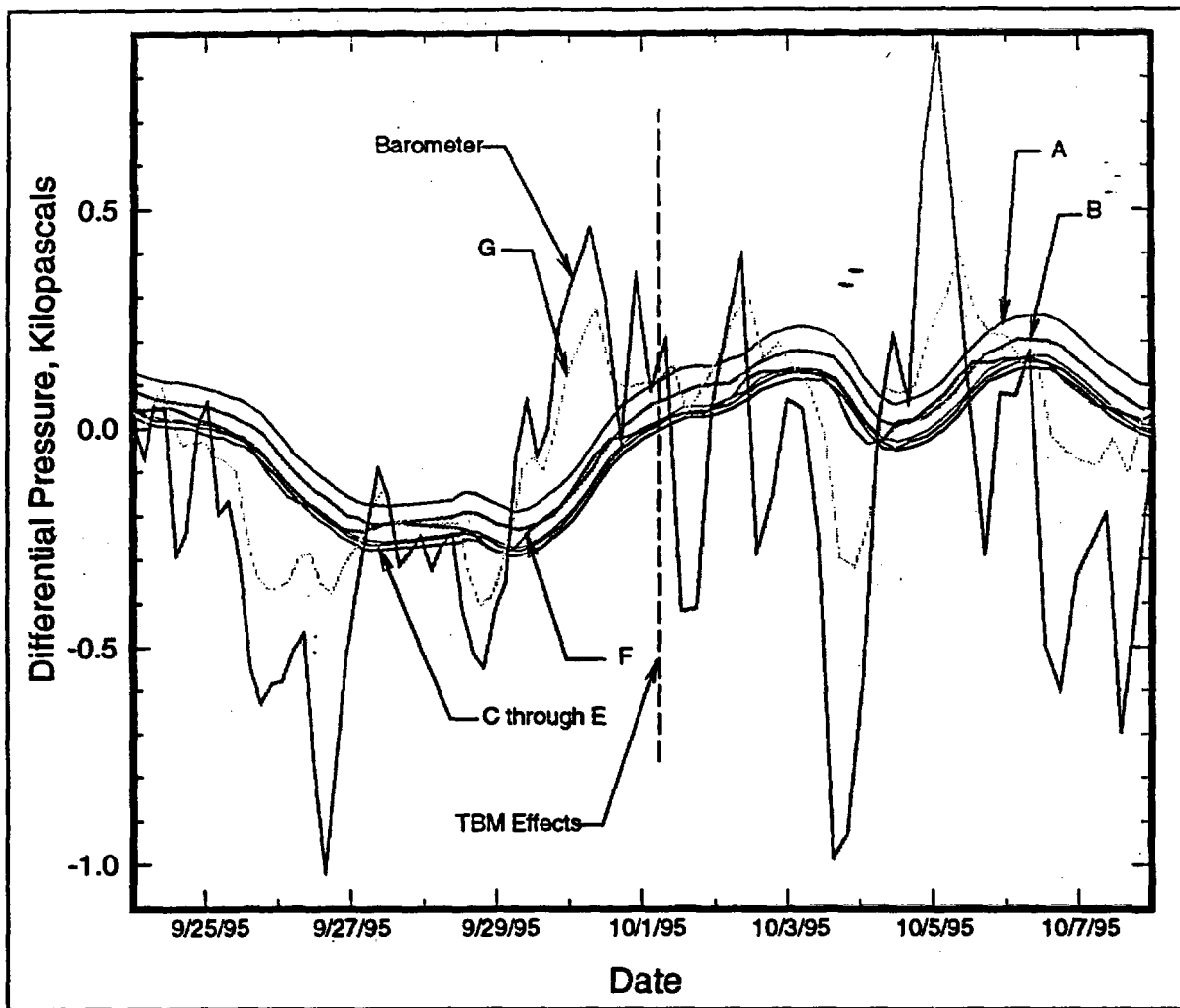


Figure 21. Selected onset of the effects of ESF excavation on pneumatic pressures at borehole USW NRG-6.

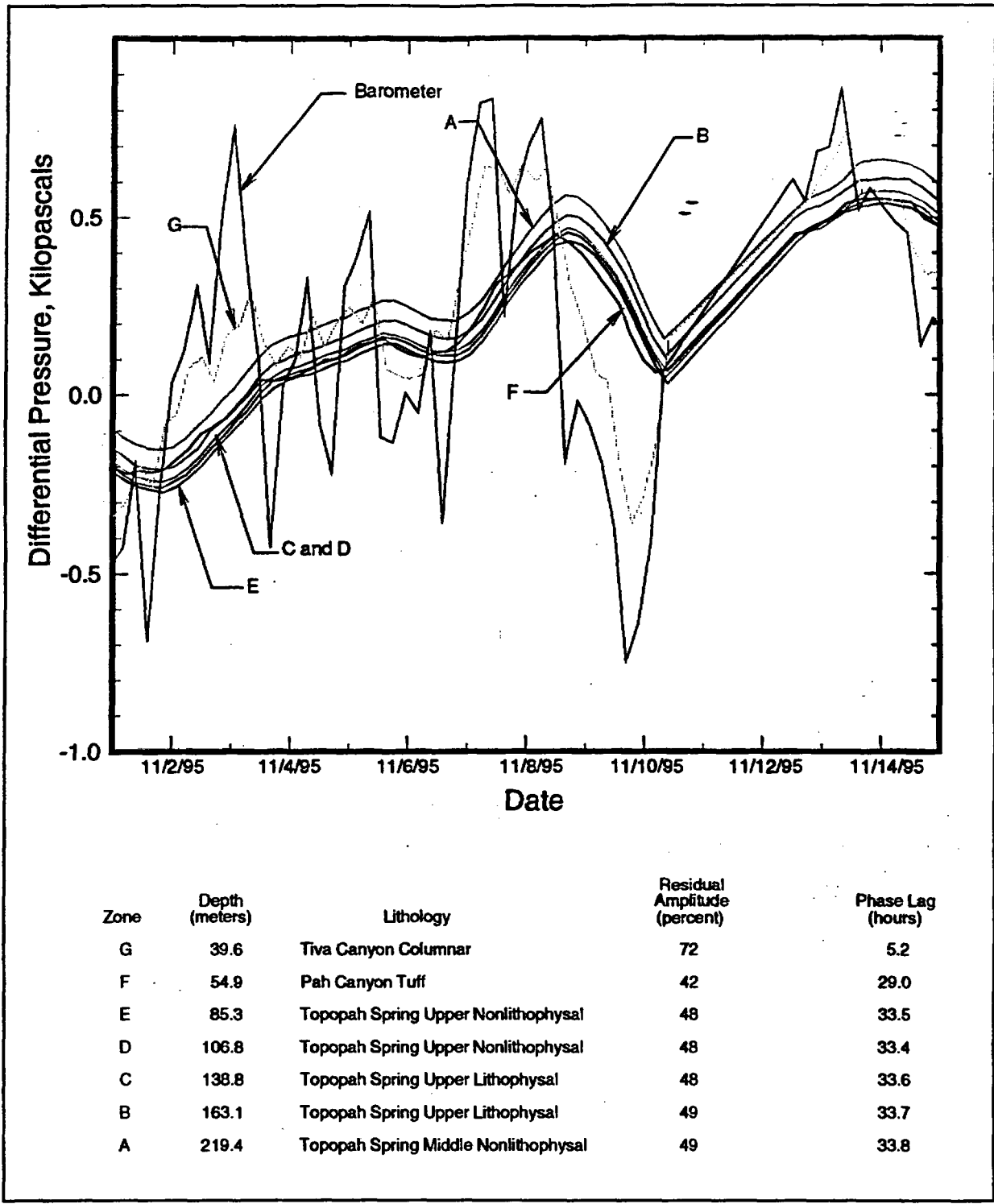


Figure 22. Pressure record and the results of cross-spectral analysis on data from borehole USW NRG-6 after the effects of ESF excavation.

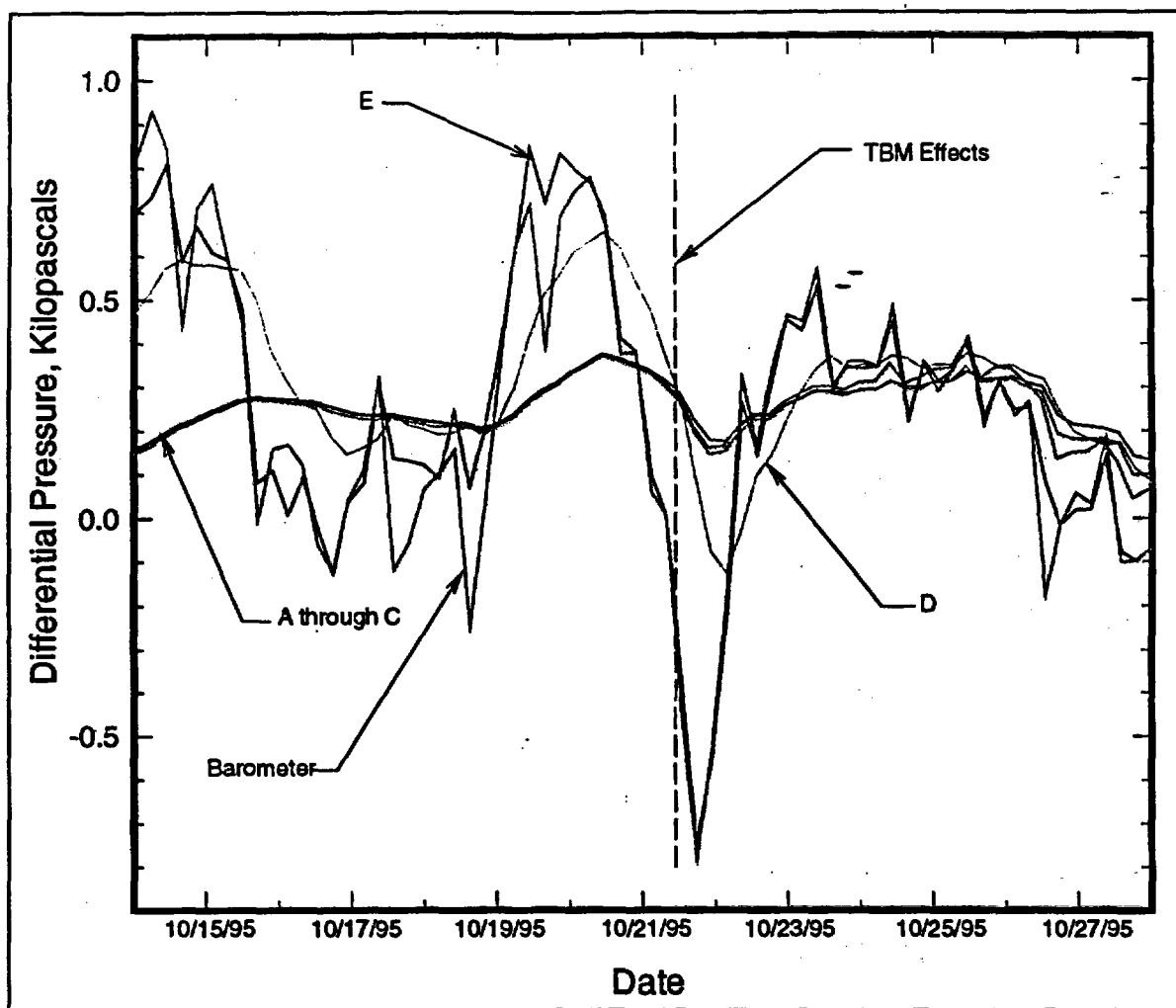


Figure 23. Selected onset of the effects of ESF excavation on pneumatic pressures at borehole USW NRG-7a.

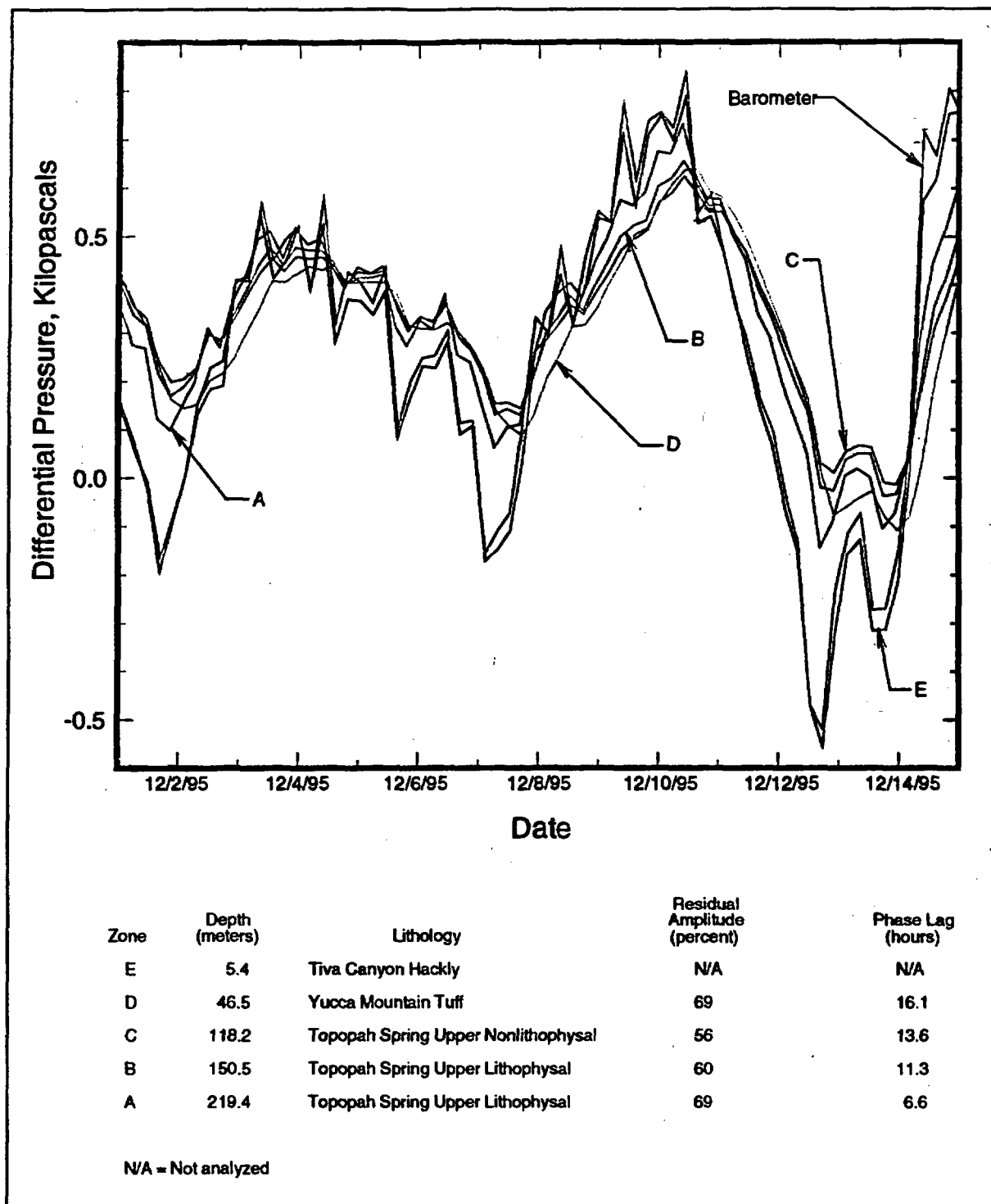


Figure 24. Pressure record and the results of cross-spectral analysis on data from borehole USW NRG-7a after the effects of ESF excavation.

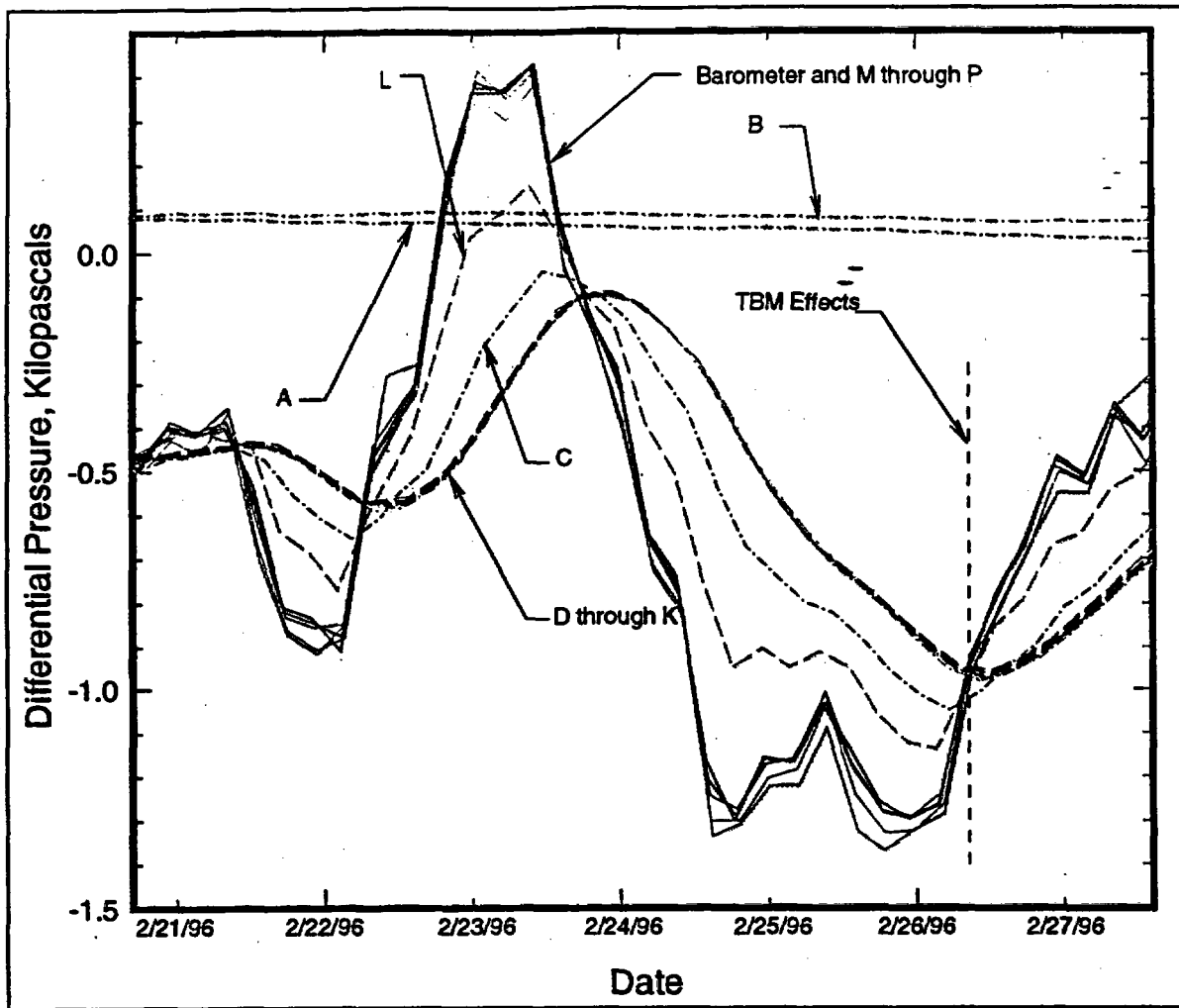
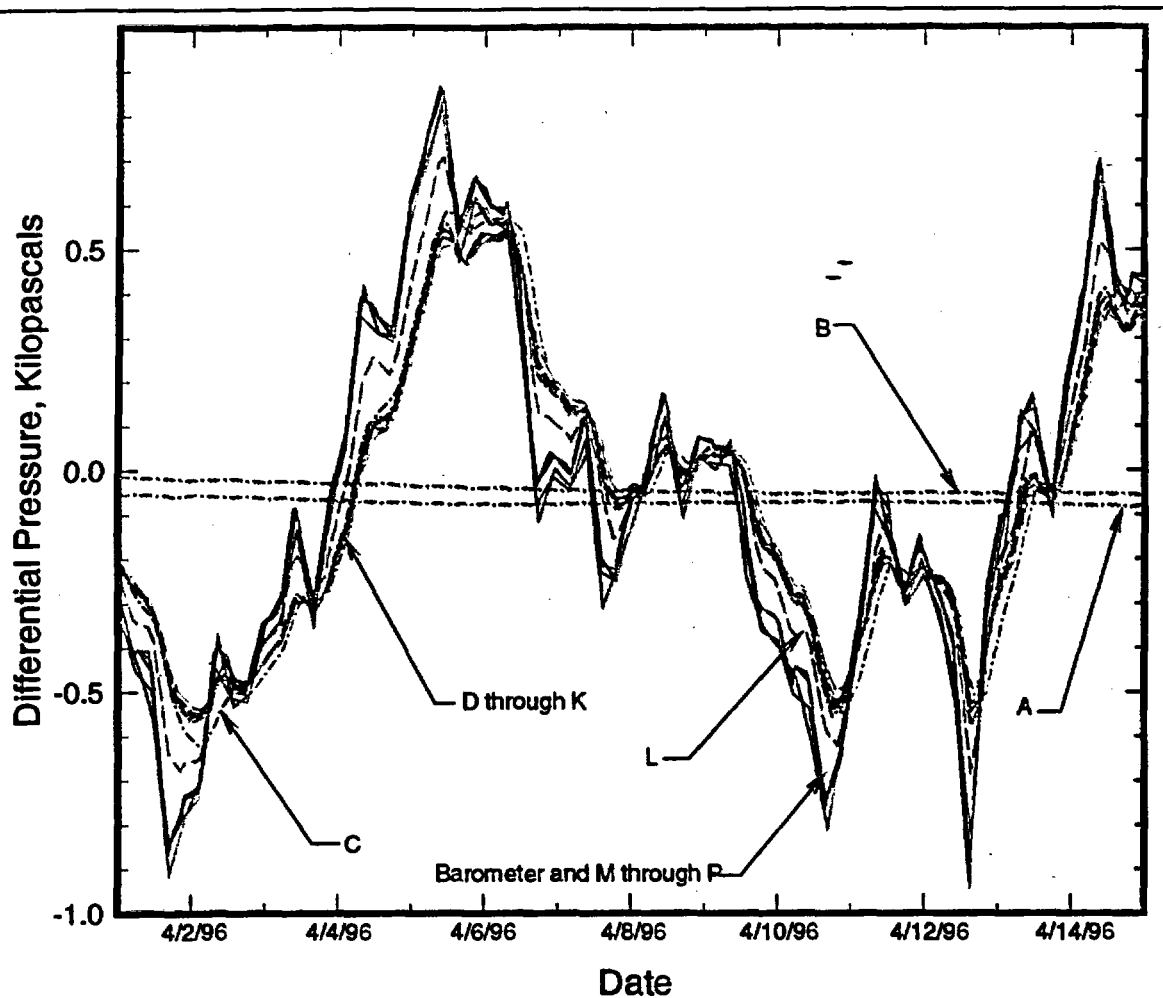


Figure 25. Selected onset of the effects of ESF excavation on pneumatic pressures at borehole USW SD-12.



Zone	Depth (meters)	Lithology	Residual Amplitude (percent)	Phase Lag (hours)
M-P	24.6-76.7	Tiva Canyon Tuff	100	0.4
L	91.8	Pre-Pah Canyon Tuff bedded tuff	85	4.4
K	106.8	Topopah Spring Upper Nonlithophysal	69	10.3
J	128.9	Topopah Spring Upper Nonlithophysal	69	10.4
I	170.8	Topopah Spring Upper Lithophysal	70	10.2
H	208.1	Topopah Spring Middle Nonlithophysal	71	9.3
G	236.8	Topopah Spring Middle Nonlithophysal	72	8.8
F	256.5	Topopah Spring Lower Lithophysal	74	8.2
E	285.1	Topopah Spring Lower Lithophysal	74	8.3
D	322.6	Topopah Spring Lower Nonlithophysal	74	8.6
C	385.7	Topopah Spring Lower Nonlithophysal	80	9.8

Figure 26. Pressure record and the results of cross-spectral analysis on data from borehole USW SD-12 after the effects of ESF excavation.

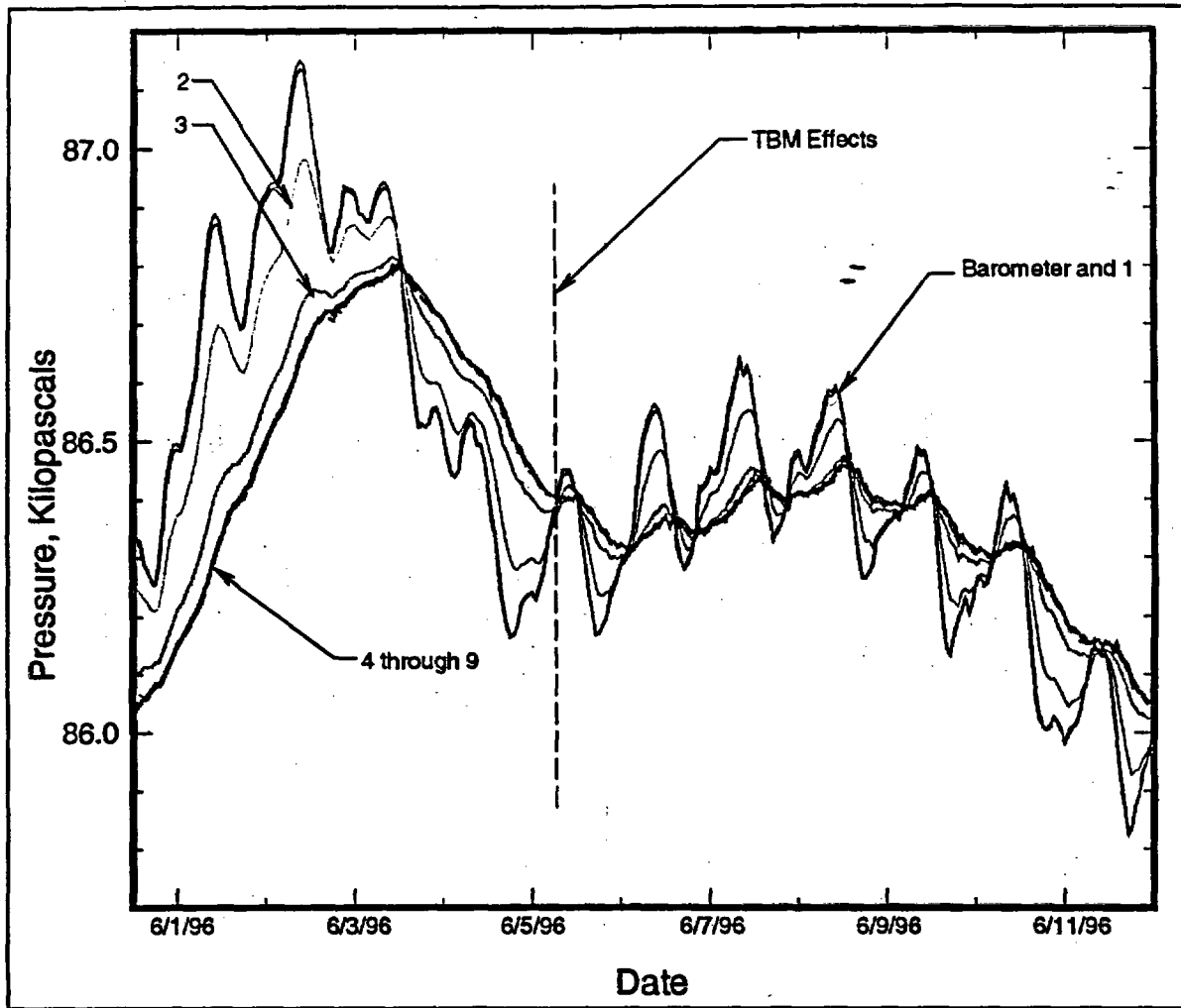


Figure 27. Selected onset of the effects of ESF excavation on pneumatic pressures at borehole USW SD-7.

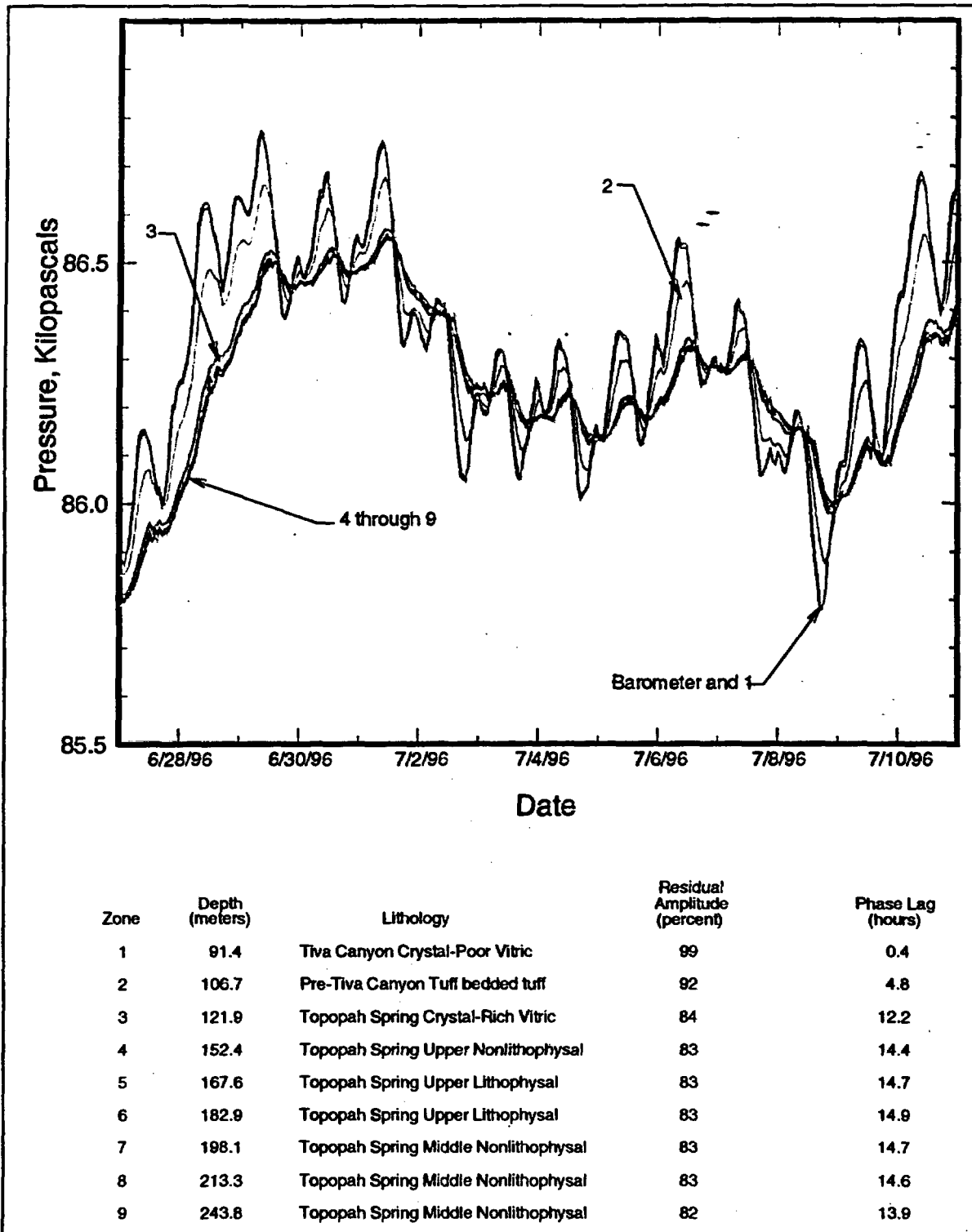


Figure 28. Pressure record and the results of cross-spectral analysis on data from borehole USW SD-7 after the effects of ESF excavation.

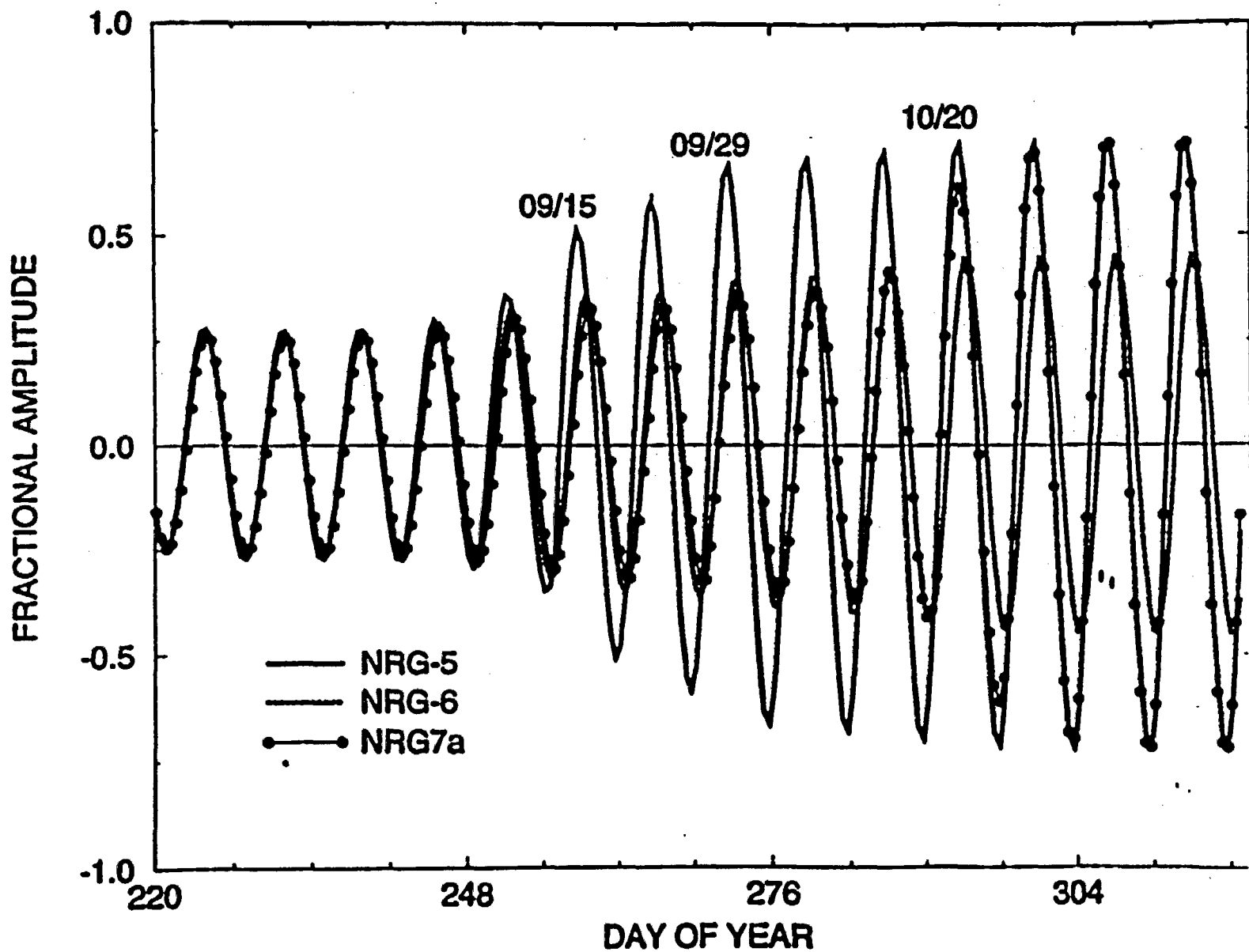
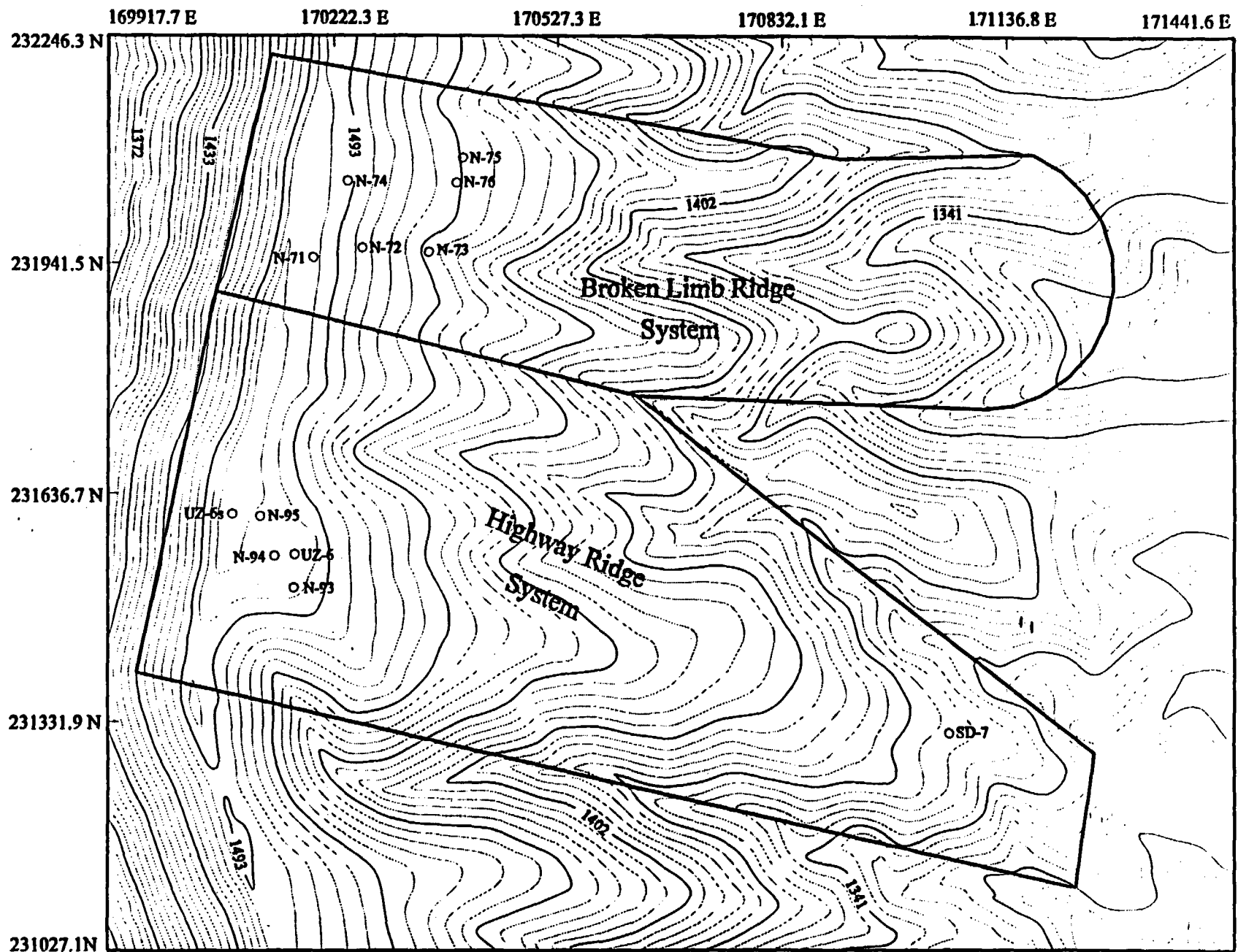


Figure 29. Results of simulation of pressure amplitudes in boreholes UE-25 NRG#5, US W NRG-6, and USW NRG-7a due to a unit amplitude barometric pressure change of one-week period with the tunnel position updated weekly.



304.8 m grid based on the Nevada State Plane coordinate system.
 6.1 m contour interval

0 100 200 300 400 500 METERS

Figure 30. Location of boreholes showing model boundaries.

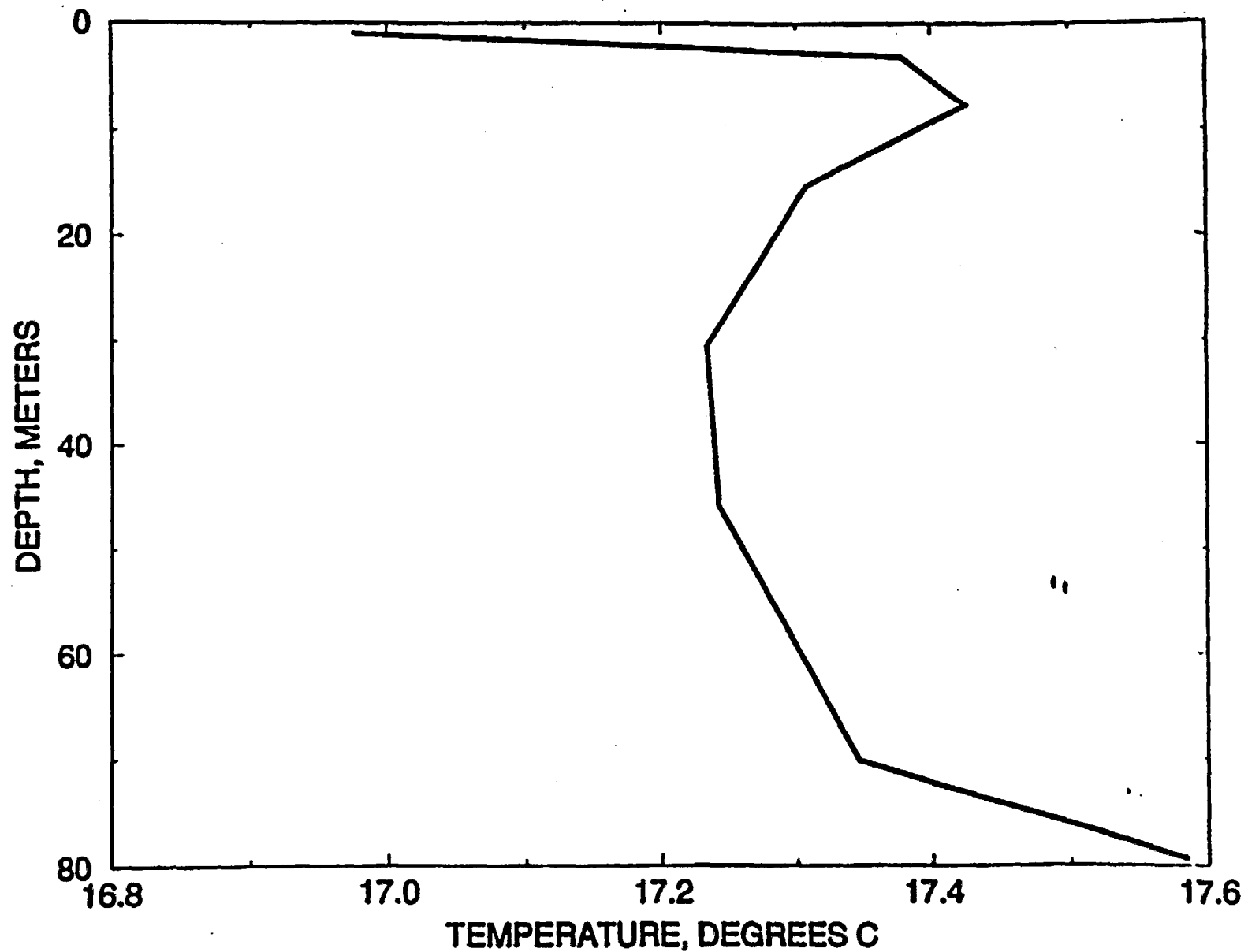


Figure 31. Gas temperature with depth during period of well exhaust, January-February, 1993.

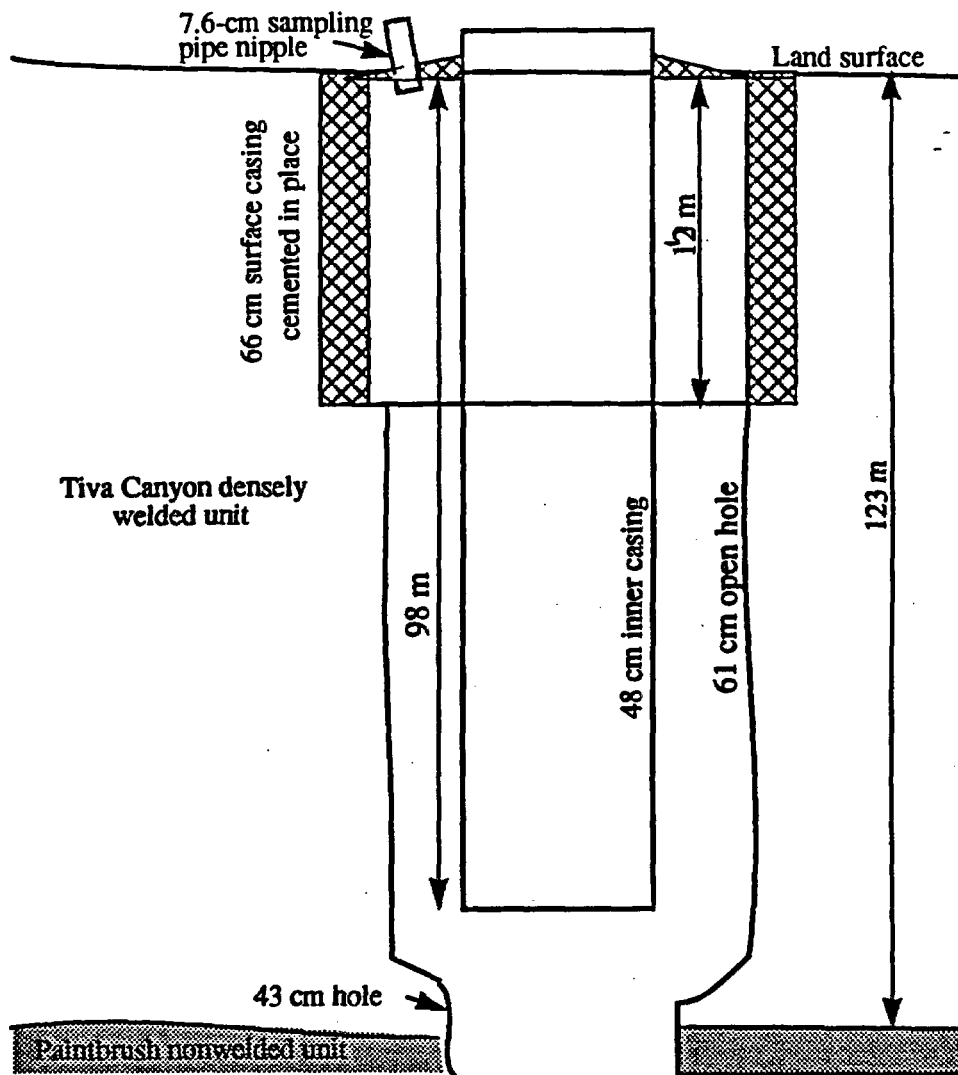


Figure 32. Sketch showing construction of upper part of well UZ6. The sampling pipe nipple has been braized into a hole in the steel cap over the surface casing, and cement has been poured around the inner casing to provide a complete seal against leakage.

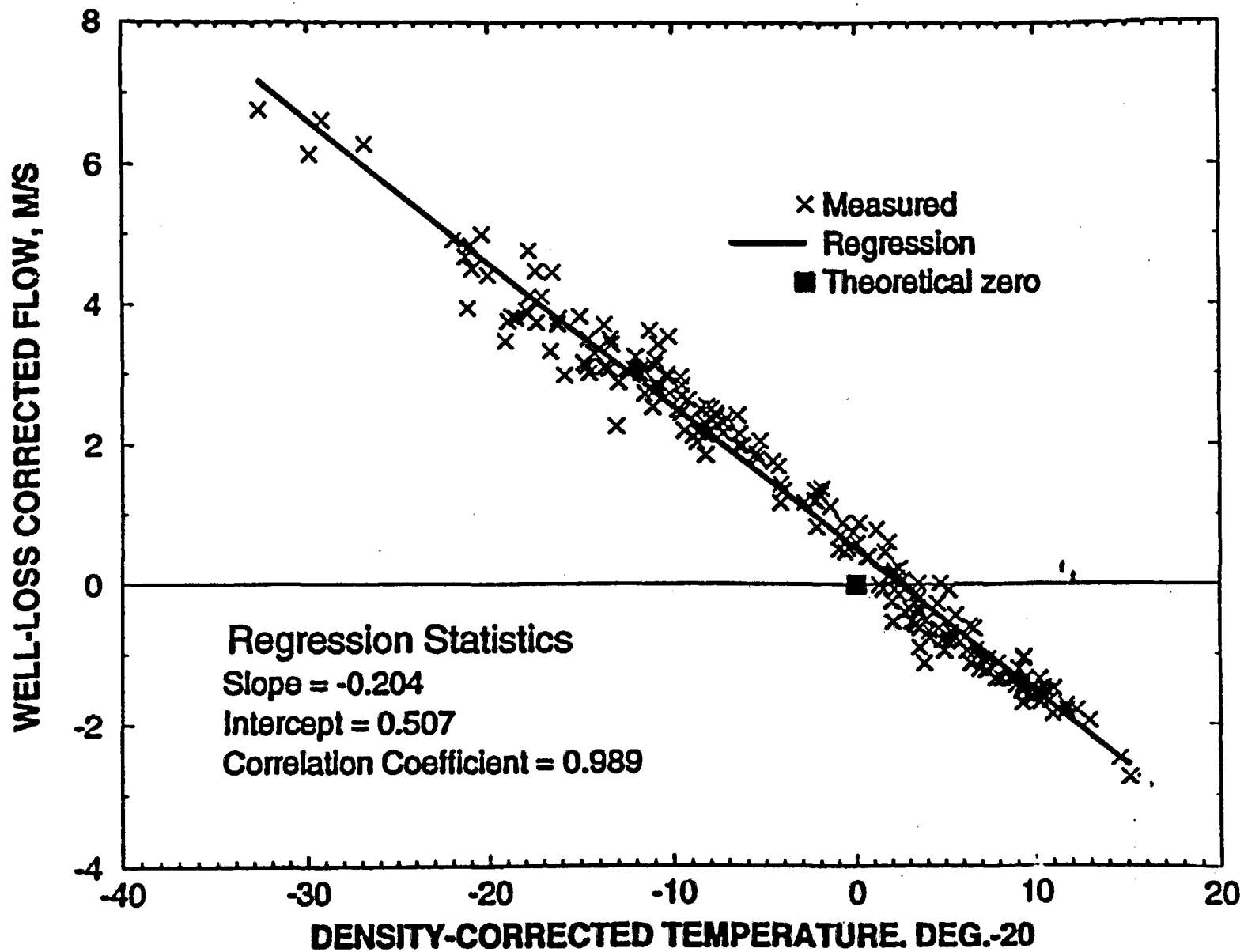


Figure 33. Thermosyphon-generated flow from borehole USW UZ-6s, computed as the residual of measured flow minus those computed for barometric pumping and for wind pumping.

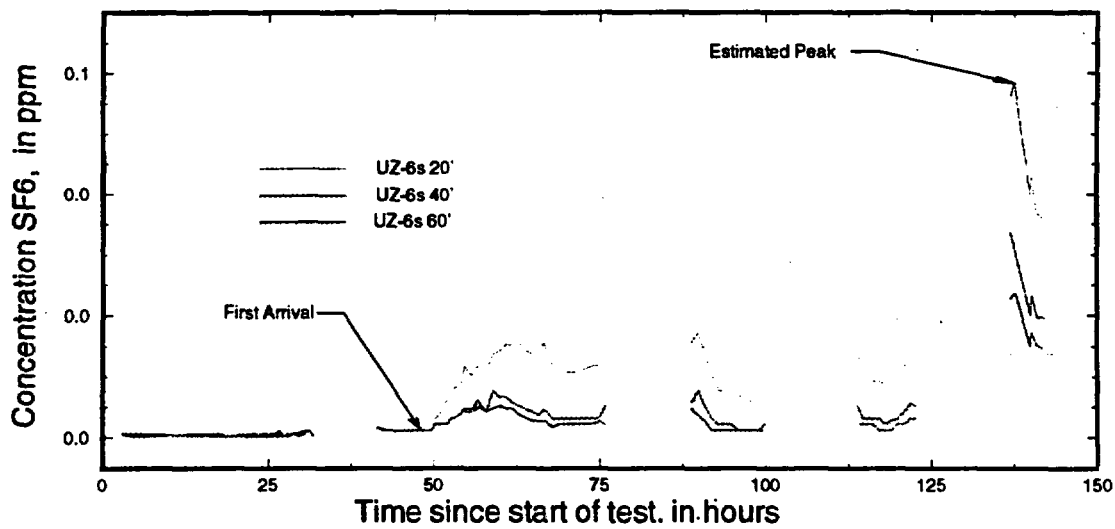
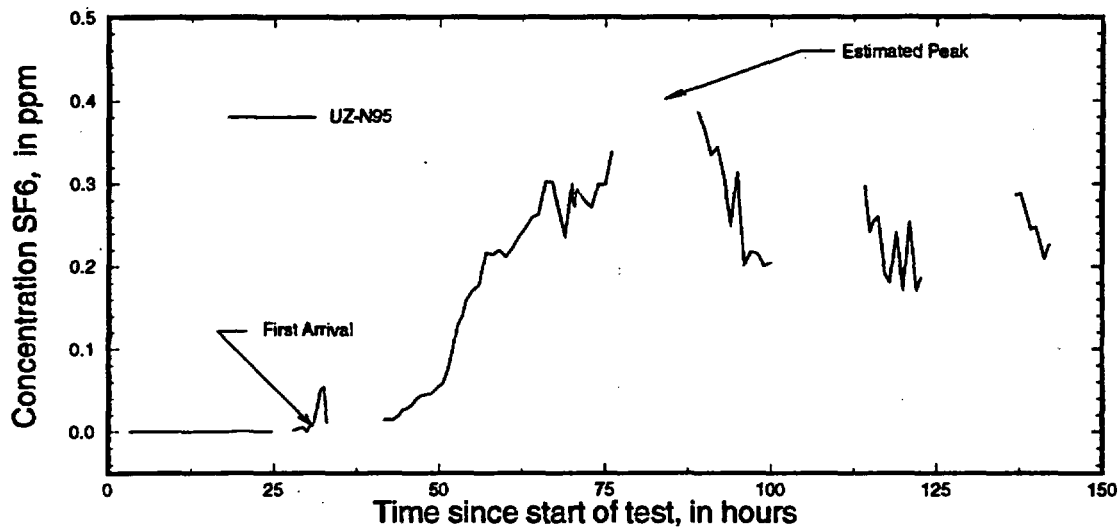
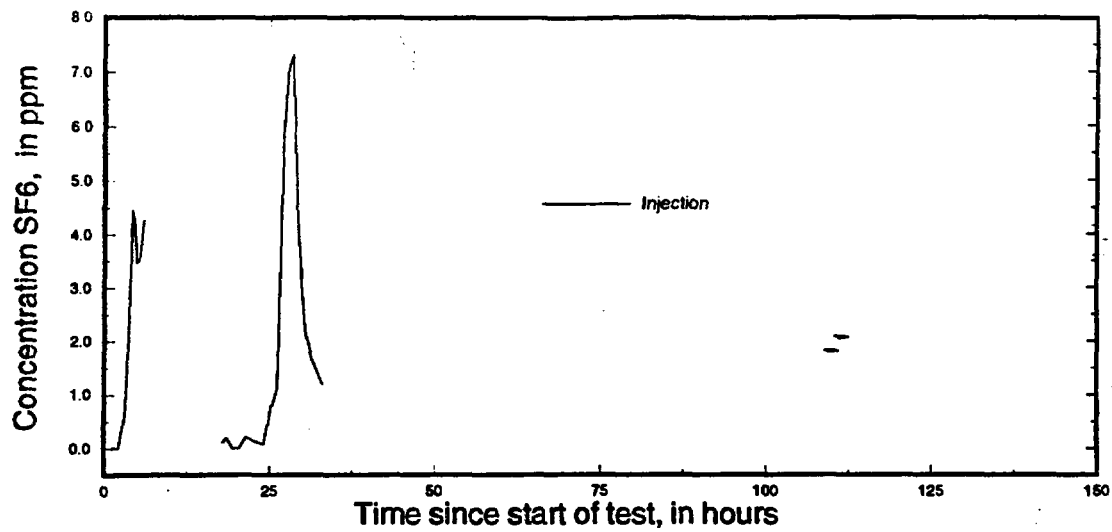


Figure 34. Tracer test SF6 concentrations in boreholes UZ-6, UZ-6s, and UZ-N95.

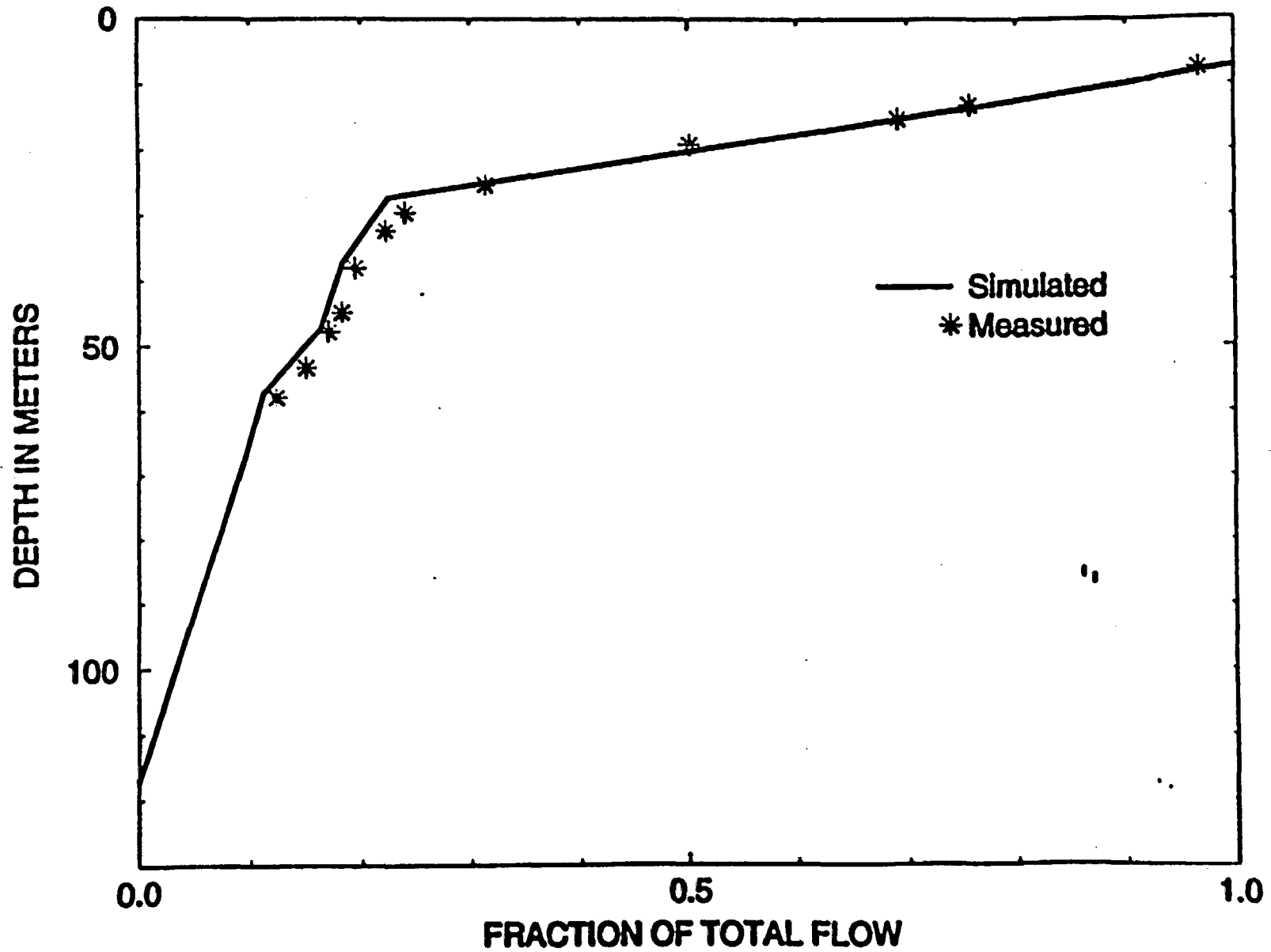
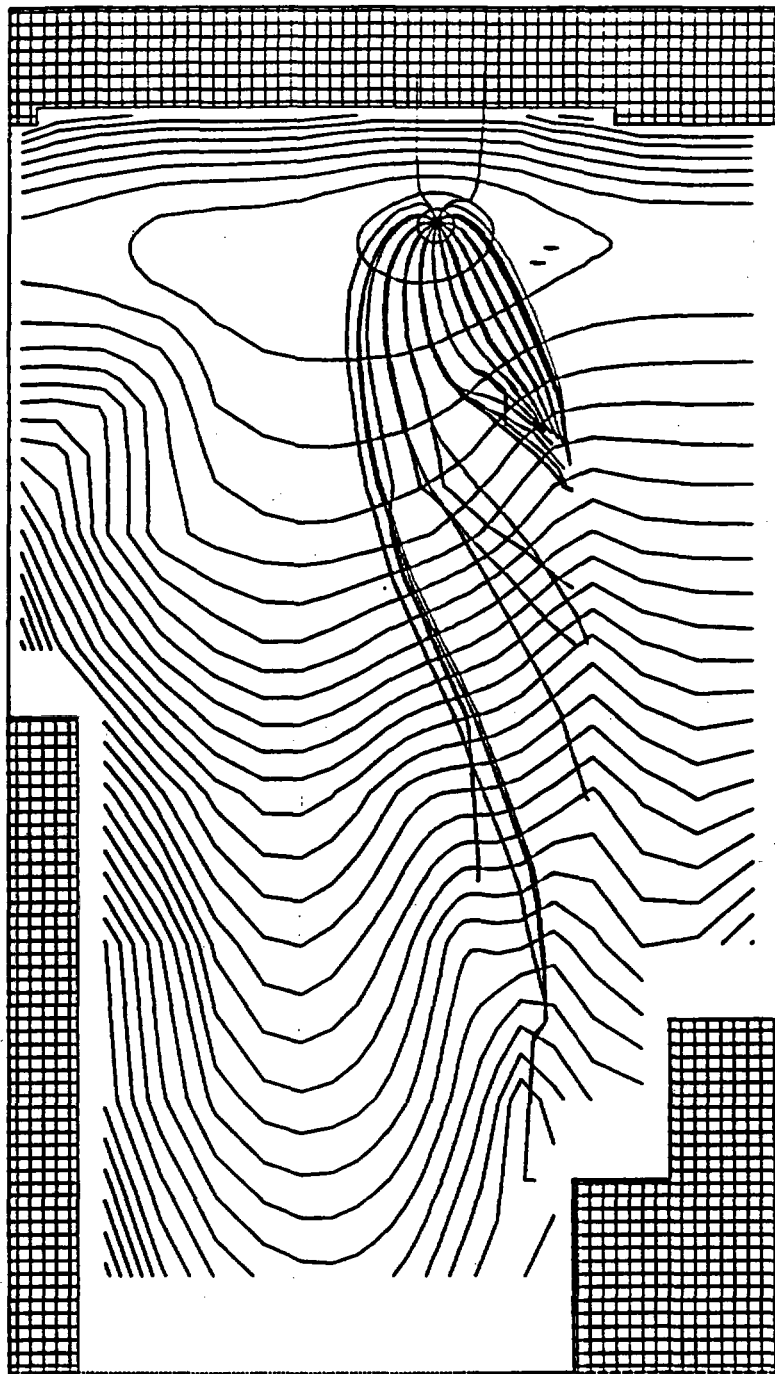
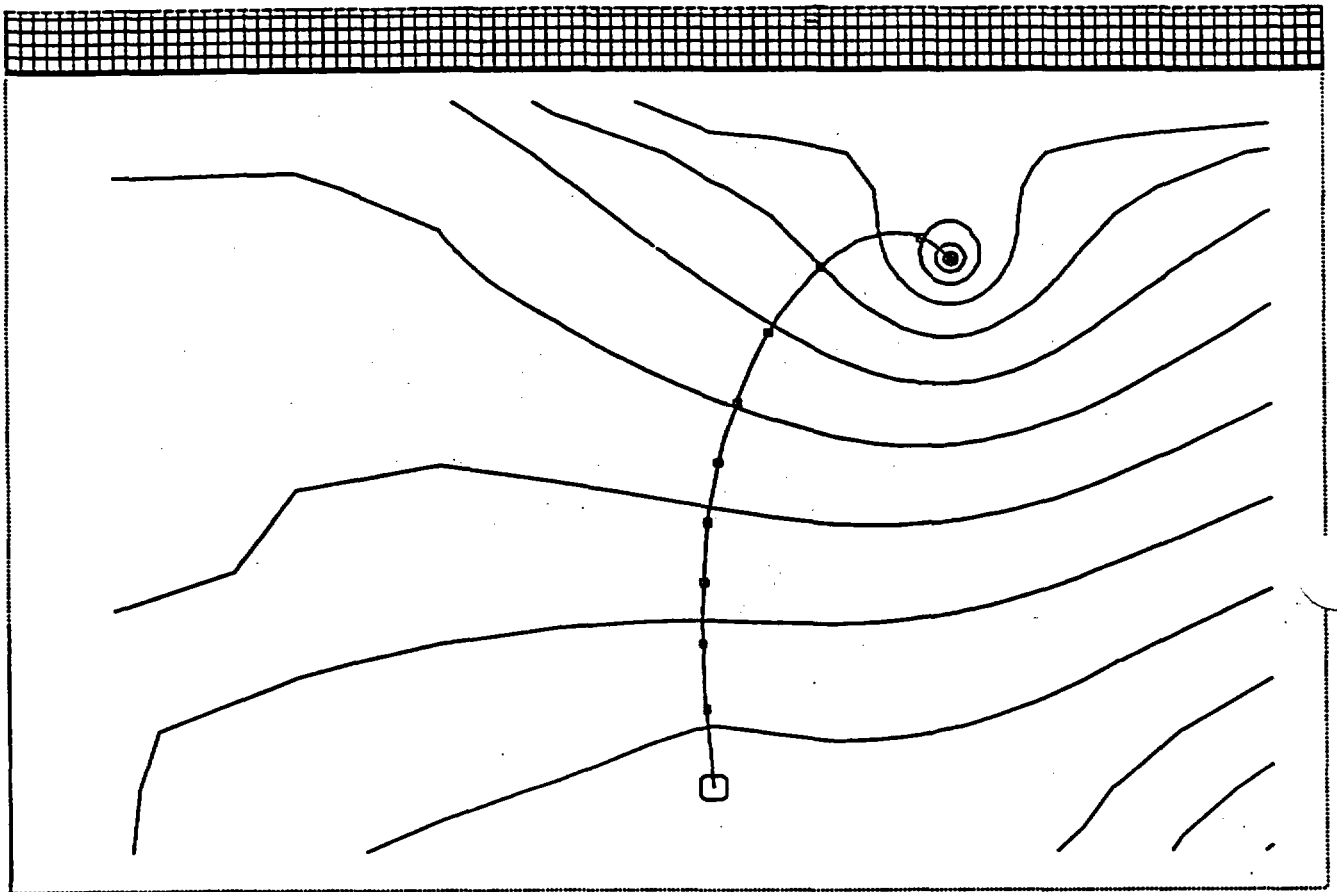


Figure 35. Comparison of simulated flow contributions to measure flow distribution with depth for calibrated model



0 100 FEET METERS

Figure 36. Particle tracking backward for nodes representing layers 3 and 4 of borehole USW UZ-6s, showing modeled source of air.



0 10 50 FEET METERS

Figure 37. Forward particle tracking from borehole USW UZ-6 to borehole USW UZ-6s. Squares represent 0.5 day intervals.

Data tracking numbers and accession numbers for references in the report entitled *Interpretation of Pneumatic and Chemical Data from the Unsaturated Zone near Yucca Mountain, Nevada*, by Gary L. Patterson, Edwin P. Weeks, Joseph P. Rousseau, and Thomas A. Oliver.

REFERENCE	DATA TRACKING #	ACCESSION #
Barracough, J.T., Teasdale, W.E., Robertson, J.B., and Jensen, R.G., 1967, Hydrology of the National Reactor Testing Station, Idaho: U.S. Geol. Survey Open File Report, 95 p.		
Bendat, J. S., and A. G. Piersol, 1986, <i>Random Data: Analysis and Measurement Procedures</i> , John Wiley, New York, 566 p.		NNA.19900727.0301
Bird, R.B., W.E. Stewart, and E.N. Lightfoot, 1960, <i>Transport phenomena</i> , McGraw-Hill, New York, p. 154-155.		NNA.19900919.0195
Buckingham, Edgar, 1904, Contributions to our knowledge of the aeration of soils: U. S. Dept Agric. Soils Bull. 25, 52 p.		
Buesch, D.C., Spengler, R.W., Nelson, P.H., Vaniman, D.T., Chipera, S.J., and Bish, D.L., 1995, Geometry of the vitric-zeolitic transition in tuffs and the relation to fault zones at Yucca Mountain, Nevada: International Union of Geodesy and Geophysics, XXI General Assembly, Boulder, Colorado, USA, Abstracts Week A, p. A426.		
Buesch, D.C., and Spengler, R.W., 1996, Geologic Framework of the North Ramp Area of the Exploratory Studies Facility, Yucca Mountain, Nevada, in Rousseau, J.P., Kwicklis E. M., and Gillies D.C., Hydrogeology of the Unsaturated Zone, North Ramp Area of the Exploratory Studies Facility, Yucca Mountain, Nevada.; U. S. Geological Survey Water Resources Investigation Report 96xxxx, <i>in press</i> , p. 44-62		
Carslaw, H.S., and Jaeger, J.C., 1959, <i>Conduction of heat in solids</i> : London, Oxford Univ. Press, p. 59, fig. 12.		NNA.19900522.0259
Colbeck, S.C., 1989, Air movement in snow due to windpumping: <i>Jour. of Glaciology</i> , v. 35, p. 209-213.		
Cooper, H.H., Bredchoeft, J.D., Papadopulos, I.S., and Bennett, R.R., 1965, The response of well-aquifer systems to seismic waves: <i>Jour. Geophys. Research</i> , v. 70, no. 16, p. 3915-3926.		HQO.19871022.0147
Cunningham, J., and Waddington, E.D., 1993, Air flow and dry deposition of non-sea salt sulfate in polar firn: paleoclimate implications: <i>Atmospheric Environment</i> , v. 27A, p. 2943-2956.		
Ferris, J.G., Knowles, D.B., Brown, R.H., and Stallman, R.W., 1962, <i>Theory of aquifer tests</i> : U.S. Geological Survey Water-Supply Paper 1536E, p. 84		NNA.901106.0145

REFERENCE

	DATA TRACKING #	ACCESSION #
French, R.H., 1983, <i>Precipitation in southern Nevada</i> ; <i>Journal of hydraulic Engineering</i> , v. 109, no. 7, p. 1023-1036.		NNA.19900104.0481
Geslin, J.K., Moyer, T.C., and Buesch, D.C., 1995, <i>Summary of lithologic logging of new and existing boreholes at Yucca Mountain, Nevada, August 1993 to February 1994</i> : U.S. Geological Survey Open-File Report 94-342, 39 p.	GS940308314211.009	MOL.19940810.0011
Geslin, J.K., and Moyer, T.C., 1995, <i>Summary of lithologic logging of new and existing boreholes at Yucca Mountain, Nevada, March 1994 to June 1994</i> : U.S. Geological Survey Open-File Report 94-451, 16 p.	GS940708314211.032	MOL.19941214.0057
Grayson, D.K., 1993, <i>The Desert's Past: a Natural Prehistory of the Great Basin</i> : Smithsonian Institution Press, Washington D.C., 356 p.		
Hantush, M.S., 1991, "Drawdown around a partially penetrating well:" <i>Am. Soc. Civil Eng. Proc.</i> , v. 87, no. 11Y5, p. 171-195.		
Hevesi, J.A., and Flint, A.L., 1996, <i>Geostatistical model for estimating precipitation and recharge in the Yucca Mountain region, Nevada-California</i> : U.S. Geological Survey Water-Resources Investigations Report 96-4123 (in press).	GS960108312111.001	
Hill, M.C., 1992, <i>A computer program (Modflowp) for estimating parameters of a transient, three-dimensional, ground-water flow model using nonlinear regression</i> : U.S. Geol. Survey Open-File Report 91-484, 358 p.		
Houghton, J.G., 1969, <i>Characteristics of rainfall in the Great Basin</i> : Desert Research Institute, University of Nevada System, Reno, Nev., 205 p.		
Imboden, D. M., and Lerman, A., 1978, <i>Chemical models of lakes</i> , in Lerman, A., <i>Lakes: Chemistry; Geology; Physics</i> : Springer-Verlag, New York, p. 343-346.		
Kume, J., and Rousseau, J. P., 1994, <i>A borehole instrumentation program for characterization of unsaturated zone percolation</i> , in <i>High-Level Radioactive Waste Management, International Conference</i> , 5th, Las Vegas, Nevada, May 22-26, 1994, <i>Proceedings</i> , Las Vegas, Nevada, p. 2076-2083.	GS940108312232.006	MOL.19960416.0127
Lewis, W.C., 1991, <i>Atmospheric pressure changes and cave airflow: a review</i> : <i>National Speleological Society Bull.</i> , June, p. 1-12.		
List, R. J., <i>Smithsonian Meteorological Tables</i> , Sixth ed., Smithsonian Institution Press, Washington, D. C., 527 pp., 1949.		IIQZ.19871031.8316

REFERENCE

Little, J. N., and Loren Shure, 1988, *Signal processing toolbox for use with MATLAB--User's Guide* [August 29, 1988 version]: Natick, Mass., The MathWorks, Inc., various pagination.

Loscot, C.L., 1993, *Geohydrologic data for test hole USW UZ-6s, Yucca Mountain area, Nye County, Nevada: U.S. Geological Survey Open-File Report 93-60, 25p.*

Lowe, P. R. 1976, An approximate polynomial for the computation of saturation vapor pressure: *Jour. Applied Meteorology*, v. 16, no. 1, p 100-103.

Massmann, Joel, and Farrier, D. F., 1992, *Effects of atmospheric pressures on gas transport in the vadose zone: Water Resour. Res.*, v. 28, no. 3, p. 777-791.

McDonald, M.G., and Harbaugh, A.W., 1988, *A modular three-dimensional finite-difference ground-water flow model: U.S. Geol. Survey Tech. of Water-Resources Investigations, Book 6, Ch. A1, 586 p.*

Montazer, P. and Wilson, W.E., 1984, *Conceptual hydrologic model of flow in the unsaturated zone, Yucca Mountain, Nevada: U.S. Geological Survey Water Resources Investigation Report 84-4345, 55 p.*

Montieth, J.L., 1973, *Principles, of environmental physics: Edward Arnold, London, p. 7*

Moyer, T.C., and Geslin, J.K., 1995, *Lithostratigraphy of the Calico Hills Formation and Prow Pass Tuff (Crater Flat Group) at Yucca Mountain, Nevada: U.S. Geological Survey Open-File Report 94-460, 59 p.*

Moyer, T.C., Geslin, J.K., and Buesch, D.C., 1995, *Summary of lithologic logging of new and existing boreholes at Yucca Mountain, Nevada, July 1994 to November 1994: U.S. Geological Survey Open-File Report 95-102, 22 p.*

Moyer, T.C., Geslin, J.K., and L.E. Flint, 1996, *Stratigraphic relations and hydrologic properties of the Paintbrush Tuff Nonwelded (PTn) hydrologic unit, Yucca Mountain, Nevada: U.S. Geological Survey Open-File Report 95-397, in press.*

Nilson, R.H., Peterson, E.W., Lie, K.H., Burkhard, N.R., And Hearst, J.R., 1991, *Atmospheric pumping: A mechanism causing vertical transport of contaminated gases through fractured porous media: Jour. Geophys. Res.*, v. 96, No. B13, p. 21,933-21,948.

Nilson, R. H., McKinnis, W.B., Lagus, P.L., Hearst, J.R., Burkhard, N.R., and Smith, C.F., 1992, *Field measurements of tracer gas transport induced by barometric pumping: Amer. Nuclear Soc. High-Level Radioactive Waste Conference Proceedings, Las Vegas, Nevada, p. 710-716.*

DATA TRACKING #

ACCESSION #

GS921208312211.013

NNA.930518.0073

GS930408312291.001

NNA.870519.0109

GS940608314211.028

MOL.19941208.0003

GS941208314211.060

MOL.19960222.0335

NNA.19921202.0002

NNA.19940203.0033

REFERENCE

DATA TRACKING #

ACCESSION #

Patterson, G. L., 1996, Occurrences of Perched Water in the Vicinity of the Exploratory Studies Facility, North Ramp, in Rousseau, J. P., Kwicklis E. M., and Gillies D. C., Hydrogeology of the Unsaturated Zone, North Ramp Area of the Exploratory Studies Facility, Yucca Mountain, Nevada.; U. S. Geological Survey Water Resources Investigation Report 96xxxx, *in press*, p. 177-179

Perry, J.H., ed., 1963, Perry's Chemical Engineers Handbook, 4th edition, McGraw-Hill, p. 14-20.

Phelan, J.M., Reavis, B. and Cheng, W.C., 1995, Passive soil venting at the chemical waste landfill site at Sandia National Laboratories, Albuquerque, New Mexico: Sandia Report SAND95-0776, UC-602, 35 p.

Pollock, D. W., 1994, User's guide for Modpath/Modpath-plot, Version 3: U.S. Geol. Survey Open-File Report 94-464, variously paged.

Purtyman, W.D., Koopman, F.C., Barr, S., and Clements, W.E., 1974, Air volume and energy transfer through test holes and atmospheric pressure effects on the main aquifer: Los Alamos Laboratory Informal Report LA-5725-MS, 14 p.

Rohay, Virginia, Rossabi, Joe, Brian Looney, Richard Cameron, and Brian Peters, 1993, Well venting and application of passive soil vapor extraction at Hanford and Savannah River: Westinghouse, Hanford Company, WHC-SA-2064-FP, p. 815-818.

Rorabaugh, M.I., 1956, Ground water in northeastern Louisville, Kentucky: U.S. Geological Survey Water-Supply Paper 1360-B, p. 122.

Rousseau, J. P., Loskot, C. L., Kume, J., Kurzmack, M., 1995, In-situ borehole instrumentation and monitoring data (October 25, 1995 through April 12, 1995) for USW NRG-7a and USW NRG-6, Yucca Mountain, Nye County, Nevada: DTN-GS950508312232.004.

Rousseau, J. P., Patterson, G. L., 1996, In-Situ Pneumatic-Pressure Response to Atmospheric-Pressure Change, in Rousseau, J. P., Kwicklis E. M., and Gillies D. C., Hydrogeology of the Unsaturated Zone, North Ramp Area of the Exploratory Studies Facility, Yucca Mountain, Nevada.; U. S. Geological Survey Water Resources Investigation Report 96xxxx, *in press*, p. 96-131

Sanford; R.L., 1982, Natural ventilation in Hartman, H.L., ed., Mine ventilation and air conditioning: Wiley Interscience, New York, p 239-253.

NNA.19910304.0107

Schlichting, Hermann, 1968, Boundary-layer theory, McGraw-Hill, New York, 744 p.

NNA.19910522.0049

Scott, R.B., and Bonk, J., 1984, Preliminary geologic map of Yucca Mountain, Nye County, Nevada, with geologic sections: U. S. Geological Survey Open-File Report 84-494, 9 p., map scale 1:12,000.

GS930208317461.001

HQS.880517.1492

REFERENCE

Spengler, R.W., Byres, F.M., and Warner, J.B., 1981, Stratigraphy and Structure of Volcanic Rocks in Drill Hole USW-G1, Yucca Mountain, Nevada: U.S. Geological Survey Open-File Report 81-1349, 50 p.

Streeter, V.L., 1962, Fluid mechanics: McGraw-Hill, New York, p. 217.

Thorstenson, D.C., Weeks, E.P., Haas, H.H., and Woodward, J.C., 1990, Physical and chemical characteristics of topographically affected airflow in an open borehole at Yucca Mountain, Nevada, in Nuclear waste isolation in the unsaturated zone, Focus '89, Sept. 17-21, 1990, Las Vegas, Nev., Proceedings: Las Vegas, Nev., p. 256-270.

Thorstenson, D.C., Haas, Herbert, Peters, C.A., and Yang, I.C., in press, The reactions and transport of CO₂ and its C-isotopes in the unsaturated zone at the crest of Yucca Mountain, Nevada: U.S. Geological Survey Administrative Report.

Vanoni, V.A., and Hwang, L.S., 1967, Relation between bedforms and friction in streams: Jour. Hyd. Div. Am. Soc. Civil Engineers, v 93, no. HY3, p. 121-144.

Weeks, E.P., 1968, Determining the ratio of horizontal to vertical permeability by aquifer-test analysis: Water Resour. Res., v. 5, no. 1, 196-214.

Weeks, E.P., 1978, Field Determination of vertical permeability to air in the unsaturated zone, Geological Survey Professional Paper 1051, 41p.

Weeks, E.P., 1978, Field determination of the vertical permeability to air: U.S. Geol. Survey Prof. Paper 1058, 41 p.

Weeks, E.P., 1987, Effect of topography on gas flow in unsaturated fractured rock--concepts and observations: in Flow and transport through unsaturated fractured rock, Evans, D.D. and Nicholas, T.J., eds., Geophysical Monograph 42, Am. Geophys. Union, Washington, D.C., p. 165-170

Weeks, E. P., 1993, Does the wind blow through Yucca Mountain: U.S. Nuclear Regulatory Commission Report NUREG/CP-0049, p. 43-53.

Whitfield, M.S., Cope, C.M. and Loskot, C.L., 1993, Borehole and geohydrologic data for test hole USW UZ-6, Yucca Mountain area, Nye County, Nevada: U.S. Geological Survey Open-File Report 92-28, 36 p.

Woodcock, A.H., 1987, Mountain breathing revisited--the hyperventilation of a volcano cinder cone: Bulletin American Meteorology Society, v. 68, no. 2, p. 125-130.

DATA TRACKING #

ACCESSION #

GS930208314211.005

HQS.880517.1492

GS930508312261.004

NNA.19900723.0196

HQS.19880517.1930

HQS.19880517.3214

GS940608312261.003

MOL.19941006.0033

GS910808312232.002

NNA.920123.0088